

THE HYDROTHERMAL SYNTHESIS OF BARIUM TITANATE POWDERS:
AN INVESTIGATION OF PREDOMINANT PROCESS
VARIABLES VIA EXPERIMENTAL DESIGN

By

JEFFREY A. KERCHNER

A DISSERTATION PRESENTED TO THE GRADUATE SCHOOL
OF THE UNIVERSITY OF FLORIDA IN PARTIAL FULFILLMENT
OF THE REQUIREMENTS FOR THE DEGREE OF DOCTOR OF PHILOSOPHY

UNIVERSITY OF FLORIDA

1998

This work is dedicated to my loving, patient, and supportive wife,

Jeannie Kerchner,

my parents,

Cliff and Suzanne Kerchner,

and

my sister,

Karen Kerchner.

Every person is touched by those around them.
I have been truly blessed.

ACKNOWLEDGMENTS

I would like to thank all of the people who made this research project successful through their support, suggestions, and sundry contributions. Sincere thanks is extended to my committee chair and advisor, Dr. James H. Adair, for his guidance in academic affairs and understanding in personal matters. I also thank the other members of my committee, Drs. Robert T. DeHoff, David E. Clark, and Michael D. Sacks, from the Department of Materials Science and Engineering, James D. Winefordner, from the Department of Chemistry, and Stephen A. Costantino, from the sponsor of the current research, Cabot Performance Materials (CPM), Boyertown, PA, for actively participating in my experience at the University of Florida. Without their combined advice and the monetary support from CPM, this research would not have been as fruitful.

I would like to extend a hearty thanks to Dr. Hassan El-Shall for his instruction in the use of experimental designs. I also greatly appreciate the efforts and advice of the entire CPM BaTiO_3 team, including Dr. David Miller, Jamie Sampson, Tracy Taggart, Ed Thompson, and Dr. Sridhar Venigalla. I acknowledge Dr. Stanley Bates and the staff at the Major Analytical Instrumentation Center (MAIC) at the University of Florida, Dr. Augusto Morrone, Eric Lambers, and Wayne Acree, for their instruction on the finer points of characterization techniques and instrumental limitations.

I am grateful to all of my colleagues in Dr. Adair's research group, both present and former, for their technical and personal support. Working beside them has been an honor and a true pleasure. Special thanks are extended to Drs. Sridhar Venigalla, Robert Chodelka, Jooho Moon, Melanie Carasso, Craig Habeger, soon-to-be Drs. Paul Demkowicz and Henrik Krarup, and the honorary Adair group members, Drs. James

Kunetz and Kevin Powers, for their assorted and enlightening academic discussions. A sincere debt of gratitude is extended to Dr. Melanie Carasso, Dr. Robert Chodelka and Paul Demkowicz for proof reading my dissertation, as well as Pam Howell for her motherly support and assistance during my enrollment at UF.

I am especially appreciative of all my friends and professors at Penn State who fostered my early academic growth. Dr. Susan Troler-McKinstry, Brady Gibbons, Doug Wolfe, and Sonya Diezhandino are just a few of these many associates. Finally, I would like to thank my wife, parents, sister, and countless friends and relatives for their herculean support, concrete guidance, and endless patience. With the foundation I was provided, it would have been difficult not to succeed.

TABLE OF CONTENTS

ACKNOWLEDGMENTS.....	iii
LIST OF TABLES.....	ix
LIST OF FIGURES.....	xi
ABSTRACT.....	xiv
CHAPTERS	
1. INTRODUCTION.....	1
2. LITERATURE REVIEW.....	5
2.1 Introduction.....	5
2.2 Aspects of Barium Titanate.....	5
2.2.1 Crystallographic Origin of the Ferroelectric Response.....	5
2.2.2 Ferroelectric Behavior of Barium Titanate.....	6
2.3 Solution Synthesis of Powders.....	8
2.3.1 Precipitation from Solution.....	8
2.3.2 Benefits and Limitations of Solution Precipitation.....	9
2.3.3 Nucleation.....	11
2.3.3.1 Classical nucleation theory.....	13
2.3.3.2 Kinetic theory.....	15
2.3.3.3 Validity of nucleation theories.....	15
2.3.4 Growth.....	16
2.3.4.1 Basic concepts of growth.....	17
2.3.4.2 Morphological theory.....	18
2.3.4.3 Continuous growth model.....	19
2.3.4.4 Two dimensional growth model.....	19
2.3.4.5 Screw dislocation theory (BCF theory).....	21
2.3.4.6 Bulk diffusion theory.....	22
2.3.4.7 Surface reaction theory.....	23
2.3.5 Physical Growth Mechanism for Monodisperse Particle Formation..	24
2.3.5.1 Monomer addition model.....	26
2.3.5.2 Aggregative growth.....	27
2.3.6 Effect of Crystal Size on Solubility.....	27
2.4 Hydrothermal Synthesis of Barium Titanate.....	28
2.4.1 History and Application in Thin Layer MLCs.....	28
2.4.2 Solubility.....	34
2.4.2.1 Titanium precursor solubility.....	34
2.4.2.2 Barium precursor solubility.....	37
2.4.2.3 Formation mechanisms based on soluble precursors.....	37
2.4.2.4 BaTiO ₃ solubility.....	38

2.4.3 Required Processing Conditions.....	40
2.4.3.1 CO ₂ -free environment.....	40
2.4.3.2 An excess precursor Ba/Ti ratio.....	42
2.4.3.3 Solution pH.....	43
2.4.4 Precursor Impurities.....	44
2.4.5 Solution Additives.....	45
2.4.6 Seeding.....	46
2.5 Experimental Designs.....	47
2.5.1 Applied Experimental Design Techniques.....	48
2.5.2 Experimental Design Limitations.....	50
2.5.3 Fractional Factorial Design.....	51
2.5.4 Basis of Significance.....	54
2.6 Powder Characterization Techniques.....	55
2.6.1 X-Ray Diffraction - Phase Purity.....	56
2.6.2 Particle Size Determination.....	56
2.6.3 X-Ray Line Broadening.....	57
2.6.4 Transmission Electron Microscopy.....	59
2.6.5 Nitrogen Adsorption/Desorption - BET.....	59
2.6.6 Helium Micropycnometry.....	61
2.6.7 X-ray Fluorescence Spectroscopy.....	62
 3. DETERMINATION OF SYNTHESIS VARIABLES AFFECTING HYDROTHERMAL BaTiO ₃ POWDERS.....	 64
3.1 Introduction.....	65
3.2 Materials and Methods.....	66
3.2.1 Hydrothermal Synthesis.....	66
3.2.2 Powder Characterization.....	70
3.3 Results and Discussion.....	73
3.3.1 Phase Purity.....	73
3.3.2 Effect of Treatments on Coulter Particle Size.....	73
3.3.2.1 Estimation of population variance.....	77
3.3.2.2 Fractional factorial matrix calculations.....	77
3.3.3 XRD Line Broadening Analysis.....	82
3.3.3.1 Effect of treatments on crystallite size.....	82
3.3.3.2 Effect of treatments on crystallite strain.....	83
3.3.4 Transmission Electron Microscopy.....	83
3.3.5 Effect of Treatments on Specific Surface Area.....	84
3.3.6 Effect of Treatments on Particle Density.....	87
3.3.7 Effects of Treatments on the Product Ba/Ti.....	88
3.4 Conclusions.....	89
 4. EFFECT OF EDTA ADDITIONS AND OTHER PROCESS VARIABLES ON THE PARTICLE ATTRIBUTES OF HYDROTHERMALLY SYNTHESIZED BaTiO ₃	 90
4.1 Introduction.....	90
4.1.1 Experimental Design.....	92
4.1.2 Hydrothermal Synthesis.....	93
4.2 Materials and Methods.....	96
4.2.1 Hydrothermal Synthesis.....	96
4.2.2 Powder Characterization.....	98

4.3 Results and Discussion	98
4.3.1 Phase Purity	98
4.3.2 Effect of Treatments on Coulter Particle Size of Barium Titanate	101
4.3.2.1 Calculation of the main effects of the treatments.....	101
4.3.2.2 Estimation of population variance	104
4.3.2.3 The 95% confidence interval and statistical significance.....	104
4.3.3 Effect of Treatments on the Barium Titanate Particle Size Distribution	107
4.3.4 XRD Line Profile Analysis.....	107
4.3.4.1 Effect of treatments on barium titanate crystallite size	107
4.3.4.2 Effect of treatments on barium titanate crystallite strain.....	108
4.3.5 Transmission Electron Microscopy.....	109
4.3.6 Effect of Treatments on Barium Titanate Specific Surface Area	109
4.3.7 Effect of Treatments on Barium Titanate Product Ba/Ti.....	111
4.4 Conclusions.....	111
5. EFFECT OF BARIUM HYDROXIDE PRECHARGING AND OTHER PROCESS VARIABLES ON HYDROTHERMALLY SYNTHESIZED BaTiO ₃	113
5.1 Introduction.....	113
5.1.1 Hydrothermal Synthesis	115
5.1.2 BaTiO ₃ Seeding	116
5.1.3 Experimental Design.....	117
5.2 Materials and Methods.....	119
5.2.1 Hydrothermal Synthesis	119
5.2.2 Powder Characterization	121
5.3 Results and Discussion	121
5.3.1 Phase Purity	121
5.3.2 Effect of Treatments on Particle Size.....	124
5.3.2.1 Estimation of population variance	126
5.3.2.2 Fractional factorial matrix calculations.....	126
5.3.3 Effect of Treatments on Particle Size Distribution.....	130
5.3.4 XRD Line Profile Analysis.....	131
5.3.4.1 Effect of treatments on crystallite size.....	131
5.3.4.2 Effect of treatments on crystallite strain.....	131
5.3.4.3 Transmission Electron Microscopy.....	133
5.3.4.4 Effect of Treatments on Specific Surface Area	133
5.3.4.5 Effect of Treatments on Product Ba/Ti.....	133
5.5 Conclusions.....	135
6. HIGH YIELD HYDROTHERMALLY SYNTHESIZED BaTiO ₃ POWDERS..	136
6.1 Introduction.....	136
6.2 Hydrothermal Synthesis	137
6.2.1 Further Decrease in the Size of Hydrothermal Product.....	138
6.2.2 Titanium Solubility	140
6.2.3 Formation Mechanisms.....	143
6.3 Materials and Methods.....	145
6.3.1 Titanium Gel Storage.....	145
6.3.2 Hydrothermal Synthesis	146
6.3.3 Powder Characterization.....	148
6.3.3.1 X-ray diffraction	148
6.3.3.2 Transmission electron microscopy	148

6.3.3.3 Specific surface area	148
6.4 Results and Discussion	149
6.4.1 Powder Lot Number 40.....	149
6.4.2 Effect of Treatments on Phase Purity.....	149
6.4.3 Transmission Electron Microscopy.....	151
6.4.4 Specific Surface Area.....	151
6.4.5 A Viable System.....	151
6.4.6 Limitations	154
6.5 Conclusions.....	155
7. CONCLUSIONS AND FUTURE WORK	157
7.1 Conclusions.....	157
7.2 Future Work.....	161
REFERENCES.....	163
BIOGRAPHICAL SKETCH.....	176

LIST OF TABLES

<u>Table</u>	<u>page</u>
2.1. Recent literature for the aqueous synthesis of BaTiO ₃ powders at elevated temperatures from various titanium precursors, precursor molar ratios, product loading, agitation rates, and Ba(OH) ₂ ·8H ₂ O introduction techniques	32
2.2. Ba(OH) ₂ ·8H ₂ O aqueous solubility with respect to temperature [Kir78]	37
2.3. Experimental design nomenclature employed within the text	49
2.4. Numerous types of experimental designs [Cau91, Hun79, Mas89]	49
2.5. The 2 ⁷⁻³ fractional factorial design matrix for the general equation I + ABCDE + ABCF + BCDG illustrating the 20 experiments and seven variables, A through G	52
2.6. Treatment levels for the seven variables of the 2 ⁷⁻³ fractional factorial design to investigate the hydrothermal synthesis of BaTiO ₃ . Note that the center values of the treatments were employed in the four replicate experiments...	53
3.1. Experimental matrix using a 2 ⁷⁻³ fractional factorial design using the general equation: I + ABCDE + ABCF + BCDG and a center point replicate analysis (in lot number 17-20)	68
3.2. The specific values employed for the low and high levels of the fractional factorial design experiment as well as the center values common to all four replicate runs	69
3.3. Characterization summary for all investigated particle attributes	76
3.4. The 2 ⁷⁻³ fractional factorial calculation matrix for effect of seven variables, A through G, on the particle size of BaTiO ₃	79
3.5. Comparison of the main effects of the investigated treatments to the calculated confidence interval which assumes a single population. The shaded regions indicate treatments which have a statistically significant effect on the given observation	80
4.1. Fractional factorial design with replicated center point to estimate variance where column A through column D represent the investigated treatments ...	92

4.2.	Investigated treatments and treatment level of the employed 2^{4-2} fractional factorial design. All experiments were performed with a stirring rate of 350 rpm, a reaction temperature of 200°C, a reaction time of 10 min, and BaTiO ₃ product loading of 0.36 mol/L assuming complete conversion of titanium gel.	94
4.3.	Summary of characterization results for the hydrothermal BaTiO ₃ powder lot numbers 22-28 with EDTA additions.....	102
4.4.	Summary of naïve main effects of treatments on the particle size where statistically significant treatments are distinguished by a shaded region.	105
5.1.	Fractional factorial design with replicated center point to estimate the variance where columns A through D represent the investigated treatments.....	118
5.2.	Investigated treatments and treatment level of the employed 2^{4-2} fractional factorial design. All experiments were performed with a stirring rate of 350 rpm, 200°C reaction temperature, 10 min reaction time, and BaTiO ₃ product loading of 0.356 mol/L assuming complete conversion of the hydrated titanium oxide gel	118
5.3.	Characterization results of the hydrothermal BaTiO ₃ powder lot numbers 29-35	125
5.4.	Summary of naïve main effects of treatments on the particle size where statistically significant treatments are distinguished by a shaded region	129

LIST OF FIGURES

<u>Figure</u>	<u>page</u>
2.1. Schematic structures illustrating two different perspectives of the perovskite BaTiO_3 lattice [Jaf71, Lin77]	7
2.2. Free-energy change during homogeneous nucleation	14
2.3. Growth models: (a) continuous, (b) two-dimensional, (c) screw dislocation or BCF [Boi88, Ran88b]. In illustration (b), the arrows indicate the direction of growth	20
2.4. LaMer and Dinegar model for monodisperse particle formation: (a) concentration of solute with respect to reaction time, and (b) dependence of precipitation rate on nucleation and growth as a function of the solute concentration [LaM50]	25
2.5. Dependence of the nucleation rate, growth rate, and mean crystal size on the supersaturation determined by a mass balance [Nyv85].	26
2.6. Scanning electron micrograph of the alternating 3.0 μm dielectric (dark) and electrode (light) layers of a cofired MLC produced from 125 nm CPM powders [Ven98]	31
2.7. Stability diagrams for the (a) titanium dioxide precursor and (b) BaTiO_3 product in the absence of CO_2 contamination at 25°C and is based on the ideal solution approximation [Moo96]	36
2.8. Formation mechanisms proposed for the hydrothermal synthesis of BaTiO_3 powders include (a) <i>in situ</i> transformation and (b) dissolution and recrystallization by either homogeneous or heterogeneous nucleation [Eck96]	39
2.9. Theoretical phase stability diagram for the $\text{Ba-Ti-CO}_2\text{-H}_2\text{O}$ system illustrates that alkaline conditions are required for the synthesis of phase pure BaTiO_3 as a function of atmospheric CO_2 at 25°C and 1 atm [Ada90, Ute90]	41
2.10. A single x-ray peak derived from crystals with (a) no strain, (b) uniform strain, and (c) nonuniform strain to illustrate the effects of crystal strain on experimental x-ray diffraction patterns [Cul78]	58
3.1. Diagram of BaTiO_3 hydrothermal synthesis and powder washing technique	67

3.2.	X-ray diffraction analysis of the as-received and hydrothermally treated precursors to demonstrate the amorphous nature of the as-received gel and the formation of crystalline anatase on heat treatment to 150°C.....	74
3.3.	X-ray diffraction analysis of barium titanate powder lot (a) 4 and (15) indicates the pattern resemblance to (c) the cubic barium titanate (JCPDS card number 31-174) and presence of unreacted anatase (JCPDS card number 21-1272) in several powders.....	75
3.4.	Transmission electron photomicrographs of powder lots (a) 17 and (b) 19 to illustrate the equiaxed nature of the typical powders.....	85
3.5.	Transmission electron photomicrographs of BaTiO ₃ powder lots (a) 15 and (b) 8 to illustrate the several aggregate and asymmetrical particles, respectively.....	86
4.1.	Hydrothermal synthesis, washing, and characterization flow diagram for BaTiO ₃ powders with EDTA addition.....	97
4.2.	XRD analysis of the as-synthesized BaTiO ₃ powder lot numbers 22-28 which illustrate XRD patterns representative of a cubic crystal structure....	99
4.3.	Experimental calculation matrix for the particle size of BaTiO ₃ powder lot numbers 22-25, including the calculation of the naïve main effects of treatments and the estimate of variance, S^2 , from the replicate powder lots 26-28	103
4.4.	TEM photomicrographs illustrate the distinct, spherical polycrystalline particles for all lots. Most powders are representative of (a) lot 22 and (b) lot 28, and exhibit a nearly monosized distribution as shown by (c) the loose agglomerate of powder lot 27	110
5.1.	Flow diagram of hydrothermal synthesis, washing, and characterization of BaTiO ₃ powder lot numbers 29-35. A percentage of the total Ba(OH) ₂ ·8H ₂ O charge was introduced at room temperature prior to the bulk Ba(OH) ₂ ·8H ₂ O injection	120
5.2.	Room temperature XRD analyses of the as-synthesized BaTiO ₃ powder lot numbers 29-35 and CPM powder lot numbers 6670-70 and R59, which illustrate XRD patterns representative of the cubic crystalline phase and some BaCO ₃ contamination	122
5.3.	Experimental calculation matrix for the particle size of BaTiO ₃ powder lot numbers 29-32, including the calculation of the naïve main effects of treatments and the estimate of variance, S^2 , from the replicate powder lots 33-35	128
5.4.	TEM photomicrographs illustrate the distinct, spherical polycrystalline particles for powder lot numbers 29-35. Most powders are equiaxed and exhibit a nearly monosized distribution, as illustrated by the powder images of (a) lot 29, (b) lot 30, (c) lot 33, and (d) lot 35	134

6.1.	Effect of precursor Ba/Ti on the particle size of hydrothermally derived BaTiO ₃ powders. The critical Ba/Ti differs by an order of magnitude in the experiments by (a) Kumazawa et al. [Kum96] and (b) Wada et al. [Wad95]. The mean particle size and crystallite size in (a) are designated by the open and filled data points, respectively	139
6.2.	Predominance diagrams for titanium and zirconium in aqueous solution. The diagrams were constructed by the OPAL software program based on the species reported by Baes and Mesmer [Baes76] and data acquired from the NBS thermodynamic tables [Wag82]	141
6.3.	Theoretical stability diagram for aqueous TiO ₂ suspensions [Bae76, Pou74]	142
6.4.	Hydrothermal synthesis, washing, and characterization flow diagram for BaTiO ₃ powders produced by the noninjection system	147
6.5.	XRD of the as-synthesized BaTiO ₃ powder lot number 39, which illustrates a cubic crystalline pattern with BaCO ₃ contamination	150
6.6.	TEM photomicrographs illustrate the distinct, spherical, polycrystalline, near-monosized particles for lot number 39	152

Abstract of Dissertation Presented to the Graduate School
of the University of Florida in Partial Fulfillment of the
Requirements for the Degree of Doctor of Philosophy

THE HYDROTHERMAL SYNTHESIS OF BARIUM TITANATE POWDERS:
AN INVESTIGATION OF PREDOMINANT PROCESS
VARIABLES VIA EXPERIMENTAL DESIGN

By

Jeffrey A. Kerchner

August, 1998

Chairman: Dr. James H. Adair

Major Department: Materials Science and Engineering

Barium titanate (BaTiO_3) is an important electronic ceramic and is employed in the powder form as the fundamental dielectric material of multilayer capacitors. Due to the closed nature of the hydrothermal system and the desire for particles of decreased size, experimental designs were employed to investigate the effects of various synthesis process treatments on the final particle attributes using low reaction temperatures ($\leq 210^\circ\text{C}$) and reaction times ≤ 30 min. Using a barium hydroxide ($\text{Ba}(\text{OH})_2 \cdot 8\text{H}_2\text{O}$) injection system, stoichiometric, polycrystalline, equiaxed particles were synthesized which exhibited a mean particle size between 73 to 120 nm and a specific surface area (SSA) from 12.5 to 25.5 m^2/g for the stoichiometric powders. The particles were believed

to exhibit the crystallite strain and a room temperature, metastable cubic crystal structure associated to hydroxyl incorporation within hydrothermal powders.

An amorphous hydrated $\text{TiO}_x(\text{OH})_y$ gel precursor was shown more desirable than anatase in performing decreased duration, low temperature reactions. When using an aqueous barium hydroxide injection system, the use of moderate injection rates and times was required. Ethylenediaminetetraacetic acid (EDTA), as a complexing agent to the $\text{TiO}_x(\text{OH})_y$ gels, showed modest alteration of the BaTiO_3 particle size in the low employed concentrations (i.e., 1 to 5 mol % of titanium). Self-seeding with BaTiO_3 seeds in 1×10^{10} to 1×10^{13} seeds/ml showed no effect on the BaTiO_3 particle size. The use of increased precursor Ba/Ti molar ratios illustrated a decrease in the particle size of BaTiO_3 powders as demonstrated by previous authors.

A non-injection system, employing the same precursors, suggested the production of polycrystalline, equiaxed particles of 50 nm and a SSA of $15.2 \text{ m}^2/\text{g}$ to be a result of an increased $\text{Ba}(\text{OH})_2 \cdot 8\text{H}_2\text{O}$ concentration rather than an elevated precursor Ba/Ti. This was permitted by a freeze-thaw technique. The phase separation caused by the freezing process provided a liquid reaction medium without the need for dilution with additional water. The net result was an increase in the current industrial yield by a factor of 2.7 while an equiaxed morphology and near monosized product were maintained. Based on the calculations from the prior literature, a dissolution and recrystallization mechanism is suggested to be dominant in sufficiently alkaline solution.

CHAPTER 1 INTRODUCTION

Since the discovery of barium titanate (BaTiO_3) in the 1940s, it remains one of the most commercially significant and widely investigated of the oxygen octahedral ferroelectrics [Her85, Kan87, Kin76, Lin77, Ras55, Ric92, Swa97]. The worldwide sales of 10.8 million pounds of BaTiO_3 -based powders for capacitor applications totaled \$72 million in revenue in 1995 [Zog96]. Whether the powder is utilized in a multilayer capacitor (MLC) [Bee97], transducer [Cro84, Hen87a], thermistor [Ish92, Zhi90], or other device, there is an increasing need for the higher purity, compositionally homogenous, submicron particle sizes achieved by the chemical methods, such as the hydrothermal technique [Bru93, Daw88]. Formulated BaTiO_3 powders are incorporated into the MLC configuration by wet powder processing methods such as tape casting, screen printing, and the waterfall technique [Bec90, Bru93, Hur72, Ree88]. In such methods, particle size and morphological control of BaTiO_3 powders, as well as adequate dispersion, are necessary to provide optimal packing conditions within ultrathin 3 μm fired dielectric layers [Ada98, Bee97, Ven98]. If the particle diameters approach the magnitude of the dielectric thickness, the voids inherent to the randomly packed layers would represent a large percentage of the total thickness and may be sufficiently large to cause a short across the dielectric layer.

Although powders made by solution-based methods are typically more expensive than the powders prepared by conventional solid state reactions, the powders are recognized to offset the increase in cost by producing a more reliable product with a uniform composition and equiaxed morphology [Hea88, Phu90], an increase in capacitor

volumetric efficiency [Kan95], and a decrease in the sintering temperatures of the co-fired package [Abe91, Daw91]. Since the dielectric material represents the MLC constituent with the highest sintering temperature, the decrease in firing temperature permits the use of less noble electrode compositions, i.e., a less expensive, increased Ag/Pd ratio or base metal composition [Spa98, Wan94]. This is significant since the current metallization systems account for approximately 90% of the materials cost and 35% of the total cost of the MLC [Phu90].

The industrial use of barium titanate and the associated academic laboratory research spanning over five decades have contributed to an extensive body of literature. A host of precursor systems and synthesis techniques have been explored, including conventional calcination [Alc91, Bea83, Fer91], electrochemical-hydrothermal methods [Bac92, Ben93, Ven95], hydrothermal methods [Dut94, Fla55, Hen91, Kut84, Men89a, Men89b, Shv79, Wad96], and solution techniques at lower temperatures [Bru93, Dog97, Kle89]. In total, the above methods have produced single crystals [Chr70], polycrystalline powders [Cha90, Daw88, Men89a], and thin films [Chi95, Kaj91, Sla96] for various applications. As common to all advanced electronic materials systems, the need for a more competitive product and price are noted. In the case of the MLC industry, powder suspensions are employed to produce thin dielectric layers. However, until recently, industrial technology was not sufficiently advanced to accommodate the processing of 100-200 nm particles. This was witnessed in the sluggish acceptance of hydrothermal BaTiO_3 during the introductory years in the market. Various researchers [Daw88, Dog97], including the author, forecast the hydrothermal method as a leading advanced electronic ceramic powder manufacturing process in the next decade due to the numerous advantages and cost effectiveness of the technique. Further explication of the advantages will be provided within the review of the literature.

Notably, the study of the hydrothermal technique is not without difficulty. The closed nature of the system at the elevated pressures and temperatures which provide enhanced reaction kinetics does not allow *in situ* observation of the reaction. The scenario is further complicated by the complexity of the dynamic reactions and chemical nature of the soluble aqueous species under reaction conditions [Dem73]. Subsequently, much trial-and-error experimentation [Len93] has been performed, and discrepancies exist in the theories of scientists with regard to the mechanisms of particle formation [Eck96, Her88, Moo96, Wad95]. Due to the difficulty of investigations under true reaction conditions, researchers entertain the option to work at decreased temperatures or perform post-mortem investigations. The author has chosen the latter, using prior low temperature studies [Eck96, Her88, Moo96] as a guide to probe the process and attempt to determine the methods necessary to tailor the final product attributes. This was accomplished in a systematic manner by the use of statistical experiments, fractional factorial designs. Experimental design techniques have gained recent popularity within the industrial community, yet to the author's knowledge have not been used to investigate either perovskite materials or the hydrothermal synthesis of inorganic materials. Therefore, a description of the advantages and the preliminary tools to perform such experiments are provided.

The following work introduces the useful properties of barium titanate and describes the underlying principles of solution synthesis with regard to the hydrothermal system. Common to all following experimentation is the use of an amorphous hydrated titanium oxide gel ($\text{TiO}_x(\text{OH})_y$) and barium hydroxide octahydrate ($\text{Ba}(\text{OH})_2 \cdot 8\text{H}_2\text{O}$) precursor system. The absence of additives to the hydrated titanium gel, use of additives of differing composition, hydrothermal treatment of the as-received gel, the use of BaTiO_3 seed particles, and alterations in the precursor introduction procedure were researched in various designs. Chapter 3 investigates the use of a fractional factorial design as a

screening experiment to determine the dominant variables from the investigated seven process variables. In this work a rapid injection of $\text{Ba}(\text{OH})_2 \cdot 8\text{H}_2\text{O}$ was employed. Chapter 4 and Chapter 5 employ identical design matrices and use a 2^{4-2} fractional factorial design with a center-point replicate analysis to investigate four process variables and the effect of ethylenediaminetetraacetic acid (EDTA) and barium hydroxide octahydrate ($\text{Ba}(\text{OH})_2 \cdot 8\text{H}_2\text{O}$) additions to the titanium gel, respectively. Also included in Chapter 5 is a three experiment series on BaTiO_3 seeding. Unlike the prior three chapters, Chapter 6 investigates the use of a noninjection system and a novel processing advantage which increases the yield of the hydrothermal reaction and decreases the observed particle size. The final section, Chapter 7, concludes the experiences of the work in a succinct manner while providing suggestions for future experimentation.

CHAPTER 2 LITERATURE REVIEW

2.1 Introduction

The following chapter illustrates the importance of the ferroelectric characteristics of barium titanate (BaTiO_3) and provides a synopsis of nucleation and growth theory as it pertains to solution synthesis. Alternative BaTiO_3 synthesis techniques are mentioned prior to the focus of the review, most notably hydrothermal synthesis and the influence of hydrothermal process variables. Once the pertinent variable effects have been discussed, an experimental design technique, fractional factorial designs, is offered which allows confident calculation of various treatment effects within a process window. Moreover, the technique also optimizes research cost and time in the arbitrary scientific endeavor. The review concludes with a brief overview of the employed powder characterization techniques.

2.2 Aspects of Barium Titanate

2.2.1 Crystallographic Origin of the Ferroelectric Response

The ferroelectric behavior of Rochelle salt was first discovered by Valasek in 1920 [Val20]. Valasek's discovery was thought to be one of "nature's great accidents" until the determination of other ferroelectric materials in the late 1930s by scientists in Zurich [Lin77]. A ferroelectric material exhibits the reorientable alignment of permanent electric dipoles when placed in an electric field [Kin76]. The origin of the polarizability is rooted in the asymmetric crystallographic nature of material and the ability of an atom

to shift or rattle within the unit cell. In contrast, centrosymmetric crystal structures cannot exhibit such an effect [Hea86].

Domains, regions of aligned dipoles, are randomly aligned in a poly-crystalline ferroelectric ceramic. When placed in a strong applied field, the domains align in the direction of the field. Upon removal of the field, some finite alignment remains (i.e., remnant polarization). An electric field of magnitude equal to the coercive field for the material must be applied in order to return the domains to an unpoled state [Kin76]. Similar polarization effects are observed when a field of opposite direction is applied and removed. This switching effect is responsible for the polarization hysteresis exhibited by ferroelectric materials. The ability to reversibly polarize and store charge permits the material's use as a capacitor to distribute finite amounts of charge in an electronic circuit. Moreover, the area of the hysteresis loop upon cycling is proportional to twice the energy (loss) required to align the domains. The loss and the dielectric constant (i.e., the normalized charge storing capacity) rank among the most important properties when considering a material for use in a capacitor application.

2.2.2 Ferroelectric Behavior of Barium Titanate

Barium titanate was the first ferroelectric perovskite material to be discovered and received a great amount of attention in the 1950s in an effort to replace mica, the capacitor material of the period [Lin77]. The perovskite structure of BaTiO_3 (shown in Figure 2.1) permits multiple positions for the octahedrally coordinated titanium atom as a function of the ambient temperature. Ideal BaTiO_3 undergoes three total transformations: rhombohedral to orthorhombic to tetragonal to the cubic phase at the transition temperatures -90°C , 5°C , and 120°C , respectively [Her85]. The most studied transition is the ferroelectric to paraelectric transformation (i.e., tetragonal to cubic). When Ti^{4+} is located at the center, the unit cell does not exhibit a permanent dipole. Hence, the high temperature, centro-symmetric cubic phase is termed paraelectric. In contrast, the

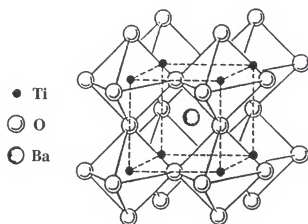
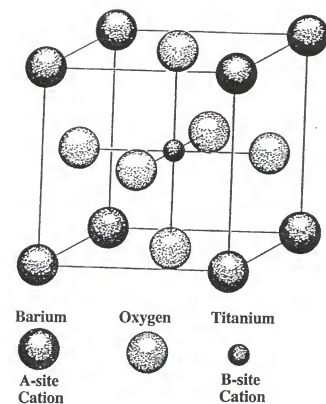


Figure 2.1. Schematic structures illustrating two different perspectives of the perovskite BaTiO_3 lattice [Jaf71, Lin77].

tetragonal phase is marked by a shift of the titanium atom toward one of the nearest neighbor oxygen atoms. The observed atomic shift is small, yet due to the high polarizability of the titanium ion, BaTiO_3 exhibits a high dielectric constant.

With increasing temperature from room temperature to 120°C , the dielectric constant rises dramatically (prior to rapid diminution at temperatures greater than 120°C). Electronic packages traverse a similar thermal path during heating on power up. Therefore, doped BaTiO_3 -based materials are employed in capacitor applications where a near temperature-independent dielectric performance is desired to enable reliable electronic circuit operation under varying temperature conditions. The synthesis of pure BaTiO_3 powders is industrially viable because dopants can be applied during postsynthesis coating procedures [Bru93, Ven98].

2.3 Solution Synthesis of Powders

Particle precipitation proceeds through multiple stages which vary in nature and kinetics as follows: (1) formation of solutes, (2) nucleation and growth of isolated primary particles, (3) aggregation of these primary particles, (4) ripening or aging to form a stable crystal [Fur85, Mer95, Nyv85, Rin96]. The above order may not be indicative of a process, nor is it mandatory that a specific stage occurs exclusively at any given time. The following sections address the driving force for precipitation and the advantages of precipitation techniques, and review the categories of keenest interest in the study of precipitation, i.e., nucleation and growth [Rin96, Soh92].

2.3.1 Precipitation from Solution

Precipitation from solution describes the formation of a desired solid from one or more species present in a liquid medium [Fur85]. Precipitation can occur only when the chemical potential of the solid is less than that of the dissolved species. When the

chemical potentials are equal, the solid and liquid are in equilibrium and the solution is deemed saturated. The concentration of the dissolved species under saturated conditions (C_0) defines the solubility of a substance. Precipitation may proceed when the concentration of the solution (C) exceeds the equilibrium concentration or solubility. The approximate driving force for precipitation is given by the difference in the actual and equilibrium concentration (ΔC) and is termed the supersaturation. Comparison of the precipitation processes of various material systems is accomplished by normalization of the concentrations by the supersaturation ratio ($S = C/C_0$). A saturated solution is described by a supersaturation ratio greater than unity.

The true driving force for precipitation is realized by the use of the activity rather than the concentration of a species. Under nonideal solution conditions, the chemical potential difference ($\Delta\mu$) describes the driving force for precipitation. The chemical potential is given by $\mu = \mu_0 + RT \ln a$, where μ_0 is the chemical potential of the standard state, a is the activity, R is the gas constant, and T is the temperature in degrees Kelvin. Thus, $\Delta\mu = RT \ln (a/a_0) = RT \ln S_a$, where S_a is the thermodynamic supersaturation ratio [Mer95].

2.3.2 Benefits and Limitations of Solution Precipitation

The advantages of solution precipitation techniques include the direct formation of high purity, homogeneous, crystalline products at low temperatures, and the relative control of the particle size, size distribution, and morphology [Ada98, Bru93, Rin96]. The solution based system also permits an increased rate of mass transport, a more intimate mixing [Dut94], and less particle growth and aggregation as caused by the high temperatures inherent to conventional solid state reactions [Bru93]. The small as-synthesized particle size eliminates the need for a cost-inefficient milling procedure and possible contamination via grinding.

The major disadvantage of solution techniques is the aggregation which occurs by capillary forces on removal of the supernatant during drying [Rin96]. However, aggregation may be avoided in wet-forming processes if employing a total aqueous processing (TAP) route [Ven98]. Thus, the as-synthesized powder suspension is never completely dewatered prior to the powder incorporation into the aqueous-based casting slurries. When complete removal of the solvent is required for dry forming methods or powder characterization, aggregation is reduced by the use of evacuated conditions.

A disadvantage typical of elevated temperature and pressure reactions is the inaccessibility of the reaction for *in situ* evaluation. This results in post-mortem product evaluation [Shi97] and/or studies at temperatures under 100°C in the case of the hydrothermal system [Eck96, Her88, Moo96]. Due to the rapid nucleation rates of BaTiO₃, observation of the nucleation and growth within measurable reaction times is possible only at temperatures < 100°C [Moo96]. The reported kinetic data offers formation mechanisms which are based on severely dissimilar conditions to that of the high temperature reactions. Most notable are the changes in the solubility of components and change in pH, both of which are significant in the evaluation of the predominant reaction species at increased temperature and pressure [Ada90, Len93, Oss88, Ven95].

Reactive precipitation processes, like that of hydrothermally derived BaTiO₃, involve the formation of a more insoluble product from multiple precursors. A process of this type often permits limited postnucleation control of the particle size and distribution due to rapid nucleation [Rin96]. First, the production of a diverse range of particle sizes or products is not likely by minor changes in the variables of a single process. Second, the rapid nucleation event may enable final product size consistency regardless of minor process variable fluctuations during the postnucleation stages of the hydrothermal run.

2.3.3 Nucleation

Speculation surrounds nucleation and growth processes due to the extremely complex observation of the inherent atomic-level dimensions of the process. Moreover, this scenario is further complicated by finite solid-solvent interactions and ordering in solution systems. Subsequently, a number of detailed texts describe both theoretical and empirical models [Isr92, Mer95, Nan66, Nyv85, Rin96, Soh92, Stu92]. The following sections attempt to succinctly describe the basic nucleation and growth concepts as well as those conditions pertinent to hydrothermal precipitation.

Under the present context, nucleation describes the original clustering of atoms from solution to form a stable phase from which growth occurs. The processes which induce nucleation are generally separated into one of two mechanisms: primary or secondary nucleation. Regardless of the nucleation mechanism, once the activation energy barrier to nucleation is overcome, rapid nucleation ensues in most systems. Primary nucleation indicates nucleation which occurs in the absence of growing crystals of the same composition and is further segmented into homogeneous and heterogeneous nucleation. Homogeneous nucleation describes the isolated combination of the solute molecules within the solvent, whereas heterogeneous nucleation occurs by attachment of the initial molecule cluster and growth from a foreign material surface [Rin96, Soh92]. Heterogeneous nucleation is observed in most real systems due to the lowering of the surface free energy by initiation on the reaction vessel walls, the surface of seed particles of the same or differing composition, or contaminant particles such as dust. However, hydrothermal systems entertain uniform solutions of aqueous complexes which can form precipitates in the absence of an initiating surface at elevated temperature and pressure conditions. Therefore, the term precipitation from homogeneous systems (PFHS) is sometimes inaccurately used to describe hydrothermal methods.

In contrast, the process which entails nuclei formation in the presence of suspended solute crystals of the same composition is termed secondary nucleation.

Secondary nucleation may be caused by several mechanisms of initiation, including contact, fracture, attrition, fluid shear, and needle breeding sources [Nyv85, Ran88a]. Of these sources, contact nucleation is most significant in mixed batch synthesis. Contact nucleation entails the contact of crystals with the agitator, pump, cooling coils, flow lines, or other crystals. Every contact involves finite fracture and usually attrition, however, the most significant effect is the displacement of the adsorbed solute layer which has not yet crystallized. Growth of the displaced clusters can occur at energy levels far less than those required for fracture or attrition, which are increasingly present in high velocity and high solids loading processes. The probability of crystal contact with other crystals increases with the time of circulation and increased solids loading, and is independent of crystal size. Also, the collision energy of a crystal is dependent on the mass of the crystal and the tip velocity of the stirrer [Ott72, Ott73]. Therefore, relatively small collision energies are expected within the hydrothermal system based on the employed low stirring rates and submicron product size. Secondary nucleation via contact in the BaTiO_3 hydrothermal system is not suspected to be dominant due to the observed small particle sizes, high nucleation rates, and near-monodispersed product.

Nucleation plays a substantial role in determining the final size of the precipitate when considering the batch reaction of a finite precursor stock. Generally, precipitation occurs from high supersaturation conditions which cause rapid nucleation rates. In turn, the rapid nucleation consumes a majority of the precursor stock, leaving little stock available for particle growth. The result is the formation of small crystals present in high concentrations of about 10^{11} to 10^{16} particles/cm³ [Soh92]. Therefore, control of nucleation and the subsequent final particle size is possible by control of the supersaturation level within a concentration region, bounded by the solubility of the precursor and the concentration at the maximum rate of nucleation [Nvy85]. The following sections discuss the importance of the concentration region and the nucleation rate, and review the prominent theories of nucleation.

2.3.3.1 Classical nucleation theory

Classical theory, also termed the thermodynamic theory, is based on the assignment of macroscopic properties, such as surface tension, to small atomic clusters. During homogeneous nucleation, an unstable critical cluster size, or embryo, is formed in the supersaturated solution [Nyv85]. Depending on the solution concentration, the embryo reversibly dissolves and grows, even if the solution is saturated. Once the minimum concentration (C^*_{\min}) necessary to overcome the activation energy of precipitation is achieved, irreversible growth of the embryo ensues. The assumption of surface tension to the nucleus allows the calculation of the energetics of formation based on the creation of a surface with respect to the creation of volume. The free energy of formation (ΔG_f) for a spherical nucleus with radius r can be given as:

$$\Delta G_f = \frac{4}{3}\pi r^3 \Delta G_v + 4\pi r^2 \gamma \quad [2.1]$$

where γ is the solid-liquid interfacial energy and ΔG_v is the volume free energy. The effective combination of the surface and volume terms is illustrated in Figure 2.2. The volume free energy is related to the supersaturation by the Gibbs-Kelvin equation as follows:

$$\Delta G_v = \frac{\Delta \mu}{V_m} = \frac{\rho}{M_w} RT \ln S_a \quad [2.2]$$

where ρ is the density of the solid, M_w is the molecular weight, and V_m is the molecular volume. Minimization of ΔG_f with respect to the radius permits calculation of the critical cluster size (r^*) as follows:

$$r^* = -\frac{2\gamma}{\Delta G_v} = -\frac{2\gamma V_m}{kT \ln S_a} \quad [2.3]$$

where k is the Boltzmann constant. Therefore, the free energy of formation for a critical size cluster is given by:

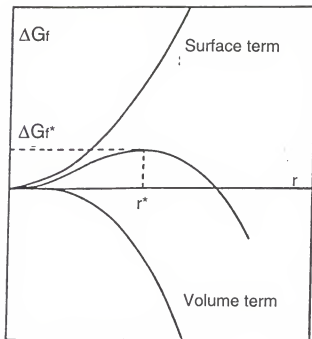


Figure 2.2. Free-energy change during homogeneous nucleation.

$$\Delta G_f^* = \frac{16\pi\gamma^3 V_m^2}{3(kT \ln S_a)^2} \quad [2.4]$$

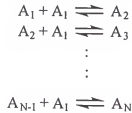
The rate of nucleation (J), assuming the rate of formation of the critical clusters transpires by a Boltzmann work function comparable to chemical reaction kinetics, is given as:

$$J = K \exp\left[-\frac{\Delta G_f^*}{kT}\right] = K \exp\left[-\frac{16\pi\gamma^3 V_m^3}{3k^3 T^3 (\ln S_a)^2}\right] \quad [2.5]$$

where K is a constant which relates the diffusional energy barrier and jump frequency. Equation 2.5 predicts that once a critical supersaturation is attained, an exponential nucleation burst occurs. The nucleation rate increases with increase of the supersaturation, increase of the temperature, and decrease of the solid-liquid surface energy.

2.3.3.2 Kinetic theory

The kinetic theory is based on molecular interactions, rather than the assumption of the macroscopic concepts to atomic clusters [Nyv85]. The kinetic model assumes the formation of a N-atom cluster by stepwise atomic or molecular collisions:



Upon attainment of N atoms, the critical size nuclei grows to a macroscopic size. A size less than N atoms results in dissolution. The dynamic equilibrium which exists between nucleation and growth can be given by the equations:



Assumption of a square-well interaction potential between a molecule and the dynamic cluster permits determination of the rate of dissociation of molecules from the cluster, radius of the critical cluster, and the rate of nucleation [Chi88a]. The net nucleation rate for the state of dynamic equilibrium is expressed by:

$$J = \frac{f(I)n(I)}{1 + \sum_{i=1}^I \prod_{j=1}^N \frac{b(j)}{f(j)}} \quad [2.6]$$

where $f(i)$ is the rate which a cluster containing I molecules grows to $I+1$ molecules, $b(i)$ is the rate which a cluster containing I molecules loses a molecule, $n(i)$ is the concentration of such a cluster, and I is a sufficiently large integer.

2.3.3.3 Validity of nucleation theories

Many scientists question the validity of the classical nucleation theory based on its implied assumptions [Nyv85]. These assumptions include:

- (a) Macroscopic thermodynamic values valid for clusters of several dozen particles or small species;
- (b) the concentrations of all the cluster sizes are constant during nucleation, i.e., time is not an included variable;
- (c) the principles of statistical mechanics can be neglected.

Various modified nucleation models have been formulated which address the objections to the classical theory. Nevertheless, predictions based on the classical theory resemble reality in most scenarios, where corrected models sometimes yield completely incorrect results [Nyv85]. The classical theory was concluded to be generally correct for homogeneous nucleation reactions, though too simplistic.

2.3.4 Growth

Crystal growth occurs by four general necessarily consecutive steps independent of the growth mechanism: transport of the solvated solute through solution, adsorption at the solid-solution interface, surface diffusion to energetically favorable sites such as a step or kink, and lastly, incorporation into the crystal lattice by chemical reaction [Mer95]. The slowest of the steps defines the rate limiting growth process. Regardless of the reaction limiting step, the solute must be desolvated prior to incorporation into the lattice. Description of the event is complicated by the different degrees of solvation exhibited by the solute in the solvated state. Thus, a variety of unit sizes, including atoms, ions, and molecules, may be present. Notably, the process of diffusion is highly dependent on the molecular size of the diffusing species.

Unlike the ease of modeling precipitation from the vapor phase, growth from solution is complex. Moreover, precipitation from solution is of great commercial significance to industry. Therefore, the literature has entertained significant discussion concerning theoretical modeling with respect to empirical observation [Nyv85]. The

basic concepts of growth and suggested theories are presented in the following sections. If one desires to measure growth rates, an explicit description of underlying assumptions is given in texts by Nyvlt and Ohara [Nvy85, Oha73].

2.3.4.1 Basic concepts of growth

An absorbed layer of solute exists on the surface of growing crystals and consists of partially ordered solute clusters [Ran88b]. The thickness of this layer varies with solution conditions such as the system composition, circulation rate, supersaturation, rate of diffusion through the layer, and solute integration to the crystal. In the presence of a layer of sufficient thickness, growth may be controlled by the diffusion of solute through this intermediate noncrystalline layer rather than bulk transportation. The two extreme growth cases are therefore termed mass transfer controlled and surface reaction controlled.

In the presence of a thick solute layer, the growth rate can be described by a mass transfer equation such as Fick's law. The mass flux density in the direction of the crystal surface due to the solute gradient is expressed by:

$$\frac{dM}{dt} = \frac{D}{\delta} A(C - C_0) \quad [2.7]$$

where t indicates time, D is the diffusion coefficient, δ is the diffusion boundary thickness, A is the surface area of the growing crystal, and $C - C_0$ is the supersaturation. The growth rate (G) also may be expressed as the change in length of a characteristic dimension (L) as shown by:

$$G = \frac{dL}{dt} = K_1(C - C_0) = K_1\Delta C \quad [2.8]$$

In nonagitated or static systems, diffusion is normally the rate controlling mechanism. Upon agitation, the growth rate increases with increasing agitation to a maximum value. Increased agitation above this point does not increase the growth rate.

Thus, at the maximum growth rate the surface reaction controls crystal growth. Intuitively, the surface reaction also is rate determining if the solute layer is thin.

Debate of growth model accuracy is rooted in the incorporation step. Most obvious when observing crystals of varying composition is the shape or habit of the crystals. Discussion revolves around the surface condition, whether pristine or exhibiting defects, and the surface energy and growth rate specific to crystallographic planes. Of the numerous theories, growth models can be separated into two major classifications: (1) those systems which deal with growth from a purely thermodynamic perspective based on the final crystal shape, and (2) theories which consider the kinetics of crystal growth such as the effect of concentration, temperature, and pressure on the final crystal shape as well as the growth rate. The following sections are devoted to the description of the solute incorporation process.

2.3.4.2 Morphological theory

During the original investigations of growth, the morphology of crystals was based merely on the surface energy of the distinct planes. One of the earliest models is the Gibbs-Wulff construction, which is based on the minimization of overall surface energy and assumes an equilibrium condition between the unimpeded solid and the mother phase, whether liquid or vapor [DeH93, Gib06, Nyv85, Wul01]. The Gibbs-Wulff equation of the equilibrium crystal shape is given by:

$$\frac{\gamma_j}{\lambda_j} = \text{constant} \quad [2.9]$$

where γ_j is the surface energy of the j th plane, and λ_j is the perpendicular distance from the centroid to the j th face and is termed the pedal function. If equilibrium is disturbed, the system will attempt to return to equilibrium by precipitation of species on those crystal faces which release the most energy. Hence, the high surface energy planes exhibit the highest linear rate of growth, largest distance from the centroid, and smallest

final surface area. It also is conceivable that a high energy surface which is adjacent to two low energy planes is consumed during reaction and is not observable in the final product.

Authors have shown that the Gibbs-Wulff construction and similar morphological based models [Don37, Har55, Har73, Har80, Kos27] are only representative of vapor-grown crystals. Dissimilar to growth in vapor, the solvent is not inert and unreactive with respect to the crystal [Giv91]. The solid-solvent interaction modifies the surface energetics and the crystal shape by the specific adsorption of ions, complexes, and organic ligands. Therefore, the solid-solvent interaction may create unanticipated results in the presence of impurities [Klu93] or allow morphological control in solution precipitation by the introduction of admixtures [Ada98, Bel97, Cho96a, Van90].

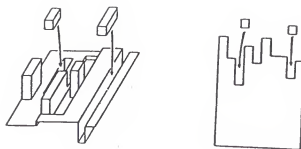
2.3.4.3 Continuous growth model

The continuous growth model is simplistic in its assumption of an atomically rough surface. Due to the rough surface, continuous growth occurs by surface assimilation at energetically favorable sites such as a kink shown in Figure 2.3(a). Under such assumptions, equation [2.8] adequately represents the growth rate.

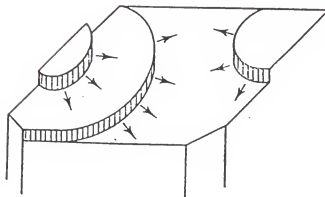
2.3.4.4 Two dimensional growth model

This model assumes an atomically smooth, defect-free surface where nucleation initiates in a two-dimensional manner. The solute adsorption on the surface is followed by transport via surface diffusion. A 2-D nucleus is formed when the number of solute species form a 2-D cluster of critical size. Growth transpires by the 2-D propagation of the newly formed steps by the adsorption of solute at the step edges, as shown in Figure 2.3(b). Thus, net growth occurs in a layering process. The rate limiting features of this model, however, differ as a function of particle size and supersaturation. For example, small crystals growing at low supersaturation require a relatively short time for one layer

(a)



(b)



(c)

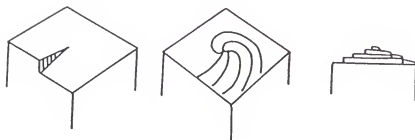


Figure 2.3. Growth models: (a) continuous, (b) two-dimensional, (c) screw dislocation or BCF [Boi88, Ran88b]. In illustration (b), the arrows indicate the direction of growth.

to propagate completely to the crystal edge in comparison to the time required for nucleation. This process is termed mononuclear growth and exhibits an infinite spreading velocity where growth is limited by nucleation. A large crystal at high supersaturation, i.e., polar conditions, requires more time for layer completion by growth than nucleation and exhibits a spreading velocity of approximately zero. Thus, a polynuclear mechanism occurs, whereby the surface is covered by multiple nuclei which grow until interconnecting with adjacent growing nuclei. A third model, the birth and spread model, is suggested to exhibit growth behavior between the two extremes of mononuclear growth and polynuclear growth. The birth and spread model is defined by a finite, constant spreading velocity which is assumed independent of the crystal size. The associated growth rate is given as:

$$G = K_2(S-1)^{2/3}[\ln S]^{1/6} \exp\left[-\frac{K_3}{T^2} \ln S\right] \quad [2.10]$$

where K_2 and K_3 are constants [Mye93]. The above equation, however, describes a noncontinuous process which assumes the preexistence of a growing step. The inability of the birth and spread model to explain crystal growth at very low supersaturation is based on the omission of bulk diffusion and surface reactions.

2.3.4.5 Screw dislocation theory (BCF theory)

Burton-Cabera-Frank (BCF) theory holds that surface terminated screw dislocations provide the initiator site for growth [Bur51]. Crystal growth occurs similar to the 2-D model in that surface diffusion follows species adsorption. However, the energy barrier for nucleation is lowered by species incorporation into the lattice at the step of the screw dislocation. After one incorporation iteration, the screw dislocation remains, but is now positioned one layer higher. The resultant spiral growth pattern is illustrated in Figure 2.3(c). Thus, the model presents a growth mechanism which does not rely on surface

nucleation under very low supersaturation conditions. The growth rate at the extremes of saturation are presented by the following equations:

$$G = K_4[(S-1)^2/S_c] \quad \text{Low supersaturation} \quad [2.11]$$

$$G = K_5(S-1) \quad \text{High supersaturation} \quad [2.12]$$

where K_4 , K_5 , and S_c are characteristic constants. Note the parabolic dependency of growth at low supersaturation and linear dependence at high supersaturation in the above equations. The assumptions of the model require that surface diffusion is the controlling step, i.e., rapid bulk diffusion is present, and only the solute incorporation at the step results in growth, i.e., the remainder of the surface is free of defects [Nyv85]. In summary, the growth rates predicted by BCF theory are quite consistent with experimental observations for systems limited by a surface diffusion mechanism [Nyv85].

2.3.4.6 Bulk diffusion theory

Unlike growth from the vapor phase where mass transfer occurs quite rapidly, bulk diffusion is not negligible in solution. Chernov modified the BCF theory to distinguish between the two systems by accounting for the bulk mass transfer limitations in solution [Che61, Nyv85]. Similar to BCF theory, the lattice incorporation is assumed to occur only at the face of the dislocation step. The model defines bulk diffusion through a solute layer of thickness δ as the controlling step in solution, yet maintains a parabolic relationship of the growth rate with supersaturation at very low supersaturations and linear relationship at high supersaturation. Moreover, the importance of hydrodynamic conditions and stirring rate are included in the crystal growth process. The growth rates for low supersaturation and high supersaturation in the simplified versions are given as follows:

$$G = K_6(S-1)^2 \quad [2.13]$$

$$G = K_7(S-1) - K_8 \quad [2.14]$$

where K_6 , K_7 , and K_8 are characteristic constants.

2.3.4.7 Surface reaction theory

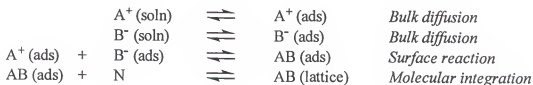
When dealing with less soluble precursors, surface reactions may describe the rate limiting step, as compared to the nucleation, surface diffusion, or bulk diffusion limited growth theories discussed above. Neilson and colleagues [Est93, Nei83] described the kinetics of insoluble salt reactions via the equation:

$$G = K_9(S-1)^q \quad [2.15]$$

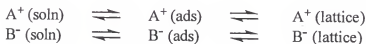
where K_9 is a constant and q is the growth order rate. Empirical studies of insoluble salt reactions such as BaSO_4 , CaCO_3 , and $\text{CaC}_2\text{O}_4 \cdot \text{H}_2\text{O}$ have shown the growth rate to exhibit a parabolic dependence (i.e., $q = 2$).

Chiang and Donohue treated the surface sites of ionic crystals as reactant species which react with adsorbed ions (rather than molecules) [Chi88b, Chi88c]. By consideration of the interaction between the electrical double layer and reacting ionic species, a second order dependence was derived for the growth rate of ionic crystals. The two most viable models, the surface reaction/molecular integration (Mechanism I) and sequential ionic integration (Mechanism II), are given for the reaction of an ionic crystal AB as follows:

Mechanism I



Mechanism II

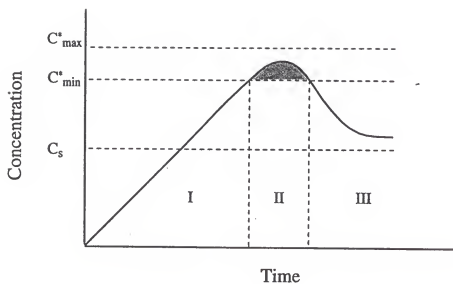


where A^+ (soln) and A^+ (ads) denote the cation in solution and the ion adsorbed on the surface, respectively, and N represents the number of lattice growth sites. The anion interactions are similarly described by the letter B .

2.3.5 Physical Growth Mechanism for Monodisperse Particle Formation

Barring secondary nucleation and aggregation, a dispersion in particle size is observed in most precipitated powders. This is attributed to the simultaneous occurrence of nucleation and growth and the finite times associated with the precipitation process. LaMer and Dinegar proposed a nucleation and growth model, the best example of which is the production of monodisperse sulfur sols by the decomposition of sodium thiosulfate [LaM50]. As demonstrated in Figure 2.4(a), if the solution concentration (C) is greater than the equilibrium concentration (C_s), embryos may reversibly grow or dissolve into the solution. However, once the minimum concentration (C^*_{\min}) necessary to overcome the activation energy of precipitation is achieved, irreversible growth of the embryo ensues. Thus, nucleation and growth occur simultaneously when the solution concentration is greater than C^*_{\min} . As the reaction proceeds, the depression of the solution concentration below C^*_{\min} results in the exclusive growth of particles. Figure 2.5 illustrates the marked increase of the nucleation rate (N) with increasing supersaturation at high supersaturations, whereas the growth rate (G) varies uniformly with increasing supersaturation [Nyv85]. Exploitation of this relationship means that a narrow particle size distribution (PSD) can be produced by rapid nucleation in a highly supersaturated environment, followed by growth, as exemplified by curve 1 in Figure 2.4(b). The net effect is a decrease in the mean particle size (L) with increase of the supersaturation (Figure 2.5).

(a)



(b)

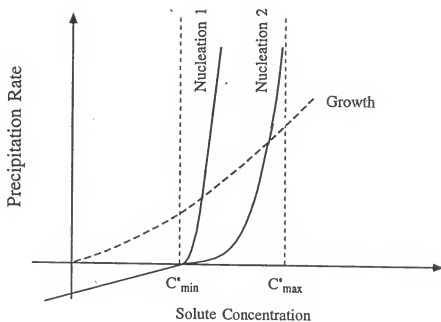


Figure 2.4. LaMer and Dinegar model for monodisperse particle formation: (a) concentration of solute with respect to reaction time, and (b) dependence of precipitation rate on nucleation and growth as a function of the solute concentration [LaM50].

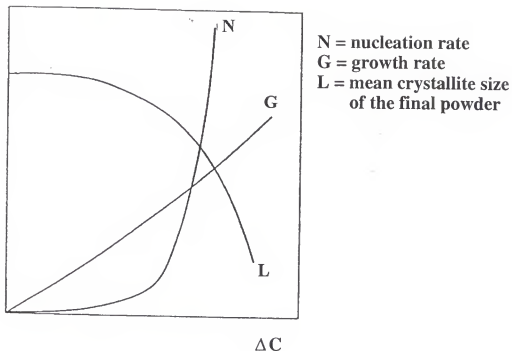


Figure 2.5. Dependence of the nucleation rate, growth rate, and mean crystal size on the supersaturation determined by a mass balance [Nyv85].

2.3.5.1 Monomer addition model

The monomer addition model was originally created for the formation of monodisperse silica particles via the Stöber process [Mat88, Stö68]. Initially, the reaction of two monomers forms nuclei. As time increases, the reaction rate of the monomer is less than the rate of monomer addition to the particles, and the monomer reaction exclusively contributes to particle growth. The affinity for monomer adsorption to the surface of growing particles rather than the formation of additional nuclei is controlled by the competing nucleation and condensation rates of the silicon alkoxide. Therefore, the particle size dispersion and final particle size can be controlled by the rate and duration of monomer addition.

2.3.5.2 Aggregative growth

The aggregative model differs from the LaMer and Dinegar model and monomer addition models since the nucleation event describes the formation of unstable primary particles. Colloidal stabilization occurs similarly to the mechanism of polymer particle growth proposed by Flory-Stockmayer theory [Bog91, Flo53]. The rapid aggregation of the unstable, small primary particles can occur by collisions due to Brownian motion or shear induced collisions [Rin96]. Two criteria must be met to form a monodisperse distribution within the aggregate model framework: (1) slow production of unstable nuclei during the entire process, and (2) the rate of aggregation must be greater than the rate of nucleation of primary particles, i.e., insufficient time for the growth of primary particles. The aggregation rate was first developed by von Smoluchowski [Smo17] and a complex differential equation was elaborated by Ring [Rin96]. Quantifiable models are founded on the assumptions of aggregation by collisions mechanisms caused by shear or Brownian motion and are based the use of a continuous or batch reactor.

2.3.6 Effect of Crystal Size on Solubility

The above nucleation and growth theories describe the respective processes with regard to a constant particle size. This is not a constraint in real systems, and a finite dispersion in growth rates may be exhibited. Also important to the discussion of nucleation and growth is the Gibbs-Thomson equation (or Ostwald-Freundlich equation if reading the German literature) which was originally derived for vapor-liquid equilibrium [Soh92] as follows:

$$\ln \frac{p(r)}{p(\infty)} = \frac{2\sigma_p V_m}{RT_r} \quad [2.16]$$

where $p(r)$ is the vapor pressure over the liquid droplet of radius r , $p(\infty)$ is the vapor pressure over a flat liquid surface, V_m is the molar volume, and σ_p is the specific surface work. In brief, the vapor pressure increases with decreased size of the droplet. However,

the above equation neglects interactions between the precursor and product phases and is not valid for precipitation from solution. A modified version which accounts for solid-liquid interactions was first described by Ostwald [Ost97] and later modified by Enüstün and Turkevich [Enü60] and Couchman and Jesser [Cou73]. The latter modified version is given as:

$$\ln \frac{a(r)}{a(\infty)} = \frac{2k_a f V_m}{3k_v v R T_r} \quad [2.17]$$

where $a(r)$ and $a(\infty)$ give the activity of the substance in equilibrium with crystals of size r and with infinitely large crystals, respectively, f is the surface stress, and v is the total number of ions into which a molecule dissociates. Similar to the liquid-vapor system, the equilibrium solubility of a substance increases with decreasing crystal size. Hence, the general growth of large solid particles at the expense of smaller particles is often called Ostwald ripening.

2.4 Hydrothermal Synthesis of Barium Titanate

2.4.1 History and Application in Thin Layer MLCs

A multitude of synthesis routes have been employed to produce BaTiO_3 powders through the decades. Some of the techniques include the conventional calcination of $\text{BaCO}_3(\text{s})$ and $\text{TiO}_2(\text{s})$ [Alc91, Bea83, Fer91], the thermal decomposition of Ba-Ti oxalates [Cla56, Kis66, Sto93], citrates [Hen78, Mul70], alkoxide salts [Bru93, Kir88, Maz72, Oza83, Suy94], and peroxide gels [Alc91, Shi97], and preparation by the sol-gel method [Kas87a, Kas87b, Suw78, Xu92]. Hydrothermal synthesis routes have employed the direct use of hydroxide salts [Her88, Kum96, Moo96], halide salts [Dut94, Her95a], acetate salts and gels [Dut94, Fla55, Hen91, Kut84, Shv79], and nitrate salts [Dut94]. The titanium precursor of the hydrothermal method generally consists of either hydrated oxide gels [Kum96, Kum95, Moo96, Shi97, Viv87, Viv89, Wad95, Wad96], anatase [Eck96, Her88, Moo96, Xia96], rutile [Kum95, Kum96], or titanium dioxide soot

[Dog97, Xia96]. The above list of authors is far from comprehensive, yet illustrates the extent of BaTiO_3 synthesis investigations in addition to the author's use of barium hydroxide octahydrate and hydrated titanium oxide gel precursors.

Hydrothermal synthesis is defined as the treatment of ceramic precursors in an aqueous environment at elevated temperature and pressure [Seg89], and was employed to synthesize BaTiO_3 for pigment applications as early 1940 [Pet40]. Research has shown the technique to be superior to other powder formation techniques due to the ability to directly produce crystalline, agglomerate-free, high purity, compositionally uniform, equiaxed powders in a relatively benign environment at low temperatures (i.e., $\leq 200^\circ\text{C}$) [Eck96, Hea88, Kum96, Ven98]. In addition, hydrothermal powders are highly reactive when sintering [Abe87, Daw91]. The subsequent reduction of the sintering temperature allows a less noble electrode composition in cofired multilayer capacitors (MLCs). This is significant since the current metallization systems account for approximately 90% of the materials cost and 35% of the total cost of an MLC [Phu90].

The drive toward miniaturized electronic components and an increase in the volumetric efficiency (i.e., capacitance/volume) of MLCs has created a demand for MLCs with $< 5 \mu\text{m}$ fired dielectric layers. Thin dielectric layers are desirable due the achieved increase in capacitance, C , in the MLC configuration and volumetric efficiency as shown in [2.18] and [2.19] respectively, and is defined by the number of dielectric layers n , dielectric layer thickness t , dielectric constant K , permittivity of free space ϵ_0 , and electrode area A .

$$C = nKA\epsilon_0/t \quad [2.18]$$

$$\frac{C}{V} = \frac{(nK\epsilon_0 A/t)}{n\Delta t} \propto \frac{K}{t^2} \quad [2.19]$$

Fired dielectric layers with a thickness of several microns require submicron powders. If the size of the particles within the dielectric slurry approaches the magnitude of dielectric layer thickness, the voids inherent to the randomly packed wet cast layers will be

sufficiently large to cause shorting and MLC failure. For example, adequately dispersed suspensions of crystalline, as-synthesized, hydrothermally derived 125 nm mean diameter particles accommodate the direct production of fired 3.0 μm dielectric layers, as shown in the MLC in Figure 2.6 [Bee97, Ven98].

Coprecipitated powders can produce particles of similar size, but require an additional pyrolysis step at elevated temperatures to produce a crystalline product. Additionally, the particles may require milling to achieve the submicron size. Milling, like the crystallization step, is energy intensive, as well as technically difficult, and poses contamination problems [Daw88]. Though less expensive in comparison to solution synthesis methods, conventional calcined powders obtain inherent milling difficulties similar to the coprecipitation system. The solid state reaction also cannot provide the intimate mixing, chemical homogeneity, and product purity gained by the hydrothermal reaction. In addition, a nonspherical, jagged morphology is produced by the calcination process.

A summary of the most recent aqueous low temperature and hydrothermal BaTiO_3 synthesis research is shown in Table 2.1. Only Her [Her95a] and Menashi [Men89a, Men89b] employ an injection system, i.e., most authors simultaneously introduce all of the precursors to the autoclave at room temperature and then ramp to the desired reaction temperature. The injection is performed in an effort to create a rapid nucleation event and thus a near monodispersed particle size distribution. Notably, the coprecipitation system of Her and Matijevic employed barium and titanium chloride salt precursors [Her95a]. To the knowledge of the author, experimental designs have not been used to quantify the effect of process variables in either the injection or noninjection systems to hydrothermally synthesize ceramic powders.

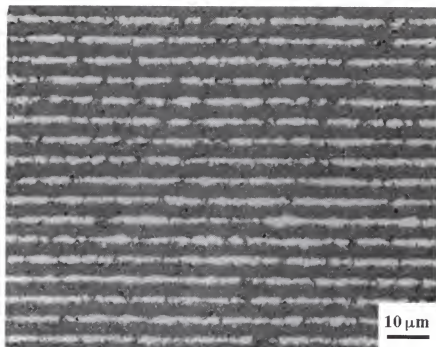


Figure 2.6. Scanning electron micrograph of the alternating 3.0 μm dielectric (dark) and electrode (light) layers of a cofired MLC produced from 125 nm CPM powders [Ven98].

Table 2.1. Recent literature for the aqueous synthesis of BaTiO_3 powders at elevated temperatures from various titanium precursors, precursor molar ratios, product loading, agitation rates, and $\text{Ba}(\text{OH})_2 \cdot 8\text{H}_2\text{O}$ introduction techniques.

Reference	Precursors	Precursor Ba/Ti	Agitation Rate	Reaction Temperature	Time at Reaction Temp.	Wash Condition	Particle Size (nm)
Abe91	$\text{Ba}(\text{OH})_2$; TiGel ⁱⁱ	1.5	stirred	200°C	5h	Acetic acid in H_2O , then H_2O	50-200
Chi95	$\text{Ba}(\text{OH})_2$; anatase	not given	not given	90°C	48h	CO_2 -free H_2O	100-200
Dog97	$\text{Ba}(\text{OH})_2$; TiO_2 soot	1.5	static	95°C	48h	H_2O	60
Dut94	Ba salts (Cl, I, Br, NO_3 , $\text{C}_2\text{H}_3\text{O}_2$, OH); Ti-gel from isopropoxide, anatase	1.0;1.6	static (agitated every 6 h)	90°C, 240°C	48h @90°C; 7days @ 240°C	Deionized H_2O	150-370
Eck96	$\text{Ba}(\text{OH})_2$; anatase	1.0	static	90°C	72 h	Formic acid in H_2O while hot	150-200
Her88	$\text{Ba}(\text{OH})_2$; anatase with 10-15% rutile	not given	static	70-103°C	24-72 h	Distilled H_2O	25-200 ⁱⁱⁱ
Her95a	BaCl_2 ; TiCl_4 with 6M NaOH or KOH	1.0-1.11	500 rpm	85°C in air	10 min	Deionized H_2O	Continuous = 220; Batch = 80
Kle89	$\text{Ba}(\text{OH})_2$; TiGel	2.0	stirred	70°-95°C	91h	1 M acetic, Hot deionized H_2O , ethanol	86
Kum95	$\text{Ba}(\text{OH})_2$; TiGel, rutile ^{iv}	2	300rpm	150-300°C	8 h	Distilled H_2O	30-110 gel; 200-700 rutile
Kum96	$\text{Ba}(\text{OH})_2$; TiGel, rutile ^{iv}	1-4	300rpm	150-300°C	8 h	Deionized H_2O	40-200 gel; 0.7-1.4 μm rutile
Mil90	$\text{Ba}(\text{OH})_2$; Ti-isopropoxide	1.0	static	90-225°C	>5 hours	Not washed	70 platelets; 200 aggregates with EDTA
Moo96	$\text{Ba}(\text{OH})_2$; TiGel, anatase	1.1	stirred	40-90°C	>100 min @ 75°C	$\text{NH}_4(\text{OH})$ in H_2O	Kinetic study; Not determined
Pfa91	$\text{Ba}(\text{OH})_2$; TiGel, anatase, rutile	1.25	stirred	60-90°C	≥ 24 h	H_2O	20-260 ⁱⁱⁱ
Shi97	$\text{Ba}(\text{OH})_2$; TiGel, tetrabutyl titanate, Ba-Ti peroxide gel, TiO_2 ^{iv}	1-3	static	75-400°C	4-72 h	Distilled H_2O and ethanol	80-500
Viv87	$\text{Ba}(\text{OH})_2$; TiGel	1	not given	$\geq 85^\circ\text{C}$	2-6 h	Dilute acetic in H_2O	200-500; 20-200 with PVA
Viv89	$\text{Ba}(\text{OH})_2$; TiGel	1	stirred	130-180°C	2-6 h	Hot H_2O	70-95
Wad95	$\text{Ba}(\text{OH})_2$; TiGel	2 to 40	stirred	50-150°C	4 h	H_2O with acetic acid	20-90
Wad96	$\text{Ba}(\text{OH})_2$; TiGel	2	stirred	150°C	4 h	H_2O with acetic acid	90
Xia96	$\text{Ba}(\text{OH})_2$; anatase with 10-15% rutile, TiGel, tetrabutyl titanate ^{iv}	1	static	75-400°C	8 h; various	H_2O with acetic acid	80-200

ⁱ $\text{Ba}(\text{OH})_2$ = hydrated $\text{Ba}(\text{OH})_2$; usually $\text{Ba}(\text{OH})_2 \cdot 8\text{H}_2\text{O}$

ⁱⁱ TiGel = amorphous hydrated titanium oxide gel, $\text{TiO}_x(\text{OH})_y$

ⁱⁱⁱ Estimated from specific surface area of BaTiO_3 powder

^{iv} $\text{TiO}_2(\text{OH})_2$ gel exhibited smallest particle size of investigated titanium precursors

^v $\text{Ba}(\text{OH})_2 \cdot 8\text{H}_2\text{O}$ aqueous solution injected into reactor

Evidenced by Table 2.1, the hydrothermal technique generally produces 20-200 nm particles. Several factors have been noted to affect the size: the titanium precursor [Kum95, Kum96, Shi97, Xia96], precursor Ba/Ti [Abe91, Kum96, Wad95], $\text{Ba}(\text{OH})_2 \cdot 8\text{H}_2\text{O}$ concentration [Her88], basicity [Sla96, Xia96], and reaction temperature [Shi97]. In conflict, Wada et al. report the particle size to be independent of the reaction temperature from 70-150°C [Wad95]. When using a $\text{Ba}(\text{OH})_2 \cdot \text{H}_2\text{O}$ precursor, amorphous hydrous titanium oxide gels produced the smallest particle sizes [Kum95, Kum96, Shi97, Xia96] and exhibit an increased reactivity with respect to crystalline TiO_2 precursors such as anatase and rutile [Kut88a, Pfa91]. Several authors noted the use of fresh gels due to an aging affect [Moo96, Shi97, Xia96]. The importance of the precursor Ba/Ti ratio, basicity, and barium hydroxide concentration will be discussed in Chapter 6.

Significant research efforts have been exerted in the examination of low temperature synthesis techniques (<150°C). However, the decreased reaction temperatures result in decreased kinetics and subsequent lengthy reaction times, which may range from 4 hours to several days depending on the reaction temperature. Such rates severely lessen the interest in low temperature reactions when considering industrial reactor throughput.

The obstacles in the investigation of hydrothermal BaTiO_3 synthesis include the inaccessibility of the reaction and the rapid kinetics of the reaction precipitation process. The closed nature of the system does not allow *in situ* determination of pH and limits sampling techniques. Specifically, the rapid nucleation and growth of BaTiO_3 at typical reaction temperatures requires the use of reduced temperatures and isothermal conditions to investigate particle formation mechanisms [Eck96, Her88, Moo96]. Therefore, the predicted mechanisms may be invalid when considering reactions at elevated temperatures. In addition to the modified reaction temperatures, multiple sampling efforts within one batch alter the reactant and product concentrations. The low temperature investigations allow determination of the incipient nucleation temperature,

thus provide the variable level regime for the injection temperature. Process mimicking experimentation, as provided by experimental design, combined with an understanding of the incipient nucleation temperature allows insight to process control within a window of multiple process variables while simulating exact hydrothermal synthesis conditions.

2.4.2 Solubility

In performing hydrothermal synthesis, the judicious selection of precursor materials is the first step necessary to provide the most economical process route, ensure the production of high quality powders, and enable process control. Knowledge of the solution chemistry of the titanium and barium precursors facilitates modification of the particle size and morphology during precipitation. However, both the dynamic solution interactions and closed nature of the system hinder absolute interpretation of the process. The following sections illustrate the importance of appreciation for the constituent solubility during precursor handling, powder synthesis, and postsynthesis processing.

2.4.2.1 Titanium precursor solubility

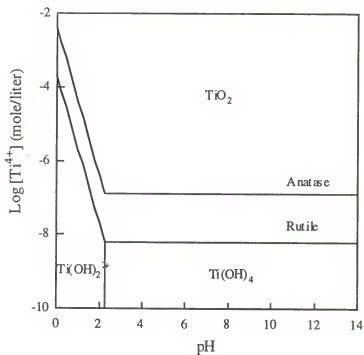
The elevated reactivity of the $\text{TiO}_x(\text{OH})_y$ gel in comparison to the crystalline oxides, anatase and rutile [Kut88a, Pfa91], is attributed to both the increased surface area and solubility. The effect of the surface area is two-fold. First, a high surface area indicates a greater number of reaction sites. Second, the inherently small colloidal sizes (and thus increased radii of curvature) of the high surface area gels cause an increase in the solubility by the previously discussed Gibbs-Thomson equation. The dissolution of the oxides in a dissolution and recrystallization reaction (to be discussed below) requires breaking of the Ti-O bonds by hydrolytic attack [Eck96]. Thus, an increase in the reactivity is also attributed to the preexisting hydroxylation of the $\text{TiO}_x(\text{OH})_y$ gel. Unless more expensive organometallic compounds are employed as in a sol-gel reaction, it is

believed that the titanium hydrated gels will allow the most cost effective synthesis for crystalline, equiaxed particles with diameters ≤ 100 nm.

Of the two precursors, $\text{Ba}(\text{OH})_2 \cdot 8\text{H}_2\text{O}$ and $\text{TiO}_x(\text{OH})_y$ gel, the gel is noted as markedly less soluble due to the high field strength of the titanium ion. Some controversy has been noted concerning the aqueous speciation of titanium at high pH. Pourbaix [Pou74] suggests the formation of $\text{HTiO}_3^-(\text{aq})$ and an increase in the solubility of titanium under alkaline conditions at room temperature. This suggestion is in disagreement with the experimentally observed stable species in aqueous solution at room temperature, $\text{Ti}(\text{OH})_4(\text{aq})$ [Lee81]. Lee's potential-pH diagrams (based on Pourbaix's approach) also do not incorporate the $\text{Ti}(\text{OH})_4(\text{aq})$ species due to a host of reasons, including a lack of thermodynamic data. However, without consideration of the tetrahydroxylated species, Lee notes the marked decrease in the stability of titanium dioxides with increasing temperature in alkaline solutions [Lee81].

In agreement with empirical observations, calculations based on the Baes and Mesmer [Bae76] cation hydrolysis approach suggest $\text{Ti}(\text{OH})_4(\text{aq})$ to be the dominant solution species over a wide pH range. Regardless of the crystal structure of the titanium dioxide, such titanium-water stability diagrams, Figure 2.7, illustrate that the solubility of the titanium compound is independent of the solution pH above pH 4 [Cho96b, Eck96, Moo96]. This finding is in contrast to most ceramic oxides, which exhibit an increase in solubility under both extremely acidic and alkaline conditions. The anomaly may be attributed to the lack of experimental data above pH 9 when the original work of Baes and Mesmer was performed. Chapter 6 discusses the possibility of a predominant pentacoordinated, $\text{Ti}(\text{OH})_5^-(\text{aq})$, species similar to that observed for Zr and Hf [Bae76]. Several authors also propose the existence of another polycordinated species, $\text{Ti}(\text{OH})_6^{2-}(\text{aq})$, by the nucleophilic attack of $\text{Ti}(\text{OR})_4$ under highly alkaline conditions [Cha90, Fla55, Kis66, Yos89]. However, Phule and Risbud report that experimental evidence of the hexacoordinated species does not exist [Phu90].

(a)



(b)

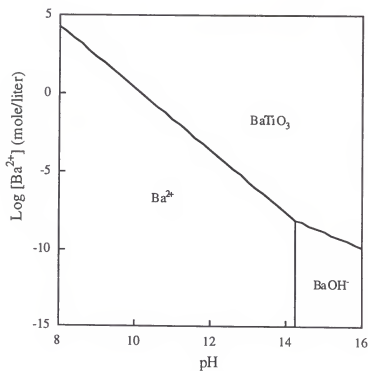


Figure 2.7. Stability diagrams for the (a) titanium dioxide precursor and (b) BaTiO_3 product in the absence of CO_2 contamination at 25°C and is based on the ideal solution approximation [Moo96].

2.4.2.2 Barium precursor solubility

$\text{Ba}(\text{OH})_2 \cdot 8\text{H}_2\text{O}$ is economical, soluble, and increases the reaction solution pH, eliminating the need for additional mineralizers such as sodium hydroxide. The increase in the solubility of $\text{Ba}(\text{OH})_2 \cdot 8\text{H}_2\text{O}$ with increasing temperature is given in Table 2.2 [Kir78]. In the absence of water, $\text{Ba}(\text{OH})_2 \cdot 8\text{H}_2\text{O}$ melts in its own water of

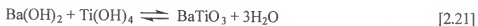
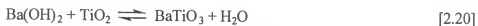
Table 2.2. $\text{Ba}(\text{OH})_2 \cdot 8\text{H}_2\text{O}$ aqueous solubility with respect to temperature [Kir78].

Temperature (°C)	0	20	40	50	60	80
Solubility (M)	0.1	0.2	0.4	0.6	1.0	6.0

crystallization at 78°C [Ovr79] and becomes nearly infinitely soluble when in aqueous solutions at temperatures above 100°C [Wad95]. As shown by Venigalla [Ven95] and the Opal© software version 1.93x, the solution species in an aqueous environment is either $\text{Ba}^{2+}(\text{aq})$ or $\text{Ba}(\text{OH})^+(\text{aq})$. With increasing temperature, the thermodynamic predominance domain of $\text{Ba}(\text{OH})^+(\text{aq})$ increases from solution conditions $\geq \text{pH } 13.5$ at 25°C to $\geq \text{pH } 11.5$ at 100°C. The solution pH of the supernatant of all forty completed reactions varied between pH 12.0 and pH 13.5, which suggests the presence of $\text{Ba}(\text{OH})^+(\text{aq})$ at elevated temperatures.

2.4.2.3 Formation mechanisms based on soluble precursors

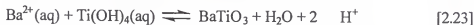
Most researchers propose generic hydrothermal equations for the reaction of barium hydroxide with titanium dioxides and hydrated gels such as [2.20] and [2.21], respectively.



This notation avoids the assignment of a formation mechanism and speculation on the reactant species. Two particle formation mechanisms, *in situ* transformation and

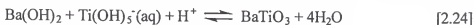
dissolution-recrystallization, have been suggested for the BaTiO₃ hydrothermal system [Den90, Eck96]. As shown in Figure 2.8, *in situ* transformation in the BaTiO₃ system requires the diffusion of the barium species through the freshly formed BaTiO₃ product layer. The dissolution and recrystallization mechanism, as the name suggests, entails the dissolution and recombination of species from solution. Notably, extremely alkaline aqueous conditions are thermodynamically required for BaTiO₃ formation [Ada90, Len93]. Comparison of experimental results of the anatase [Her88, Moo96] and gel reactions [Kum96, Moo96, Wad95] with Ba(OH)₂·8H₂O is provided in Chapter 6, where a dissolution and recrystallization mechanism is proposed under highly alkaline conditions. Quite possibly, the species BaOH⁺(aq) and Ti(OH)₅⁻(aq) or Ti(OH)₄⁰(aq) are involved, and the solubility of Ti is not nearly as low as conventionally proposed under high pH conditions [Bae76].

Assuming a dissolution and recrystallization mechanism and the reaction of Ti(OH)₄(aq), possible reactions (without considering possible intermediate reactions) may be given by:



where the solution pH decreases with increasing time of reaction in both reactions.

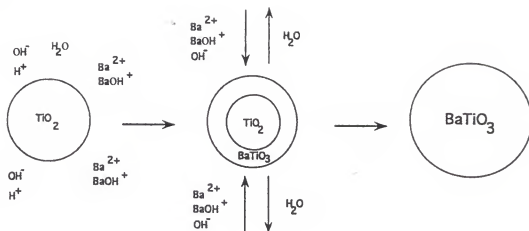
Assuming the existence of the pentacoordinate Ti complex, the following reactions may describe the generic and solution-based formation reactions [2.24], [2.25], and [2.26]:



2.4.2.4 BaTiO₃ solubility

The incongruent dissolution of BaTiO₃ has been documented by both experimental analysis [Cho96b, Ute90] and theoretical calculation [Ada90, Len93] as

(a)



(b)

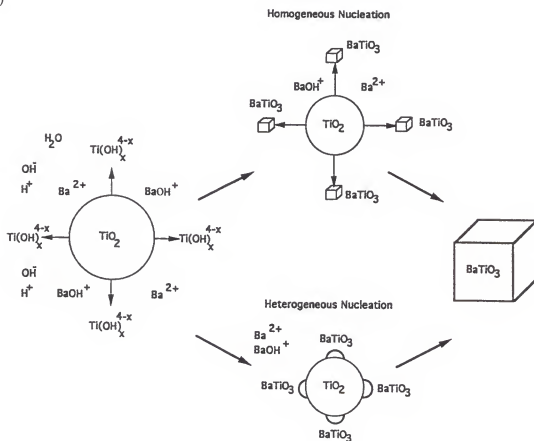


Figure 2.8. Formation mechanisms proposed for the hydrothermal synthesis of BaTiO_3 powders include (a) *in situ* transformation and (b) dissolution and recrystallization by either homogeneous or heterogeneous nucleation [Eck96].

illustrated in Figure 2.7b and Figure 2.9 in the absence and presence of carbon dioxide, respectively. In acidic to moderately alkaline solutions (i.e., solution pH approximately \leq pH 9), barium ions are depleted from the surface, leaving behind a barium-depleted zone or titanium-rich layer. Barium depletion from titanate-based powders is further enhanced when working with the hydrothermally-derived submicron powder sizes as witnessed by the modified Gibbs-Thomson equation. Therefore, solution processing conditions, such as powder washing and solvent addition in aqueous based forming techniques, must be controlled if a stoichiometric product is desired. As shown by Chodelka, stoichiometric stability versus pH over a moderate range may be optimized through the addition of a passivation layer [Cho96b].

Based on thermodynamic calculations BaTiO_3 is very insoluble under extremely alkaline conditions (i.e., \geq pH 13) under the employed reaction conditions [Ada90, Len93]. This is experimentally supported by the rapid nucleation rates as the temperature approaches 100°C and the onset of nucleation at temperatures as low as $50\text{--}60^\circ\text{C}$ [Moo96]. In addition, once completely crystalline, the insoluble BaTiO_3 particles do not exhibit coarsening during increased times at high temperatures [Hen91, Wad95].

2.4.3 Required Processing Conditions

2.4.3.1 CO_2 -free environment

Processing reactive submicron, advanced ceramic materials for electronic components requires additional precautions to ensure a homogenous, electronically useful product. Several processing conditions are crucial if a high purity BaTiO_3 powder is desired. The high stability of BaCO_3 in a moderate-alkaline solution pH at low temperatures [Ada90, Len93] indicates that a CO_2 -free synthesis and postsynthesis atmosphere must be maintained [Cha90]. The contamination process is further enhanced by the increased solubility of the submicron powders and increased surface area available

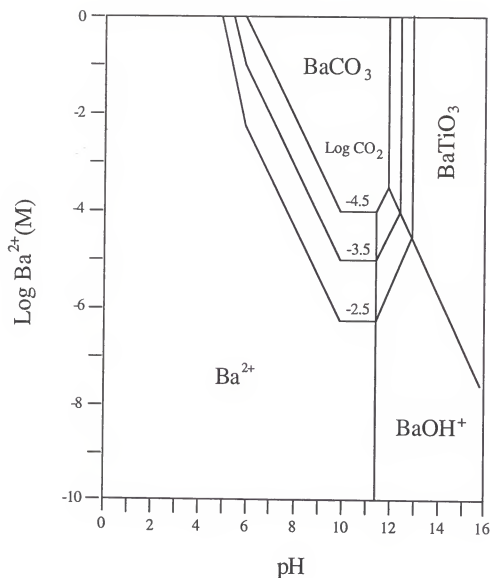


Figure 2.9. Theoretical phase stability diagram for the Ba-Ti-CO₂-H₂O system illustrates that alkaline conditions are required for the synthesis of phase pure BaTiO₃ as a function of atmospheric CO₂ at 25°C and 1 atm [Ada90, Ute90].

for reaction. High purity BaTiO_3 is most easily maintained by using CO_2 -free water as the reaction medium [Bru93, Her88, Wad95] and purging the autoclave with nitrogen prior to synthesis [Dut94, Moo96]. Unlike sealed industrial processes, centrifugation and decantation on the laboratory scale involves the inevitable exposure of the barium-laden mother liquor to the atmosphere during powder washing. After washed and dried, the powder must remain sealed since exposure to atmospheric CO_2 and humidity causes barium dissolution from the particle surface. Subsequently, the high pH caused by the dissolution process promotes the crystallization of barium carbonate [Suy94].

2.4.3.2 An excess precursor Ba/Ti ratio

Due to the finite solubility of the barium ion [Ada90, Len93], the production of stoichiometric BaTiO_3 is possible only when the precursor $\text{Ba/Ti} > 1$. In the event that a slightly deficient Ba/Ti is employed, the excess titanium gel is transformed to anatase during the hydrothermal treatment [Che95, Kut88b, Moo96]. In extremely low Ba/Ti (i.e., $\text{Ba/Ti} \leq 0.25$), $\text{BaTi}_5\text{O}_{11}$ or a combination of $\text{BaTi}_5\text{O}_{11}$ and anatase are formed [Kut88b]. On heating to temperatures $> 1200^\circ\text{C}$ in air, the $\text{BaTi}_5\text{O}_{11}$ decomposes to BaTi_4O_9 and rutile. In contrast, a large Ba/Ti results in additional barium in solution which may precipitate as $\text{Ba}(\text{OH})_2 \cdot 8\text{H}_2\text{O}$ on cooling to room temperature. Barium hydroxide can be avoided by the use of a precursor ratio near unity or a hot ammoniated water wash. Excessively high Ba/Ti ratios (often in conjunction with high reaction temperatures) have been noted by some authors to produce the stable tetragonal phase [Dut94, Kaj91, Shi97] rather than the metastable cubic phase typically observed from hydrothermal products with a precursor ratio near unity. In summary, BaTiO_3 is thermodynamically favored over differently ordered Ba-Ti-O compounds in a wide range of ratios surrounding $\text{Ba/Ti} = 1$ [Kan75, Ovr79]. However, the ratio and impurity levels must be controlled or the powder may coexist as a mixture with contaminant TiO_2 , BaCO_3 , or $\text{Ba}(\text{OH})_2 \cdot 8\text{H}_2\text{O}$ phases.

Several authors note that an increase of the precursor Ba/Ti decreases the particle size of the final product and attribute this phenomena to a rapid nucleation event [Kum96, Wad95]. The nature of this relationship is further discussed and tested in Chapter 6. Also noted is an increase in reaction kinetics due to an increase in the $[\text{Ba}(\text{OH})_2 \cdot 8\text{H}_2\text{O}]$ [Cha90, Her88]. Hertl reported an independence of the rate of reaction after attaining a $[\text{Ba}(\text{OH})_2 \cdot 8\text{H}_2\text{O}] \geq 1 \text{ M}$ and a subsequently saturated TiO_2 interface [Her88]. Unfortunately, the precursor Ba/Ti was not supplied by Hertl.

2.4.3.3 Solution pH

The pH of the reaction medium is a key variable in the synthesis of BaTiO_3 powders since it dictates the chemical nature of the aqueous species from the precursors [Bae76, Fox91, Hen92a, Liv92, Liv90]. An elevated solution pH is noted to perform at least three functions: (1) promote the BaTiO_3 reaction kinetics [Cha90, Sla96], (2) increase the solubility of the titanium precursor [Cha90, Kee66, Pou74, Sla96, Yos89], (3) fulfill the thermodynamic requirement for phase pure synthesis [Ada90, Len93]. Remarkably, the thermodynamic predictions have been reproduced in the laboratory [Kan75, Moo96, Ovr79, Shv79]. For example, Moon observed the necessity for a 0.2 M $[\text{Ba}(\text{OH})_2 \cdot \text{H}_2\text{O}]$ and subsequent solution pH of 13.1 to produce phase pure BaTiO_3 .

As discussed in the previous section, the need for a precursor Ba/Ti > 1 demands a postsynthesis powder wash to remove the excess barium from solution. Researchers report the incongruent dissolution of the barium ions from BaTiO_3 powders in solutions of low $[\text{OH}^-]$ [Ada90, Cho96b, Ute90]. A nonstoichiometric powder is anticipated from powder washes using a moderate to acidic solution pH, yet many authors employed deionized or distilled water [Dog97, Her88, Her95a, Kum95, Kum96, Shi97, Viv89] or acidified aqueous washes [Eck96, Viv87, Wad95, Wad96, Xia96]. Thus, the solution pH remains an important, and much neglected, variable in postsynthesis processing. In addition, pH control plays an integral role in the production of dispersed aqueous slurries

for wet-forming as illustrated by the Gouy-Chapman double layer model and DLVO theory calculations [Der41, Ove52, Ver48, Hun81, Hun93].

2.4.4 Precursor Impurities

Omnipresent to all BaTiO₃ synthesis techniques previously mentioned is the finite contamination by the main precursor species, precursor impurity, and or undesirable product of the precursor which remains within the lattice or grain boundaries of the BaTiO₃ powder (at least) until firing. Commonly, the use of various BaTiO₃ synthesis techniques are restricted by the sensitivity of dielectric properties to incorporated precursor contaminants or the adverse decomposition of the contaminant at high temperatures [Dut94, Kle89]. For example, BaTiO₃ compacts formed from acetate and nitrate derived powders dedensify on sintering [Dut94] while BaCO₃ impurities inhibit complete densification [Cha90]. In addition to residue from the main precursor constituents, impurities within the precursors may be as equally damaging to the electronic characteristics of the final powder. Thus, similar to other advanced ceramics destined for electronic applications, special attention is required to minimize impurity levels at all stages of the process.

The TiO_x(OH)_y gel is synthesized by the neutralization of titanium oxychloride (TiOCl₂(aq)) in an aqueous ammonium hydroxide solution under agitation. The as-synthesized gel is washed with hot water on a vacuum filtration belt to ensure chloride removal. However, a finite amount remains. Chloride is the major contaminant of the CPM hydrated titanium oxide gel slurry which translates to a typical level of chloride contamination within CPM BT-8 lots of ≤ 200 ppm [Tracy Taggart, personal communication, May 23, 1998].

Four significant impurities are contained in the Ba(OH)₂·8H₂O precursor, ≤ 0.81 mol% BaCO₃ and ≤ 0.065 mol% Sr, and ≤ 0.12 mol% Cl, and ≤ 0.069 mol% Na.

All other noted impurities are present in trace amounts. Barium carbonate, the inevitable and major impurity, is removed prior to synthesis (during the injection process of the experimental designs research of this experimentation). The $\text{Ba}(\text{OH})_2 \cdot 8\text{H}_2\text{O}$ dissolves when heating the aqueous solution prior to injection, leaving the insoluble carbonate which is removed by an in-line filter. Carbon concentration determination within the final BaTiO_3 powders is a convoluted measure of both the precursor, gel, atmospheric exposure during the wash process, and handling of powder. Thus, the final concentration of the produced powders cannot be directly compared to the precursor contamination levels or present CPM BT-8 powders. Sr contamination is noted in concentrations ≤ 700 ppm within typical CPM BT-8 lots. All other cation impurities are present in concentrations ≤ 100 ppm.

2.4.5 Solution Additives

The general control of ceramic particle attributes such as size, shape, and dispersion can be manipulated by the prudent introduction of additives to the primary precursors at room temperature prior to the nucleation event [Ada98, Bel97, Li96,]. The use of alkaline mineralizers, such as NaOH or KOH, to promote rapid BaTiO_3 nucleation by dissolution of the titanium network has been reported [Dut94, Her95a, Xia96]. However, unless alkali contamination can be avoided, undesirable dielectric properties result from the compensatory defect chemistry of the lattice [Her85, Kle89]. If employed, other basic mineralizers may provide undesirable decomposition products during the sintering of the dielectric. Therefore, pH control by the addition of the original barium precursor, $\text{Ba}(\text{OH})_2 \cdot 8\text{H}_2\text{O}$, is desirable because it does not unnecessarily complicate the system with species foreign to the product lattice.

Efforts to increase the *in situ* dispersion during the synthesis of BaTiO_3 powders have employed EDTA [Mil90], 85,000 MW polyvinyl alcohol [Viv87], and fish bone

gelatin, Triton X-100, Dextran 250, and β -cyclodextrin by Her and Matijevic [Her95a]. The work by Miller is discussed in Chapter 4. Using a gel-hydroxide, noninjection system, Vivekanandan noted smaller particles via a steric stabilization mechanism when PVA was added during both the gel neutralization and BaTiO_3 synthesis steps [Viv87]. The final size of the BaTiO_3 particles was reported to drop from 200-500 nm to 20-200 nm in the presence of PVA. The utility of the powders is not known due to the ambiguity of the manuscript in reporting thermoanalytical and dielectric characteristics. In addition, photomicrographs of the particle synthesized with PVA were not provided. Of the assorted polymeric additives employed by Her et al., the gelatin exhibited no effect on the dispersion of the coprecipitated powder. All other polymers were reported to cause agglomeration [Her95a].

2.4.6 Seeding

Generally, precipitation occurs from high supersaturation conditions which cause rapid nucleation rates. In turn, the rapid nucleation consumes a majority of the precursor stock prior to particle growth in a batch reaction. The result of solution precipitation methods is small crystals present in high concentrations of about 10^{11} to 10^{16} particles/cm³ [Soh92]. Growth by seeding techniques therefore requires the use of a high seed concentration. For example, Bell successfully used large hematite seed concentrations to seed the glycothermal production of α -alumina powders under reaction temperatures and pressures similar to the hydrothermal technique [Bel98]. The hydrothermal heterogeneous nucleation of BaTiO_3 on anatase particles in the hydroxide-anatase reaction [Chi95, Zha96], titanium metal (precursor) substrates [Bac92, Ben93, Kaj91, Ven95], and single crystal SrTiO_3 [Chi95] suggest the possibility of BaTiO_3 seeding techniques. Also noted is the work of various authors in single crystal synthesis [Gar96, Reh98, Yoo97] and chemical vapor deposition seeding [Cho97].

2.5 Experimental Designs

The utilization of experimental designs lends statistically based quantification of the main effects of process variables in a decreased number of experiments. Such methods, also called the design of experiments (DOE) technique, have been developed since the 1950s and have been used to study ceramic systems [McC96, Pou91], but have not been employed in the hydrothermal or solution synthesis of ceramics to the knowledge of the author. Typically, general research conclusions are often based on the experimental results of the instinctive one-variable-at-a-time strategy, which is both inefficient and leads to inaccurate broad conclusions drawn from two-dimensional data. This is because data obtained by the one-variable-at-a-time method on the effect of an alteration of the variable (or treatment) A is valid only under one specific condition (i.e., the exact values of the j other variables in an arbitrary process) and cannot be accurately extrapolated to encompass a process window. In addition, the one-variable-at-a-time approach does not assess process or characterization variability. The use of statistical experimental design provides information which is proven to be statistically significant (with respect to inherent experimental variability), is valid within a processing window of multiple variables, and is known to be reproducible. The technique also produces knowledge of multivariable effects, such as the simultaneous variation of temperature and time. Such information is not possible with the one-variable-at-a-time strategy. In summary, conservation of research time and cost is possible by confident acquisition of an increased amount of data while employing a decreased number of experiments. Due to these advantages, three fractional factorial experimental designs with a center point replicate analysis were performed to investigate the main effect of the various process variables on the physical attributes of a patented BaTiO_3 hydrothermal process [Men89a, Men89b]. The following section contains the general strategies employed during proper experimental design, the limitations of the technique, and the methodology used in all

designs by using the initial twenty experiment, 2^{7-3} fractional factorial design as an example.

2.5.1 Applied Experimental Design Techniques

Depending on the design type, designs can screen a process to determine the most dominant variables, optimize the yield or efficiency of a process, or allow process tailoring to acquire a desired product attribute. Many textbooks describe the basic strategies of experimental designs as well as the numerous types of designs available to the practicing scientist [And52, Box78, Cau91, Coc57, Fed55, Kem52]. Therefore, a succinct functional plan is given which highlights the experimental design process rather than the selection of a design.

The following discussion of statistical designs employs nomenclature which may be confusing to one who is first learning DOE techniques or is familiar with another DOE text. Table 2.3 outlines the definitions for terms utilized within the following chapters. Notably, the words variable and treatment are used interchangeably within the text. Equally as numerous as the authored texts, many experimental designs have been formulated. A limited list of design names is given in Table 2.4. Most designs can be easily applied with the aid of experimental design software such as ECHIP (ECHIP Inc., Hockessin, DE) or MINITAB (MINITAB Inc., State College, PA).

Initially in an industrial setting, project teams are formed which are sufficiently small to be manageable, yet include all necessary talents. In academia, this research team consists of the graduate assistant and research advisor. Upon assembly of the project and/or project team, the objective should be specifically defined. An appropriately narrow objective would be "to screen the variables which significantly affect particle

Table 2.3. Experimental design nomenclature employed within the text.

Term	Definition	Example
Variable or Treatment	Parameter which is modified	Reaction time or temperature
Level or Variable level	Magnitude of the variable	50°C or 90°C
Observation	Measured result	Particle size
Main effect	Calculated effect of a variable	Increase in the particle size causes a decrease in the settling time from solution

Table 2.4. Numerous types of experimental designs [Cau91, Hun79, Mas89].

Taguchi	Youden Squares
Plackett-Burman	Nested
Factorial	Tree Technique
Central Composite (square or cube)	Least Squares
Completely Randomized Blocks	Split-Plot
Randomized Blocks	Mixture Models
Latin Squares	Polynomial
Graeco-Latin Squares	Response Surface Methods
Hyper-Graeco-Latin Squares	Box-Behnken
Balanced Incomplete Blocks	Linear with Center Point
Fractional Factorial	Canonical Analysis

size.” The objective describes the expected results of the project, however, the path to that goal is the most important portion of the design process. Thus the merit of the results of an experimental design is based on the selection of the variables and variable levels, for example, reaction temperature and 50°C, 70°C, and 90°C, respectively. The type of design is chosen and the design matrix is constructed based on the project goal and variable selection. After the experiments are conducted, main effects of the variables are calculated by inserting the values/observations of the particle attributes into the design matrix. The main effects are tested for statistical significance, and conclusions are drawn with respect to the effectiveness of each treatment in altering a given attribute (such as particle size).

2.5.2 Experimental Design Limitations

The limitations of DOE techniques rely on the selection of the most significant variables, use of variable levels within the physical constraints of the experimental apparatus, and/or the ability to choose variables within an important regime. For example, one would not investigate the function of temperature on the sintering of alumina at temperatures of 300°C and 400°C. A project team is well advised to conduct lengthy discussion of the list of variables and levels. If a major variable is completely neglected or the level improperly selected, it is difficult, if not impossible, to rework experimental data by performing several additional experiments. Often the entire design must be repeated. Prior to conducting experiments, one must ensure the process variables are controllable and characterization methods reproducible. The success of the design, as true of any experiment, relies on the consistency and control of all variables, whether included or excluded from the design matrix.

2.5.3 Fractional Factorial Design

Experimental designs are broadly defined in two categories, complete and incomplete designs. Most fall under the latter category. A full factorial design is termed a complete design, and describes a series of experiments which perform all combinations of the variables and variable levels. In order to analyze seven variables at two levels, a large number (2^7 or 128) of experiments are required. In order to construct a more workable matrix, a 2^{7-3} fractional factorial design was employed. This indicates that the design is a one-eighth replicate of a full factorial 2^7 design and that 7 variables are investigated at two levels (i.e., at a high and low value such as 100°C and 200°C). The advantage of this “incomplete design” is the ability to gain information concerning the main effects of all variables in only 16 experiments as opposed to 128. The matrix for the selected design is shown in Table 2.5 and is described by the general equation $I+ABCDE+ABCF+BCD G$ [Hun79]. The fractional factorial design is contained within rows (or experiments) one through sixteen. The seven variables are indicated by columns A through G. Rows seventeen through twenty designate the four replicated runs at a center point and are designated by a “0”. The high and low variable levels are designated by a “+1” and “-1”, respectively. To further elucidate the variable designation see Table 2.6 for the listing of the variable levels investigated in the 2^{7-3} design.

The final column in Table 2.5 indicates the observations (i.e., the obtained results) for the twenty experiments. Arbitrary observations can be placed into this column, such as specific surface area, density, or porosity, etc., to investigate the effect of any treatments on that selected particle attribute. However, the objective of the original design was defined to investigate one or several attributes. Additional investigation of arbitrary attributes must be made with caution since the measured effect may be an indirect artifact of the treatment.

The choice of the 2^{7-3} design rather than a 2^{7-2} or 2^{7-4} fractional factorial design is based on personal choice. A 2^{7-2} experiment would require a less time effective

Table 2.6. Treatment levels for the seven variables of the 2^{7-3} fractional factorial design to investigate the hydrothermal synthesis of BaTiO_3 . Note that the center values of the treatments were employed in the four replicate experiments.

	Treatment (variable)	Low Value (-)	Center Value (0)	High Value (+)
A	Injection Temperature ($^{\circ}\text{C}$)	60	80	100
B	Injection Rate (metering valve)	9	10	11
C	Final Reaction Time (min)	10	20	30
D	Final Reaction Temperature ($^{\circ}\text{C}$)	170	190	210
E	Precursor Ba/Ti Ratio	1.10	1.20	1.30
F	Solids Loading ($\text{g}_{\text{BaTiO}_3}/\text{L}_{\text{H}_2\text{O}}$)	63	73	83
G	Ti-gel Treatment at 150°C (min)	0	30	60

thirty-two experiments to screen the process, whereas the eight experiments required for a 2^{7-4} design does not allow resolution of the main effects from two-parameter interactions. In the 2^{7-4} design, the calculated main effect of any variable is “confounded” or “aliased” with two parameter effects [Box78, Cau91], thus it is considered mathematically inseparable from the two-parameter effects. For example, the calculated effect for the reaction temperature indicates the combined effect of the reaction temperature and the effect of the reaction temperature-reaction time parameter interaction. Though the employed 2^{7-3} fractional factorial design does not allow determination of two-parameter interactions, it ensures that the estimates of the main treatment effects are confounded with only third-order, fourth-order, and fifth-order interactions. Such high-order interactions are typically assumed to represent nil effects and are sometimes used to calculate the variance of a distribution by the analysis of variance technique [Hun79]. The calculated main effects are termed “naïve main effects” because of the confounded nature with other higher order parameters.

2.5.4 Basis of Significance

The use of DOE generally requires three steps when using the acquired data: the estimation of the population variance (or width), calculation of the main effects of the treatments, and comparison of the main effects to the population variance to qualify a treatment as significant or insignificant. The variance and main effects calculations will be provided within the experimental chapters, but the general approach follows. The population variance, S^2 , may be calculated from the analysis of variance (ANOVA) table [Hun79], Yates algorithm, large multiparameter effects, or, as in the employed technique, observations from experiments performed at the center point (or level) between the high and low levels of the design. The S^2 value is applied in the calculation of the Student's t -distribution based on the data from the experimental design, here the fractional factorial design, to produce a 95% confidence interval. The separately calculated main effects are

compared against the 95% confidence interval. One first assumes the null hypothesis that a treatment does not exhibit an effect on an attribute (or the attribute population). Thus, it is assumed that all treatments effects, τ_i , equal zero in the model $y_i = \eta + \tau_i + \epsilon_i$. The physical description of the null hypothesis model defines each particle size observation (y_i) as the result of the particle size population mean (η) plus inherent experimental error (ϵ_i). If the treatments have no effect (as defined by the null hypothesis), then all main effects should lie within a 95% confidence interval for the total powder population. However, if the calculated main effect lies outside the confidence interval, the effect has a 5% chance of belonging to the confidence interval. Thus, the effect is defined as a "rare event," and the treatment is deemed "statistically significant."

The number of necessary experiments depends largely on the desired objective (whether screening or optimization) and the balance of experiment and characterization costs to the product and process worth. Intuitively, a researcher who acquires more data is able to provide enhanced representation of the observed population. This increase in confidence is quantified by the decrease in the value of the Student's t-distribution with increasing degrees of freedom. The result is a reduction in the confidence interval width for the population.

2.6 Powder Characterization Techniques

Postsynthesis powder characterization is used to inspect the particle size and morphology as well as provide the values necessary to calculate the effects of treatments on the powder attributes. Quantitative characterization includes the determination of the mean particle size, particle size distribution, x-ray peak broadening to measure crystallite size and strain, specific surface area, density, and Ba/Ti molar ratio of the final powder. In addition, several observations were employed in a qualitative manner. These include conventional x-ray diffraction and transmission electron microscopy. The remainder of the chapter conveys the underlying theory of the employed characterization techniques.

2.6.1 X-Ray Diffraction - Phase Purity

Conventional x-ray diffraction (XRD) is employed to discern the atomic arrangement of atoms within crystalline samples. Monochromatic x-ray generation occurs by the emission of electrons via a tungsten filament, acceleration by a potential difference, and bombardment of a metal target, typically Cu. Electronic transitions within the Cu target subsequently produce monochromatic or near monochromatic x-rays which are directed across a sample over a range of incident angles. A scintillation detector records the intensity of the observed diffraction as a function of the angle of incidence (2θ). Compositional determination of a crystalline substance from the count intensity versus angle data is described by the Bragg Law [Cul78]:

$$n\lambda = 2d\sin\theta \quad [2.27]$$

where n is an integral number which represents the order of reflection, λ is the wavelength of the incident x-rays (1.54 Å for a Cu target), d is the interplanar spacing, and θ is the half angle of the diffraction. Thus, every crystalline material possesses a distinct x-ray pattern due to unique atomic sizes and configurations. X-ray diffraction may be used to directly measure the crystallographic transformations of BaTiO₃ (section 2.2.2) and the lattice constant of the unit cell ($a_{\text{cubic}} = 4.031 \text{ Å}$ and $a_{\text{tetragonal}} = 3.994 \text{ Å}$ from the JCPDS cards 31-174 and 5-626, respectively). With minor mathematical analysis of the x-ray data, the technique also can provide the diffraction generated crystallite size and strain (as later discussed).

2.6.2 Particle Size Determination

The measurement of particle size may be accomplished by various sizing methods which include optical and electron microscopy, sieving, sedimentation methods, electrical pulse counting, light scattering, hydrodynamic methods, and electroacoustics [Hun93].

Most techniques report an equivalent spherical diameter and range in limitation based on the optical properties, density, size, and other parameters.

Polarization intensity differential scattering (PIDS), a form of light scattering, is useful for particles of sizes ranging between 40 nm to 400 nm and enhances the PSD resolution for sizes less than 800 nm. Unlike the symmetric scattering patterns typical of Rayleigh and Fraunhofer scattering (for particle sizes of a few nanometers and greater than ten microns, respectively), the scattering produced by particle sizes near the range of the incident radiation is complicated. In the PIDS system, the scattering events of multiple wavelengths of polarized monochromatic light within the visible to near-visible range are recorded by a photodiode array. The recorded intensity patterns are then deconvoluted with respect to angle of scattering, the various incident wavelengths, and the initial angle of polarization to produce a time-averaged, spherical-equivalent particle size distribution.

2.6.3 X-Ray Line Broadening

Conventional XRD is used to determine the phase purity of unknown materials via the characteristic position of x-ray peaks centered at a specific angles of incidence. Contrarily, x-ray line broadening techniques determine the crystallite size and/or crystallite strain by measurement of the respective peak widening or skewing around the idealistic angle of the peak as shown in Figure 2.10. Peak broadening occurs when the 1.54Å wavelength from a $\text{CuK}\alpha$ x-ray source interacts with small crystals of sizes less than 200 nm and/or when a nonuniform strain exists [Cul56, Tay61]. Skewing of the peak toward low or high angles occurs in the presence of a uniform strain. Methods of measurement of the two effects and discrimination between them were first investigated by Scherrer and Laue [Cul78, Eck96, Lau26, Sch20], however, the equations do not account for instrumental broadening and assume stress-free crystallites [Tay61]. More

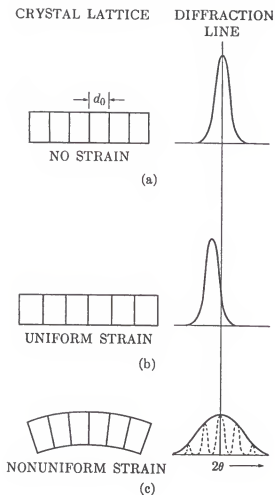


Figure 2.10. A single x-ray peak derived from crystals with (a) no strain, (b) uniform strain, and (c) nonuniform strain to illustrate the effects of crystal strain on experimental x-ray diffraction patterns [Cul78].

recent reported techniques employ curve fits based on the assumption of the generic x-ray peak curve comparison to Cauchy, Gaussian, and Voigt functions [Del82, Hal49, Kum95, Tay61, Viv89, Wil53]. The following research employs the Warren-Averbach technique, a line broadening method which calculates the crystallite size and strain from a Fourier transform deconvolution of the experimentally derived peaks. Moreover, the reliability of the data is further enhanced by the use of two orders of a reflection of the (hkl) plane in question.

2.6.4 Transmission Electron Microscopy

Transmission electron microscopy may be employed to view the particle size, morphology, defect structure, and/or crystal nature of ceramic powders, and is based on electron transmission through a sufficiently thin sample. Both thin milled samples or grids with dispersed powder can be imaged by the coherent, focused electron beam provided that the mean sample thickness (or particle size) is less than 200 to 300 nm. Electrons produced via the thermionic emission of a tungsten filament are accelerated by a high voltage bias, transmitted through the sample, and focused to either produce an image of the sample or a diffraction pattern dependent on the placement of the focal plane of the lens system. Both the elastic and inelastic scattering of electrons by sample-beam interaction causes the observed diffraction and phase contrast [Lor94].

2.6.5 Nitrogen Adsorption/Desorption - BET

The use of nitrogen adsorption/desorption to quantify the specific surface area of powders is termed the BET technique in honor of the inventors, Brunauer, Emmet, and Teller [Bru40]. Measurements are based on the weight of the nitrogen which is absorbed to the powder surfaces of a known weight of powder at a given pressure at the boiling temperature of liquid nitrogen, 77.35 K at 1.0 atm. The technique is predicated on the

assumption of a monolayer of nitrogen adsorption, where perfect monolayer formation is influenced by the interaction of the solid and the nitrogen gas. This interaction is pseudo-quantified by the BET C constant as calculated in equation [2.31]. An increase in the magnitude of the C constant represents an increase in the solid-gas interaction and therefore an increase in the accuracy of the calculated surface area. Weak interaction, represented by a C constant less than 20, is marked by the formation of multiple adsorbate layers before completion of a monolayer and results in questionable surface area calculations. The C constant of ceramic powders is typically equal to 100. For silica powder, the C constant ranges between 50 to 250 [Pow98].

In practice, an accurate powder weight and pristine surface, with respect to water adsorption, are ensured by sample outgassing under vacuum at elevated temperatures. After weight measurement of the dried powder in the BET cell, the cell is evacuated on the BET instrument and the cell volume is determined by recording the amount of He gas required to obtain a given pressure. The cell is again evacuated and the amount of nitrogen gas required to obtain a given pressure is recorded. During a multipoint BET, pressure equilibration is performed at multiple pressures, P , relative to the atmospheric pressure, P_o . Knowledge of the weight of gas absorbed, the molecular weight of the adsorbate, M , and the cross sectional area of the adsorbate molecule, A_{cs} , allows determination of the specific surface area, SSA, and C constant via a linear regression. Calculation of the surface area of solids is given by the equation:

$$\frac{1}{W \left[\left(\frac{P_o}{P} \right) - 1 \right]} = \frac{1}{W_m C} + \frac{C-1}{W_m C} \left(\frac{P}{P_o} \right) \quad [2.28]$$

where W indicates the weight of nitrogen adsorbed at the relative pressure of P/P_o and W_m is the weight of the monolayer of adsorbate. The plot of the left side of [2.28] against P/P_o between $0.05 < P/P_o < 0.35$ results in a line for solids provided that an

adsorbate monolayer is formed. Solving for W_m in both the equation of the slope, s , and the intercept, i , from [2.29] permits determination of W_m as shown below:

$$s = \frac{C-1}{W_m C} \text{ and } i = \frac{1}{W_m C} \Rightarrow W_m = \frac{1}{s+i} \quad [2.29]$$

Calculation of the weight of the adsorbate by equation [2.30] permits determination of the total surface area of the sample, S_t , within the BET cell using the equation:

$$S_t = \frac{W_m N A_{cs}}{M} \quad [2.30]$$

where N is Avogadro's number. The reported surface area for solids is conventionally provided in the form of a specific surface area, i.e., the total surface area of the sample divided by the sample weight after outgassing. The reliability of the calculated specific surface area is quantified by the C constant as discussed above. Similar to the calculation of W_m , the C constant can be determined from the equation of the line from equation [2.31]:

$$C = (s/i) + 1 \quad [2.31]$$

2.6.6 Helium Micropycnometry

Pycnometry utilizes gas displacement measurement by the Archimedes principle to determine the volume of small amounts of solid materials, powders, and porous materials. Use of the ideal-gas equation and calibration normalization permit the calculation of the powder volume, V_p , by measuring the pressure difference before and after helium gas is leaked into the sample cell as shown by:

$$V_p = V_c - V_R[(P_1/P_2)-1] \quad [2.32]$$

where V_c indicates the total volume of the sample cell including the powder, V_R indicates the reference volume of the reservoir, P_1 is the pressure of helium when confined to the reservoir, P_2 is the pressure of helium when the gas is permitted to occupy the reservoir

and sample cells. Both the total volume and volume of the reservoir are calculated by calibration to a steel shot standard.

2.6.7 X-ray Fluorescence Spectroscopy

X-ray fluorescence spectroscopy (XRF) is a nondestructive technique which was first invented in the 1930s and is commonly employed in industry [Wil87]. This is largely attributed to the ability to quantify elements of nearly all atomic weights with only a single analysis, ease of instrument use, rapid preparation and analysis time, and the lack of a need for consumable solution standards as necessary for wet chemical methods [Ben92]. XRF entails x-ray excitation of the inner shell electrons of the unknown sample. This is accomplished similar to procedures employed in conventional x-ray diffractometers: thermionic emission of an electron beam from a tungsten filament, x-ray production by a target material, electron excitation within the sample, sample x-ray emission, collection of the emitted spectrum via a detector, and amplification. In order to quantify the elemental presence of Ba and Ti, the respective emission intensity of the characteristic x-ray peaks from the sample in question are compared with intensity of the characteristic x-ray peaks from a reusable BaTiO₃ calibration standard with a known Ba/Ti. Calculation of the ratio is possible based on the relationship between the concentration c_A of element A and the respective emitted x-ray intensity I_A , as shown in [2.33], if the relationship is linear. The proportionality constant k_A is specific to element:

$$c_A / I_A = k_A \quad [2.33]$$

and can be experimentally determined easily by analyzing samples comprised of varying known concentrations of element A. Using the XRF technique, acquisition of a high precision quantitative ratio is possible [Ben92, Wil87], i.e., ± 0.002 , as reported by CPM. In comparison, inductively coupled plasma spectroscopy provides a precision $\geq 1\%$, as

reported by Bennett [Ben92]. This value was experimentally verified by prior experimentation on CPM BaTiO₃ powder lot number R59.

CHAPTER 3

DETERMINATION OF SYNTHESIS VARIABLES AFFECTING HYDROTHERMAL BaTiO₃ POWDERS

3.1 Introduction

Mineral crystallization under elevated temperatures and pressures in aqueous environments was known to geologists as early as the nineteenth century [Daw88]. Some of the landmark hydrothermal investigations were performed on quartz and other mineral systems by Morey and Laudise et al. [Lau62, Mor53]. The process was first employed to synthesize BaTiO₃ for pigment applications by Peterson in 1940 [Pet40]. In the following forty years, the use and commercial production of hydrothermal BaTiO₃ was limited due to the ease and lower cost of the solids state reaction of BaCO₃ and TiO₂ [Alc91, Bea83, Fer91]. However, technological advancement in colloidal dispersion, industrial wet casting and printing, and the miniaturization and increase in the reliability of microelectronic devices have provided a demand for the high purity, chemically homogeneous, and equiaxed submicron powders provided by hydrothermal techniques. The increased cost of hydrothermal powders is offset by the decrease in the sintering temperature of a cofired multilayer capacitor (MLC) and the use of less noble electrode compositions [Abe91, Daw91, Phu90].

Commercial dielectric powder formulations are incorporated in the MLC configuration by wet powder processing methods such as tape casting, screen printing, and the waterfall technique [Bec90, Bru93, Hur72, Ree88]. In the multilayer capacitor (MLC) configuration, a decreased dielectric thickness is desirable due to the increase in the capacitor volumetric efficiency (i.e., capacitance/volume). Industry trends are noted by comparison of the current industrially produced 3 μm fired dielectric layer thickness of a high performance MLC [Bee97, Ven98] to the 15 μm layer thickness produced in 1984

[Kan95]. The need for equiaxed powders on the order of <200 nm in forming micron-sized layers is apparent when considering the ratio of the particle diameter to the overall dielectric layer thickness and the size of the packing voids inherent to the wet-cast powder suspension. If nearly equal in magnitude, a short-circuit results across the dielectric and the part is rendered useless with respect to the desired function as a charge storing device.

Previous hydrothermal research illustrated the effects of the titanium precursor [Kum95, Kum96, Moo96, Shi97, Xia96], the BT precursor ratio (Ba/Ti) [Kan75, Kum96, Wad95], basicity [Ish90, Moo96, Xia96], and barium concentration [Her88] on the final particle size in noninjection systems (i.e., all precursors were added to the reaction vessel at room temperature and ramped directly to the reaction temperature). However, like most closed systems, some discrepancy exists in the assignment of treatment effects. Turbulence is especially noted in the areas of particle formation and the factors which control particle size, allowing ample opportunity for experimentation.

Few authors studied either coprecipitation [Her95a] or hydrothermal systems [Men89a, Men89b] using injection systems at elevated temperatures to control the concentration of solution species. In addition, the use of experimental designs in the synthesis of BaTiO_3 has not been reported to the author's knowledge. The inability to measure the *in situ* reaction of the high temperature and pressure hydrothermal system has forced two routes of research. First, the study of low temperature systems is employed to evaluate BaTiO_3 particle formation mechanisms under measurable growth conditions, since the kinetics of the high temperature reaction are quite rapid. The second method, trial and error experimentation, entails measurement of the final particle attributes following typical hydrothermal reaction conditions. However, such a study provides information on the most desirable characteristics, those of the powder product. Combination of the literature associated with thermodynamic studies [Ada90, Len93] and the two experimental methods provides a large data base from which the dominant variables and variable levels can be selected for investigation.

Experimental design, or the design of experiments (DOE), has been well documented by texts throughout the 1940s to 1950s [And52, Coc57, Fed55, Kem52, Pla46]. Such analysis of the hydrothermal method allows one to screen the process efficiently to determine the predominant variables and variable interactions which affect powder attributes. In addition, the statistical-based approach permits quantifiable estimation of the reproducibility of the process and calculation of confidence intervals for all variable effects. In this research, a screening fractional factorial design was employed to gain an understanding of variable effects over a processing window, something not possible using the one-variable-at-a-time approach of trial-and-error experimentation. In addition, the process simulation provided by the experimental design method is advantageous in comparison to low temperature studies.

3.2 Materials and Methods

3.2.1 Hydrothermal Synthesis

Twenty BaTiO₃ powder batches were synthesized with CO₂-free deionized water, as illustrated in the process flow diagram in Figure 3.1. Variable levels and the specific variable levels for every batch are listed in Table 3.1 and Table 3.2, respectively. The titanium precursor, an amorphous hydrated TiO_x(OH)_y gel, was prepared by CPM, Boyertown, PA, by the neutralization of titanium oxychloride (TiOCl₂(aq)). Upon receipt at the University of Florida, the gel was separated into 100 ml aliquots and frozen to avoid gel aging. The gel was thawed before weighing the desired amounts for each hydrothermal reaction. Hereafter, the thawed gel is termed the “as-received” gel. Prior to a hydrothermal run, an aqueous slurry of the as-received gel was sometimes pretreated (as dictated by the experimental design) by autoclaving the slurry at 150°C under autogenous pressure in a Ti reaction liner. If a pretreatment was not desired, the gel slurry (pH 3.5 prior to the addition of water) was added to the reaction liner, and the autoclave was sealed and ramped to the injection temperature. Simultaneously, an aqueous solution

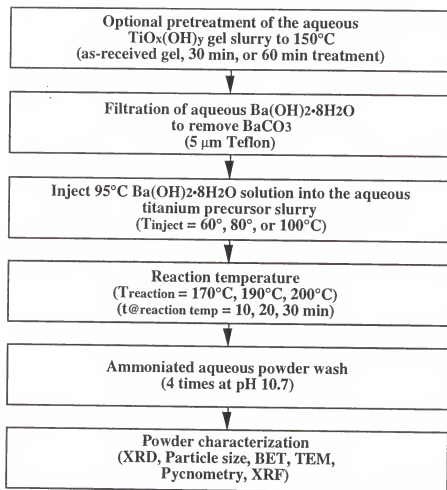


Figure 3.1. Diagram of BaTiO_3 hydrothermal synthesis and powder washing technique.

Table 3.1. Experimental matrix using a 2^{7-3} fractional factorial design using the general equation: $I + ABCDE + ABCF + BCDG$ and a center point replicate analysis (in lot number 17-20).

Lot #	A	B	C	D	E	F	G	Observation
1	-1	-1	-1	-1	+1	-1	-1	
2	+1	-1	-1	-1	-1	+1	-1	
3	-1	+1	-1	-1	-1	+1	+1	
4	+1	+1	-1	-1	+1	-1	+1	
5	-1	-1	+1	-1	-1	+1	+1	
6	+1	-1	+1	-1	+1	-1	+1	
7	-1	+1	+1	-1	+1	-1	-1	
8	+1	+1	+1	-1	-1	+1	-1	
9	-1	-1	-1	+1	-1	-1	+1	
10	+1	-1	-1	+1	+1	+1	+1	
11	-1	+1	-1	+1	+1	+1	-1	
12	+1	+1	-1	+1	-1	-1	-1	
13	-1	-1	+1	+1	+1	+1	-1	
14	+1	-1	+1	+1	-1	-1	-1	
15	-1	+1	+1	+1	-1	-1	+1	
16	+1	+1	+1	+1	+1	+1	+1	
17	0	0	0	0	0	0	0	
18	0	0	0	0	0	0	0	
19	0	0	0	0	0	0	0	
20	0	0	0	0	0	0	0	

Table 3.2. The specific values employed for the low and high levels of the fractional factorial design experiment as well as the center values common to all four replicate runs.

	Treatment	Low Value	Center Value	High Value
A	Injection Temperature (°C)	60	80	100
B	Injection Rate of Aqueous Ba(OH) ₂ ·8H ₂ O Solution*	--	--	--
C	Final Reaction Time (min)	10	20	30
D	Final Reaction Temperature (°C)	170	190	210
E	Precursor Ba/Ti Ratio	1.10	1.20	1.30
F	Solids Loading (g _{BaTiO₃} /l _{H₂O})	63	73	83
G	TiO ₂ (OH) _x gel treatment at 150°C (min)	0	30	60

* Adjustment of the injection rate was insufficient to evaluate the effect of the injection rate on particle attributes.

of $\text{Ba}(\text{OH})_2 \cdot 8\text{H}_2\text{O}$ was heated to 95°C in a separate container. On achievement of the desired injection temperature (i.e., the temperature of the $\text{TiO}_x(\text{OH})_y$ gel slurry in the autoclave), the 95°C $\text{Ba}(\text{OH})_2 \cdot 8\text{H}_2\text{O}$ solution was introduced to the injection apparatus, filtered through a $5\ \mu\text{m}$ Teflon filter (to remove possible BaCO_3 contamination), and injected into the autoclave. After injection, the autoclave was ramped to a desired reaction temperature for a predetermined reaction time under autogenous pressure and cooled to room temperature. All autoclave reactions and pretreatments were performed under mechanical agitation at 350 rpm since this variable was shown to be relatively insignificant between 100-600 rpm [Kum95]. In addition, the authors tried to limit the large number (i.e., seven) of variables investigated. Though turnover and shear are required to describe reactor agitation, the physical constraints of the autoclave agitation head and reactor geometry afford only simplistic control of agitator rpm. It was assumed that the investigated rpm regime by previous authors encompassed a reasonable shear range.

Following autoclave disassembly, the powders were rinsed with a deionized, ammoniated water wash (adjusted to pH 10.7 with ammonium hydroxide) using a centrifugation (3500 rpm) and decantation technique. The wash was necessary to remove the excess barium in solution, yet the wash solution pH required adjustment to avoid incongruent dissolution of barium from the BaTiO_3 surface [Ada87, Cho96b]. After the fourth and final wash, the powders were stored in the wash solution until the powders were vacuum dried at 160°C for ≥ 8 hours prior to characterization.

3.2.2 Powder Characterization

BaTiO_3 samples for x-ray diffraction (XRD) analysis were prepared by weighing a known amount of powder onto an amorphous silica slide, wetting the powder with isopropanol to distribute the powder over the sample portion of the slide, and allowing the samples to air dry. Similarly, the aqueous slurry of the as-received and treated $\text{TiO}_x(\text{OH})_y$ gels was agitated, sampled, deposited, and allowed to air dry. Phase purity

XRD analysis was performed from 10° to 90° 2θ using $\text{CuK}\alpha$ radiation at 40 kV and 20 mA using a Philips Powder Diffractometer model APD 3720 (Mount Vernon, NY) in combination with a Philips automated diffraction software PW1877, version 3.6g.

Quantitative particle size analysis was performed via light scattering with a Coulter Corporation Particle Size Analyzer (Model LS230, Miami, FL). Powder sampling was conducted by agitation of the final wash suspension prior to the withdrawal of 15 ml of suspension. The high solids loading 15 ml sample suspension was then sonicated for one minute via an ultrasonic horn before introduction to the 1.5 L water reservoir of the LS230. The dispersed particles in the water reservoir are constantly sonicated and recirculated through the internal light scattering test cell during an analysis run. Therefore, the resultant distribution for a single analysis is based on a 120 s time-averaged distribution. The reported mean particle sizes consist of an average of two separate analyses for each powder lot and are based on a number frequency distribution.

X-ray line broadening analysis samples were deposited on a cut off-angle quartz slide similar to the aforementioned XRD procedure. Quartz slides were utilized to reduce background radiation and enhance peak measurement. The employed Warren-Averbach method requires the comparison of two dissimilar order peaks on an "infinite" crystal size calibration standard and two dissimilar order peaks of the unknown sample to determine the difference between sample and instrumental broadening (Philips Line Profile 1.0 analysis software). Instrumental peak breadth was determined by a step scan of the quartz standard at a step size of 0.005° 2θ for 6.0 s over the (100) and higher order (200) peaks at $19.0\text{--}23.0^\circ$ 2θ and $41.1\text{--}43.5^\circ$ 2θ , respectively. Step scans of the cubic BaTiO_3 (100) and higher order (200) peaks were performed on every sample at $21.0\text{--}23.0^\circ$ 2θ and $43.5\text{--}46.0^\circ$ 2θ , respectively, using a 0.01° 2θ step size and a 15 s scan time. Unlike other line broadening measurement techniques, the Warren-Averbach method is based on a Fourier series curve fit and does not require an assumption of the sample and standard XRD profiles to represent a Voigt, Cauchy, or Gaussian curve [Tay61]. In addition to the measurement of two peaks per sample, rather than only one peak in other methods,

the Warren-Averbach technique has been successfully used to evaluate hydrothermally synthesized BaTiO_3 powders [Viv89].

Transmission electron microscopy (TEM) samples were prepared by dispersion of approximately 0.01 g of vacuum dried BaTiO_3 powder in 12 ml of isopropanol by sonication. Carbon coated Cu grids were vertically dipped into the suspension and stored under vacuum prior to TEM analysis. TEM analysis was performed at 200 kV on a JEOL 200cx transmission electron microscope (Boston, MA).

The measurement of specific surface area of the twenty powders was performed by conventional nitrogen adsorption/desorption by the Brunauer, Emmett, and Teller (BET) technique on a Quantachrome Autosorb-6 Sorption System (Boca Raton, FL). After drying the as-washed powders in a vacuum oven, arid conditions were ensured by outgassing the powder and the 6 ml amorphous SiO_2 BET cell for ≥ 8 hours at 160°C under a 300 mtorr vacuum. The ascertained specific surface area for every powder is based on the linear regression of a five-point analysis. All analyses provided a C constant ≥ 50 , thereby signifying reliable data, as discussed in Chapter 2.

A helium pycnometer, Quantachrome model MPY-1 (Boca Raton, FL), was utilized to calculate particle densities. The reported density values reflect the average of four measurements after samples were outgassed >12 hours at 160°C at approximately 300 mtorr and placed in the pycnometer cell under flowing helium for 10 min. Similar to other physical attributes, the results were inserted into the experimental design matrix in order to estimate the main effects of the synthesis treatments.

Analysis of the Ba/Ti of the final powder, hereafter called the powder Ba/Ti, was performed at CPM with an X'Unique II x-ray fluorescence (XRF) spectrometer (Philips Electronics, Mahwah, NJ). The sample preparation procedure entailed mixing 3.00 g of the dry desired powder lot with 2.00 g of #PH101 Avicel, a microcrystalline cellulose (FMC Corporation, Philadelphia, PA) which provides green pellet integrity after uniaxial pressing. Sample pellets were analyzed using 75 kV and 40 mA accelerating voltage conditions with a He flow-through sample cup. The reported ratio was obtained by

comparison to the peak emissions of CPM BaTiO₃ calibration standards, is based on the analysis of a single pellet, and is accurate to ± 0.002 by a repeatability and reproducibility (Gage R&R) analysis by CPM.

3.3 Results and Discussion

3.3.1 Phase Purity

XRD of the TiO_x(OH)_y gel (Figure 3.2) indicated that the as-received amorphous gel transformed to the crystalline anatase phase upon hydrothermal treatment at 150°C for both the 30 min and 60 min treatments. The observation is in agreement with the prior experimentation [Che95, Moo96]. XRD of the BaTiO₃ powders (Figure 3.3) illustrated a crystalline phase representative of the cubic BaTiO₃ phase for all powders. Also noted in several powders was a diminutive peak at 25° 2 θ which is attributed to the (101) anatase peak at 25.3° 2 θ and signifies incomplete reaction of the titanium precursor. However, the unreacted anatase concentration was expected to be present in minor concentrations since the (101) anatase peak exhibits the most intense peak of the pattern and the 25°C peak was the only observed peak not attributed to the BaTiO₃ matrix. As later illustrated by XRF analysis, the presence of anatase and/or amorphous titanium gel was significant in some powders. Comparison of the lot numbers which exhibited an anatase contaminant phase with the level of the gel hydrothermal treatment indicates that the anatase was noted only in the BaTiO₃ powders which were formed from a 150°C treated titanium precursor slurry.

3.3.2 Effect of Treatments on Coulter Particle Size

Particle size distributions measured by the Coulter LS230 indicated a number frequency mean particle size between 76 nm to 115 nm as shown in Table 3.3, the summary of characterization results. Estimation of the main effect of the treatments was performed by placing the particle size raw data within the design matrix, as described below.

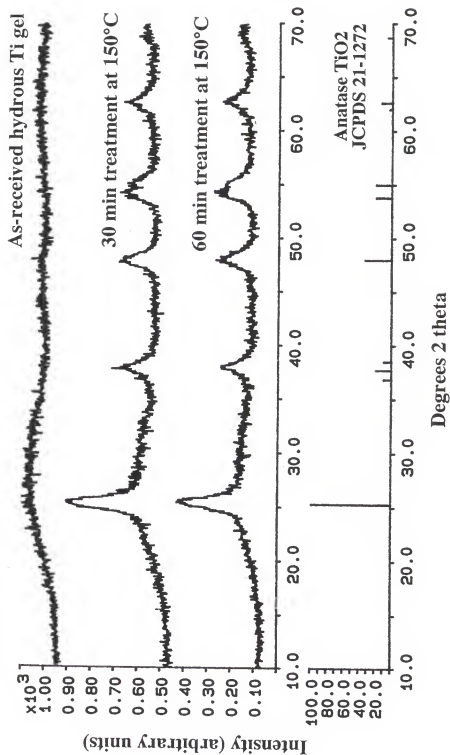


Figure 3.2. X-ray diffraction analysis of the as-received and hydrothermally treated precursors to demonstrate the amorphous nature of the as-received gel and the formation of crystalline anatase on heat treatment to 150°C.

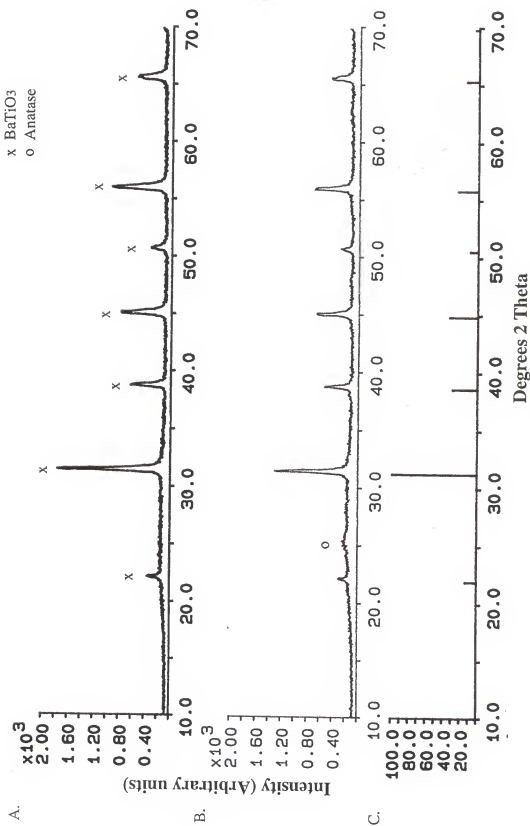


Figure 3.3. X-ray diffraction analysis of barium titanate powder lot (a) and (b) 15 indicates the pattern resemblance to (c) the cubic barium titanate (JCPDS card number 31-174) and presence of unreacted anatase (JCPDS number 21-1272) in several powders.

Table 3.3 Characterization summary for all investigated particle attributes.

Lot No.	Crystalline Phase via XRD	Particle Morphology via TEM	Mean Particle Size via Coulter (nm)	Specific Surface Area via 5-pnt. BET (m ² /g)	Particle Density via Helium Pycnometer (g/cc)	XRD Crystallite Size (nm)	XRD Crystallite Strain (%)	Product Ba/Ti via XRF
1	Cubic BaTiO ₃	a'	108	73.8	4.99	29.0	0.223	0.778
2	Cubic BaTiO ₃	e	97	83.8	5.01	23.0	0.306	0.715
3	Cubic BaTiO ₃ ⁱⁱ	e	81	39.1	5.21	26.7	0.241	0.711
4	Cubic BaTiO ₃	e	76	15.1	5.75	24.8	0.274	0.982
5	Cubic BaTiO ₃ ⁱⁱ	e,s	87	40.5	5.15	29.2	0.231	0.670
6	Cubic BaTiO ₃	e	77	18.7	5.73	21.6	0.296	0.975
7	Cubic BaTiO ₃	a	115	74.9	4.99	26.9	0.255	0.738
8	Cubic BaTiO ₃	a	90	114	4.81	18.9	0.382	0.609
9	Cubic BaTiO ₃	e,s	104	31.7	5.34	21.9	0.227	0.744
10	Cubic BaTiO ₃ ⁱⁱ	e	82	37.0	5.07	27.2	0.238	0.780
11	Cubic BaTiO ₃	e,a	107	42.0	4.78	23.4	0.255	0.848
12	Cubic BaTiO ₃	e	97	52.1	4.66	27.2	0.252	0.753
13	Cubic BaTiO ₃	e	106	38.5	5.00	19.0	0.296	0.852
14	Cubic BaTiO ₃	e	112	41.2	5.17	23.5	0.290	0.879
15	Cubic BaTiO ₃ ⁱⁱ	e,s	94	50.4	4.68	24.8	0.210	0.605
16	Cubic BaTiO ₃ ⁱⁱ	e,s	85	53.6	4.72	19.3	0.289	0.677
17	Cubic BaTiO ₃ ⁱⁱ	e	86	39.1	5.05	25.0	0.253	0.773
18	Cubic BaTiO ₃ ⁱⁱ	e,a	87	46.1	4.92	18.5	0.330	0.736
19	Cubic BaTiO ₃	e	88	19.4	5.38	28.2	0.230	0.968
20	Cubic BaTiO ₃ ⁱⁱ	e,s	89	49.9	4.76	22.3	0.293	0.707
Average ⁱⁱⁱ			94.8	50.4	5.07	24.14	0.267	0.770
95% CI ^{iv}			± 1.0	± 14.5	± 0.28	± 4.36	± 0.046	± 0.126
Physical Range ^v			76-115	15.1-114	4.66-5.75	18.9-29.2	0.210-0.382	0.605-0.982
CPM R59	Cubic BaTiO ₃	e	190	7.4	5.38	27.7	0.261	1.003

i e = equiaxed morphology, a = some asymmetrical particles, s = several secondary particles comprised of small crystallites (~10 nm).

ii Anatase contamination visible from x-ray diffraction.

iii Average of powder lots 1-16.

iv Confidence interval calculated for lots 1-16 assuming a single population based on the replicate lots 17-20.

v Measured range of lots 1-16.

3.3.2.1 Estimation of population variance

The confidence interval for the sixteen batches of the fractional factorial design was calculated by first estimating the particle size variance of the four replicate runs, experiments 17 through 20, at the center point of the design. The estimate of variance, S^2 , was calculated by equation [3.1] where y_i is the particle size for each experiment (i.e., 86.4, 87.4, 87.8, or 88.6 nm), Avg. Y is the average of the four experiments (i.e., 87.55 nm), and n is the total number of experiments (i.e., four):

$$S^2 = \Sigma [(y_i - \text{Avg. Y})^2] / (n-1) = 0.84 \quad [3.1]$$

The estimate of variance, 0.84, is utilized in the 16 powder fractional factorial design calculations to determine the statistical significance of the treatment effects.

3.3.2.2 Fractional factorial matrix calculations

In determination of the statistical significance of data, the null hypothesis is first assumed, that is, that the treatments have no effect on the observation, i.e., the particle size. Therefore, it is assumed that all treatments effects, τ_i , equal zero in the model $y_i = \eta + \tau_i + \epsilon_i$. The physical description of the null hypothesis model defines each particle size observation (y_i) as the result of the particle size population mean (η) plus an arbitrary inherent experimental error (ϵ_i). If the treatments have no effect as defined by the null hypothesis, then all main effects should lie within a 95% confidence interval for the 16 powder population, which is given by [3.2] or [3.3].

$$\eta = \text{Avg. Y} + t_{v,0.025}(S^2/n)^{1/2} = 94.8 \pm 1.0 \quad [3.2]$$

$$P(93.8 < \eta < 95.8) = 0.95 \quad [3.3]$$

where the Avg. Y is the average particle size of the 16 runs, $t_{v,0.025}$ is the value of the Student's t-distribution for fifteen degrees of freedom, S^2 is the estimate of variance calculated from the four replicate runs, n is the total number of experiments, sixteen. If the naïve estimate of the main effect for any one treatment lies outside the confidence

interval (CI), then the null hypothesis is refuted and the main effect cannot be assumed to belong to the single population. Therefore, the effect of the treatment is considered to be statistically significant. Conversely, if the calculated main effect of a variable lies within the CI, then it cannot be distinguished from the main population. The treatment/variable would be deemed statistically insignificant in affecting the particle size.

After calculating the 95% confidence interval for the 16 powder matrix, the naïve main effects for each treatment must be computed. This is accomplished by multiplying the particle size observation of lot number 1 (108 nm from Table 3.3) by the variable level value (i.e., -1 or +1) present in each column of the design matrix, Table 3.1, and inserting the product into columns A, B, C, D, etc. as shown in Table 3.4. Particle size insertion is performed similarly for the remaining experimental lots number 2 through 16 to produce the completed calculation matrix, Table 3.4. The naïve estimate for the main effect of treatment A is calculated by summing column A of Table 3.4 and dividing the result by half of the total number of experiments (i.e., $n/2$ or 8). The calculated main effects are located within both Table 3.4 and Table 3.5, where a negative value for the main effect indicates that the particle size varies inversely with the low and high level designations of the treatment effect.

From Table 3.5, five treatments exhibit a significant effect on the particle size of BaTiO₃ powders: the temperature of the titanium precursor slurry upon injection (injection temperature), the final reaction temperature, the final reaction time, the solids loading of the reactor, and the occurrence or absence of the 150°C hydrothermal treatment of the gel. The two most effective in magnitude, the injection temperature and TiO_x(OH)_y gel treatment, vary inversely with the particle size. Increase of the injection temperature may be expected to increase reaction kinetics, increase the solubility of titanium, and increase the exposure time of TiO_x(OH)_y gel at the injection temperature regime. Hence, smaller particles are produced by a more rapid nucleation event and are thought to be

Table 3.4. The 2^{7-3} fractional factorial calculation matrix for effect of seven variables, A through G, on the particle size of BaTiO_3 .

Lot #	A	B	C	D	E	F	G	Mean Particle Size (nm)
1	-108	-108	-108	-108	108	-108	-108	108
2	96.8	-96.8	-96.8	-96.8	-96.8	96.8	-96.8	96.8
3	-81.0	81.0	-81.0	-81.0	-81.0	81.0	81.0	81.0
4	76.2	76.2	-76.2	-76.2	76.2	-76.2	76.2	76.2
5	-87.2	-87.2	87.2	-87.2	-87.2	87.2	87.2	87.2
6	77.0	-77.0	77.0	-77.0	77.0	-77.0	77.0	77.0
7	-115	115	115	-115	115	-115	-115	115
8	89.6	89.6	89.6	-89.6	-89.6	89.6	-89.6	89.6
9	-104	-104	-104	104	-104	-104	104	104
10	81.8	-81.8	-81.8	81.8	81.8	81.8	81.8	81.8
11	-107	107	-107	107	107	107	-107	107
12	97.4	97.4	-97.4	97.4	-97.4	-97.4	-97.4	97.4
13	-106	-106	106	106	106	106	-106	106
14	112	-112	112	112	-112	-112	-112	112
15	-93.6	93.6	93.6	93.6	-93.6	-93.6	93.6	93.6
16	84.9	84.9	84.9	84.9	84.9	84.9	84.9	84.9
Estimated Main Effect	-10.7	-3.5	1.6	7.0	-0.7	-6.1	-18.3	Σ Column = Avg. Y = 94.8

Table 3.5. Comparison of the main effects of the investigated treatments to the calculated confidence interval which assumes a single population. The shaded regions indicate treatments which have a statistically significant effect on the given observation.

	Treatment / Main Effect of Treatment on Listed Measurement	Mean Particle Size via Coulter LS230 (nm)	Specific Surface Area via BET (m^2/g)	Particle Density via He pycnometer (g/cm^3)	XRD Crystallite Size (nm)	XRD Crystallite Strain (%)	Product Ba/Ti via XRF
A	Temperature of Ti precursor slurry on injection of $\text{Ba}(\text{OH})_2 \cdot 8\text{H}_2\text{O}$ ($^{\circ}\text{C}$)	-10.8	3.1	0.096	-1.92	0.049	0.053
C	Final Reaction Time (min)	1.6	7.2	-0.071	-2.49	0.029	-0.038
D	Final Reaction Temperature ($^{\circ}\text{C}$)	7.0	-14.2	-0.277	-1.73	-0.019	-0.005
E	Precursor Ba/Ti Ratio	-0.7	-12.5	0.125	-0.50	-0.002	0.118
F	Solids Loading ($g_{\text{BaTiO}_3}/L_{\text{H}_2\text{O}}$)	-6.1	11.4	-0.194	-1.61	0.026	-0.074
G	Treatment of $\text{TiO}_2(\text{OH})_2$ gel at 150°C (min)	-18.3	-29.3	0.284	0.58	-0.032	-0.003
	95% Confidence Interval	± 1.0	± 14.5	± 0.280	± 4.36	± 0.046	± 0.126

representative of the highly hydroxylated, aqueous titanium precursor species. Smaller particles are also measured by heat treatment of the $\text{TiO}_x(\text{OH})_y$ gel. The 150°C hydrothermal product, anatase, exhibits a lower reactivity than the as-received gel [Eck96, Pfa91]. In addition, the titanium-based hydrothermal treatment product has coarsened (if not completely crystallized) and exhibits a lower surface area with respect to the untreated gel, as shown by the BET results. Subsequently, a decreased reactivity is expected from the smaller surface area hydrothermally treated reactant. Conventional nucleation and growth theory suggests that larger particles are produced by less reactive precursors [Rin96]. This effect also was also reported by Kumazawa when rutile derived BaTiO_3 particles were shown to be consistently >5 times larger than the hydrated gel derived particles for the $\text{Ba}(\text{OH})_2 \cdot 8\text{H}_2\text{O}$ system and similar Ba/Ti between 1.0 to 4.0 [Kum96]. Quite possibly, the residual, unreacted titanium-based particles, as illustrated by XRF, account for the smaller observed particle size.

Though not as effective in alteration of the BaTiO_3 particle size, the effects of the final reaction temperature and precursor solids loading also are statistically significant. BaTiO_3 coarsening was not expected due to the relatively short time that the powders were subjected to the reaction temperature and the observation of the independence of the reaction temperature and particle size from 70-150°C [Wad95]. Thus, the observed increase in the particle size with increased reaction temperature and reaction time at the reaction temperature might be attributed to the more complete reaction of the residual titanium precursor and subsequent growth of the BaTiO_3 particles. Equally possible is the enhanced crystallization and coarsening of the gel to the anatase structure. Similar to the results of Chapter 5 and Chapter 6, smaller particles are formed by the increase of the precursor solids loading. Under all experimental conditions, the $[\text{Ba}(\text{OH})_2 \cdot 8\text{H}_2\text{O}]$ aqueous solution is not saturated [Kir78, Ovr79]. Therefore, increased total loading increases the barium concentration in solution and increases the solution pH. The ramifications of these increases are further discussed in the later chapters, yet the result is a more rapid

nucleation event which is thought to be promoted by the enhanced digestion of the gel network or anatase lattice.

Several additional points are notable. First, the light scattering technique is a measure of the particle dispersion. Therefore, the measured particle size may be attributed to porous aggregates or agglomerates rather than fully dense particles. Further characterization to discern the particle density and particle size by electron microscopy is necessary before acceptance of the light scattering derived particle size. However, the reported particle sizes are similar in magnitude to the sizes reported by previous authors in Table 2.1. Finally, after completion of the experimental series, control of the injection rate was determined insufficient to enable evaluation of its effectiveness on the final particle size. Therefore, the study actually evaluated six variables at a rapid injection rate (2.5 l/min) and an injection time < 15 s.

3.3.3 XRD Line Broadening Analysis

3.3.3.1 Effect of treatments on crystallite size

The average crystallite size of the sixteen powders was equal to 24.1 ± 4.4 nm via calculation of a 95% confidence interval from the four replicate powders. The actual particle sizes of the sixteen lots ranged between 18.9 nm to 29.2 nm via the Warren-Averbach XRD technique. Through design analysis similar to that used to determine the Coulter particle size in Table 3.4, all treatments were shown to exhibit a statistically negligible effect on the crystallite size derived from planes normal to the (100). The null hypothesis was accepted.

The observed crystallite sizes are comparable to the 68-95 nm and 40-52 nm hydrothermally derived BaTiO_3 crystallites reported by independent laboratories [Kum95, Viv89] which employed the amorphous $\text{TiO}_x(\text{OH})_y$ gel and $\text{Ba}(\text{OH})_2 \cdot 8\text{H}_2\text{O}$ systems without $\text{Ba}(\text{OH})_2 \cdot 8\text{H}_2\text{O}$ injection. The research of Vivekanandan et al. [Viv89] compared three different line broadening techniques: two separate Hall Williamson analyses using Cauchy and Voigt approximations and a Warren-Averbach analysis. It

was determined that all three techniques provided similar results. The Warren-Averbach technique was reported to be superior since the method was most representative of the single-crystal particles viewed by TEM. Comparison of the measured 80-110 nm particles and the calculated 18.9 nm to 29.2 nm crystallite size suggests the particle to be polycrystalline. This was confirmed by TEM analysis.

3.3.3.2 Effect of treatments on crystallite strain

In performing the Warren-Averbach line profile technique, calculation of the crystallite strain within a given direction is possible. The strain perpendicular to the (100) of the twenty powders provided an average value of $0.267 \pm 0.046\%$, where all measured strains ranged between 0.223-0.382%. In contrast to the evaluation of crystallite size, analysis of the treatment effects on strain proved one treatment effect, the temperature of the titanium-based precursor prior to injection of barium hydroxide, to lie outside the calculated 95% confidence interval. Estimation of the main effect of the injection temperature, 0.049%, to be just beyond the 95% confidence interval given by $\pm 0.046\%$. Though statistically significant from the definition of the population, the effect is sufficiently close to the general population that it might be considered as a sample from the general population. If the effect is assumed real, it might be described by the more rapid particle formation process expected at increased temperatures. Speculation of the event proposes any or all of the following: (1) the rapid kinetics allow insufficient time for complete reaction and removal of the byproduct water, (2) hydroxyl removal is inhibited by encapsulation by the freshly forming product, (3) if residual anatase is present at the particle core, the encapsulation may increase the observed strain based on the strain at the anatase-BaTiO₃ interface.

3.3.4 Transmission Electron Microscopy

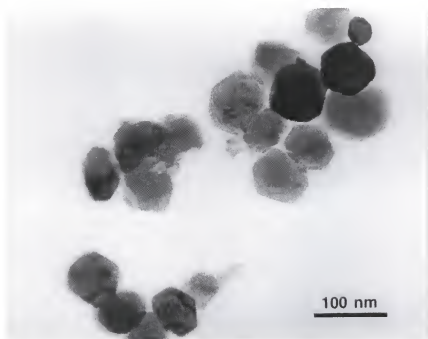
Most powders exhibit particle diameters between 20 nm to 170 nm and an equiaxed morphology similar to the particles shown in the TEM photomicrographs

in Figure 3.4. Some particles exhibit a hexagonal plate-like shape. The observation is atypical of the usually equiaxed morphology of hydrothermal products synthesized at low temperature. However, nonspherical powders are not completely without mention in other studies. Hexagonal particles also were noted by Miller [Mil90] when using EDTA in a static system. Rectangular particles are noted in the highly tetragonal BaTiO_3 produced by Kajiyoshi et al. at reaction temperatures $\geq 400^\circ\text{C}$ [Kaj91]. Similarly, visual inspection of the powders produced by Xia et al. show an increase in the presence of cubic/rectangular faceted crystals with increasing reaction temperature from 100°C through 400°C when using a constant reaction time of 8 hours [Xia96]. Both observations of rectangular particles are consistent with the noted increase in tetragonality as a result of increase in the reaction temperature [Dut94, Kaj91, Shi97, Xia96], increase in the reaction time [Dut94], and the simultaneous decrease in the lattice hydroxyl concentration with regard to these reaction conditions [Shi97, Viv87]. Thus, the observed particle morphology appears to be consistent with the underlying crystalline structure. Another BaTiO_3 morphology observed in the literature is best explained by a raspberry-like appearance [Moo96, Zha96]. Such a nodular surface is attributed to an aggregative growth model in rapidly reacting systems or the heterogeneous nucleation of BaTiO_3 on less soluble crystalline precursors such as anatase. Several raspberry-like 100-200 nm aggregates of smaller crystallites, approximately 5-10 nm in diameter, were noted in powders 5, 9, 15, and 20 as illustrated in Figure 3.5a. In addition, several irregular asymmetrical single particles were noted in powders 7, 8, 11, and 18, as shown in Figure 3.5b. Independent of the observed morphology, visual inspection of the powder lots corroborated the particle size analysis by the Coulter light scattering technique.

3.3.5 Effect of Treatments on Specific Surface Area

In both the 150°C hydrothermally treated and as-received state, the hydrated $\text{TiO}_x(\text{OH})_y$ gel exhibited a relatively high surface area. Gel samples from the as-received, 30 min treatment at 150°C , and 60 min treatment at 150°C slurries yielded a specific

A.



B.

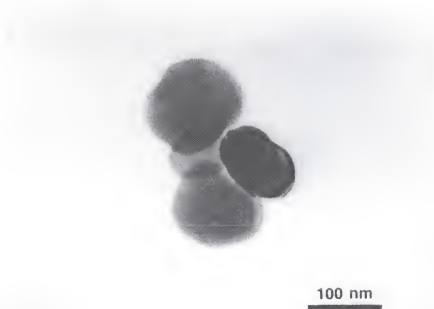
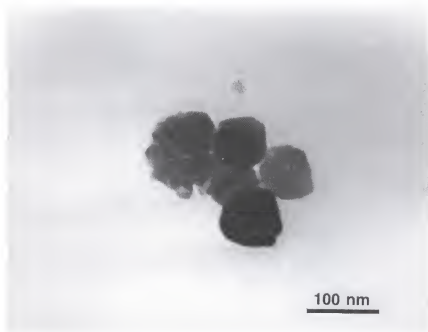


Figure 3.4. Transmission electron photomicrographs of powder lots (a) 17 and (b) 19 to illustrate the equiaxed nature of the typical powders.

A.



B.

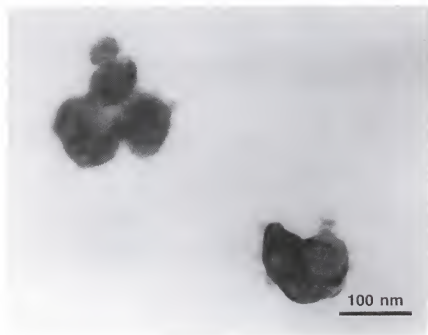


Figure 3.5. Transmission electron photomicrographs of BaTiO₃ powder lots (a) 15 and (b) 8 to illustrate the several aggregate and asymmetrical particles, respectively.

surface area of 241 m²/g, 195 m²/g, and 193 m²/g, respectively. Thus, treatment of the gel at 150°C caused some coarsening of the powders. This effect is expected from the increase in density from 2.5 g/cm³ to 3.48 g/cm³ [Lid94] which occurs during the amorphous to anatase transformation. However, increase in the time of aging at 150°C did not cause significant decrease of the surface area.

The specific surface area of the powders ranged from 15.1 to 114 m²/g. Upon insertion of the surface area results into the statistical matrix, the calculated 95% confidence interval was determined as 50.4 ± 14.5 m²/g. Therefore, one treatment, the hydrothermal treatment of the TiO_x(OH)_y gel, exhibited a statistically significant effect on the surface area. The inverse effect, -29.3, indicates that 150°C treatment of the gel results in a powder with a decreased surface area. However, the assignment of treatment effectiveness based on the observed particle size and BET measurements is speculative due to the phase impurity. High surface areas of some lots may be attributed to an asymmetrical particle geometry, agglomerates of smaller crystallites, increased surface roughness or porosity, but is most likely attributed to the presence of unreacted high surface area amorphous or anatase residuals. The above hypotheses are plausible when realizing the rapid Ba(OH)₂·8H₂O injection rate and time. Calculation of a contaminant concentration of 5 % of 200 m²/g anatase indicates that the contaminant would contribute an increase of 10 m² of surface area per one gram of the mixed TiO₂-BaTiO₃ powder. The titania concentrations suggested by XRF suggest an even stronger influence on the surface area. Notably, the three powders which exhibited a product Ba/Ti > 0.968 exhibited an SSA between 15.1 and 19.4 m²/g. All other powders exhibited a SSA > 31.7 m²/g and a product Ba/Ti < 0.879.

3.3.6 Effect of Treatments on Particle Density

The density of the particles varied between 4.66-5.75 g/cm³. However, the majority of the powders exhibited a density less than the CPM R59 powder, 5.38 g/cm³, and all densities were lower than the generally accepted theoretical density, 6.02 g/cm³, of

hydrothermally derived BaTiO_3 . The 95% confidence interval for the density values is described by $\pm 0.28 \text{ g/cm}^3$. Thus, the only statistically significant treatment is the $\text{TiO}_x(\text{OH})_y$ gel treatment, where treatment of the gel at 150°C results in particles of increased density. This may be probable if the slower anatase reaction does not cause encapsulation of the titanium precursor and allows more time for molecular rearrangement. In general, the low densities may be attributed to a contaminant phase. If a contaminant phase is present, anatase (3.48 g/cm^3 [Lid94]) exhibits a higher density than the amorphous gel (2.5 g/cm^3) and may contribute to the measured increase in the density.

The common contaminant in hydrothermally derived powders is water, which resides as both physically and structurally bound water and hydroxyls [Hen92b, Her95b, Shi97, Sla96, Viv87, Wad95, Xia96]. TG/DTA of four selected powders indicated a constant weight loss with respect to temperature. At the final temperature of 1000°C , a loss of 4-6 % was recorded (ignoring the initial 2 % of physically adsorbed water since powders were not outgassed prior to TG/DTA and accounting for the 1 % discrepancy after postanalysis calibration with a CaCO_3 standard). This amount of water incorporation corresponds to a final particle density between 5.00 g/cm^3 and 4.62 g/cm^3 , and is similar to the observed densities. Thus, the generally low observed densities strongly correspond to the presence of a low density unreacted titanium precursor and the hydroxyls associated with the titanium precursor and BaTiO_3 .

3.3.7 Effects of Treatments on the Product Ba/Ti

X-ray fluorescence illustrated a large variation in the product Ba/Ti from 0.605 to 0.982. No treatment was shown to exhibit a statistically significant effect on the product ratio. Notably, the precursor Ba/Ti shows the largest dependence, though not statistically significant. The Ba/Ti precursor was varied by maintaining a constant batch size with respect to the gel (0.214 mol/batch). The titanium molarity was calculated based on the pyrolysis of the gel and the assumption that pure TiO_2 was formed. Therefore, the $\text{Ba}(\text{OH})_2 \cdot 8\text{H}_2\text{O}$ concentration in this design varied between 0.30-0.46 M.

This concentration is greater than the 0.2 M concentration shown by Moon to produce phase pure BaTiO_3 in a noninjection system [Moo96], yet is lower than the concentration employed in the future chapters. The inconsistent and sometimes inhomogeneous product may be attributed to the rapid injection rate, the use of a less reactive anatase precursor, and the need for an increased $\text{Ba(OH)}_2 \cdot 8\text{H}_2\text{O}$ concentration.

3.4 Conclusions

Experimental design is useful in investigating the hydrothermal technique provided that variables and variable levels are judiciously selected and controlled. Such designs provide quantifiable conclusions of particle attribute effects based on real-world process conditions. Rapid injection of $\text{Ba(OH)}_2 \cdot 8\text{H}_2\text{O}$ to the suspended titanium precursor produces a phase mixture of cubic polycrystalline BaTiO_3 and unreacted anatase and/or amorphous titanium-based particles under most of the investigated conditions. The production of phase pure BaTiO_3 with the rapid injection system is most probable with a decreased injection rate, increased time at the reaction temperature, and increased $[\text{Ba(OH)}_2 \cdot 8\text{H}_2\text{O}]$ in the final solution. This may be accomplished by increase in the Ba/Ti ratio and/or the use of increased solids loading of the autoclave. The reported particle attributes approximate those attributes reported in the literature for pure BaTiO_3 , yet also represent a finite mixture of the titania particles. Finally, the hydrothermal pretreatment of the $\text{TiO}_x(\text{OH})_y$ gel greatly affected the powder size attributes in the rapid injection rate process. Though the products of this design are not anticipated to be viable dielectric powders, the experimental series has provided direction to the experimentation which follows.

CHAPTER 4

EFFECT OF EDTA ADDITIONS AND OTHER PROCESS VARIABLES ON THE PARTICLE ATTRIBUTES OF HYDROTHERMALLY SYNTHESIZED BaTiO₃

4.1 Introduction

For solution-based formation mechanisms which involve dissolution and recrystallization, the mean particle size of solution derived powders typically can be altered by control of the competition between the nucleation and growth processes. In general, solution seeding [Bel98], micellar encapsulation [Li96], alteration of the stirring rate [Soh92], and modification of the solubility of the reactant species [Ada98, LaM50] can be employed to promote either nucleation or growth [Rin96]. The latter is most probable in the BaTiO₃ hydrothermal system due to the observed rapid nucleation rates and the desired high solids loading. Changes in reactant concentrations may be accomplished by adjustment of the reaction temperature and/or solution pH, addition rate of a precursor(s), addition of a complexing agent, use of a different reaction medium, and/or using a different chemical, physical, or crystalline form of the precursors. Previous investigations have illustrated the significance of the type of titanium precursor employed during hydrothermal synthesis of BaTiO₃ powders [Kum95, Kum96, Moo96, Shi97, Xia96]. Of the investigated precursors, the amorphous hydrated gels have shown an increased reactivity and thus smallest BaTiO₃ particle size with respect to crystalline anatase and rutile precursors [Kum96, Moo96, Xia96, Shi97]. The following experimental design investigates the use of (1) a complexing agent introduced to a hydrated titanium oxide gel, (2) a range of Ba(OH)₂·8H₂O injection rates, not investigated in the rapid injection work of the initial 20 experiment design, (3) a range of increased precursor BT molar ratios (Ba/Ti), and (4) a range of injection temperatures.

The complexing agent, ethylenediaminetetraacetic acid (EDTA), was employed to alter the solubility of titanium species available for reaction upon the injection of the aqueous barium hydroxide solution. In researching the tables of stability constants by Smith and Martell, the ligands which complex the high field strength titanium ions are fairly limited due to the extreme stability of titanium dioxide [Smi89]. In various solution synthesis reactions, the use of other complexing agents, such as oxalic acid in the oxalate coprecipitation process, produce an intermediate insoluble precipitate which must undergo thermal treatment in order to form crystalline BaTiO_3 powders [Cla56, Mil90, Sto93]. Furthermore, the thermal decomposition products of the several other titanium complexing agents contain noxious vapors upon ramping to binder burnout and/or sintering temperatures. Miller also employed EDTA in BaTiO_3 synthesis research, however, the process employed a titanium isopropoxide based precursor and a static system without hydroxide injection, i.e., all precursors were placed in the reaction vessel prior to heating from room temperature [Mil90]. The static system produced large aggregates with mean diameters of approximately 200 nm with increasing EDTA concentration. Though the mechanism of formation and reaction kinetics were not determined, the presence of EDTA was suggested to decrease the degree of powder aggregation [Mil90]. The objective of the following text is to determine the effects of EDTA additions and other process variables on particle attributes in an agitated, injection-based system by using experimental designs.

Experimental designs have been well documented by texts throughout the 1940s to 1950s, but to the author's knowledge have yet to be employed in the solution synthesis of ferroelectric powders [And52, Coc57, Fed55, Kem52, Pla46]. Due to the inaccessibility of the hydrothermal process at elevated temperatures and pressures, researchers may resort to particle formation analysis at low temperatures. However, the validity of extrapolating these conclusions to more extreme conditions is questionable. In contrast, actual process scenarios may be probed by post-mortem analysis of the hydrothermal method via

experimental design. A host of available statistically based designs allow one to efficiently screen or optimize the process to determine the predominant variables which affect powder attributes using fewer total experiments. In addition, the statistical-based approach permits quantifiable estimation of the repeatability of the process and calculation of confidence intervals for all variable effects. In this research, a screening fractional factorial design was employed to gain an understanding of the variable effects in the presence of EDTA and gain knowledge of the viable processing window.

4.1.1 Experimental Design

A 2^{4-2} fractional factorial design was employed in order to analyze four treatments (or variables) in one matrix. Thus four treatments are investigated at two levels (i.e., at a high and low value such as 100°C and 200°C). The advantage of this design is the ability to gain data concerning all treatments in fewer experiments than the 16 experiments (i.e., 2^4) necessary to perform all combinations of the four treatments at two levels. The matrix for the design is shown in Table 4.1 and is described by the general equation $I + ABC - ACD$ [Box78]. The conditions for the four experiments within the fractional factorial design are

Table 4.1. Fractional factorial design with replicated center point to estimate variance where column A through column D represent the investigated treatments.

Lot #	A	B	C	D	Observation
22	-1	-1	+1	+1	
23	+1	-1	-1	+1	
24	-1	+1	-1	-1	
25	+1	+1	+1	-1	
26	0	0	0	0	
27	0	0	0	0	
28	0	0	0	0	

contained within powder lots 22-25 and the four treatments are indicated by column A through column D. Powder lots 26-28 designate the three replicated runs performed at the center point of the experiment (or center level between the high and low levels) and are designated by a "0". The high and low levels of the treatments are designated by a "+1" and "-1", respectively. To further elucidate the treatment designation, see Table 4.2 for the listing of the treatment levels investigated.

The final column in Table 4.1 indicates the observations (i.e., the obtained data) for the seven experiments. Any quantifiable particle attribute data may be placed into the observation column, such as specific surface area, particle size, porosity, etc. However, the treatments and treatment levels for this research were chosen with the intention to investigate the effect(s) on the particle size of BaTiO₃ powders. Caution must be exercised in concluding the effects of the treatments on arbitrary characteristics which are substituted into the original design matrix. Therefore, the calculated effect of the treatments may or may not be related to the investigated particle attributes, but the treatments were statistically analyzed to acquire a more complete understanding of the system. Calculation of the naïve estimate of main effects, estimate of the particle distribution variance, and determination of statistical significance of the treatment (or variable) effects will be presented within the results portion of this manuscript.

4.1.2 Hydrothermal Synthesis

Hydrothermal synthesis is defined as the treatment of precursors in an aqueous environment at elevated temperature and pressure, and was employed to synthesize BaTiO₃ for pigment applications as early 1940 [Pet40]. Research has shown the technique to be superior to other powder formation techniques due to the ability to directly produce crystalline, agglomerate-free, high purity powders in a relatively benign environment at low temperatures (i.e., $\leq 200^{\circ}\text{C}$). For example, dispersed suspensions of the typical crystalline as-synthesized 100-150 nm particle diameters via the Cabot Performance Materials (CPM)

Table 4.2. Investigated treatments and treatment level of the employed 2^{4-2} fractional factorial design. All experiments were performed with a stirring rate of 350 rpm, a reaction temperature of 200°C, a reaction time of 10 min, and BaTiO₃ product loading of 0.356 mol/L assuming complete conversion of titanium gel.

Treatment		Low Value	Center Value	High Value
A	Temperature of TiO _x (OH) _y gel on injection of Ba(OH) ₂ ·8H ₂ O solution (°C)	50	70	90
B	Injection Rate (ml/min)	15	30	45
C	Ba/Ti Precursor Ratio	1.2	1.5	1.8
D	EDTA Concentration (mol%)	1	3	5
	or (M)	7.07×10^{-3}	2.12×10^{-2}	3.53×10^{-2}
	or (g)	0.6266	1.8797	3.1326

hydrothermal process accommodate the direct production of fired $3.0\text{ }\mu\text{m}$ dielectric layers [Bee97]. BaTiO_3 powders produced via other techniques, such as conventional calcination, oxalate-derived, sol-gel-derived methods, may require additional crystallization heat treatments and/or milling prior to use in forming operations [Fax70, Her95a, Phu90, Suy94]. In both scenarios, application of the respective secondary processes may produce aggregated powders and/or nonequiaxed morphologies unsuited for use in ultra-thin layers. The competitiveness of such techniques is further lessened if the solution chemistry is not appreciated during wet milling and an unanticipated nonstoichiometric surface results due to the incongruent dissolution of barium [Ada87, And87, Cho96b, Len93]. Finally, the use of an aqueous-based synthesis technique is relatively inexpensive and benign in comparison to the hazards, raw material cost, and disposal cost of organic solutions.

The major commercial disadvantages of hydrothermal synthesis include the stability of the selected material within the aqueous environment, the appreciable capital equipment expenditures, and the aggregation of particles during solvent extraction [Rin96]. The first two disadvantages may be negated by adequate control of solution pH and cost analysis of the entire process lifetime and sales of a superior product, respectively. The latter, aggregation on drying, can be surmounted by avoiding solvent removal from the powder until drying of the final tape [Ven98]. Thus, the as-synthesized wet-cake is not completely dewatered when introduced to the polymeric plasticizer, binder and other casting additives. With respect to academic interests, the disadvantages of the hydrothermal BaTiO_3 synthesis include the inaccessibility of the reaction and the rapid kinetics of the reaction precipitation process. The closed nature of the system does not allow *in situ* determination of pH and limits sampling techniques. Specifically, the rapid nucleation and growth of BaTiO_3 at typical reaction temperatures requires the use of reduced temperatures and isothermal conditions to investigate particle formation mechanisms [Eck96, Her88, Moo96]. In addition to the modified reaction temperatures, multiple sampling efforts within one batch

alter the concentrations of reactants and products. Such incipient nucleation temperature studies provide the treatment level range for the injection temperature, yet do not provide data on the effect of specific variables with regard to final product characteristics. Contrarily, process mimicking experimentation as provided by experimental design allows insight to process control within a window of multiple process variables while simulating hydrothermal synthesis conditions.

4.2 Materials and Methods

4.2.1 Hydrothermal Synthesis

Seven BaTiO₃ powder batches were synthesized with CO₂-free deionized water, as illustrated in the process flow diagram in Figure 4.1. Variable levels and the specific variable levels for every batch are listed in Table 4.1 and Table 4.2, respectively. The titanium precursor consisted of a high surface area, 240 m²/g, amorphous hydrated Ti-gel from CPM, Boyertown, PA. The gel and a desired amount of EDTA were weighed into the Ti reaction vessel, placed in the autoclave, purged with nitrogen, sealed to the atmosphere, and ramped at approximately 1.2°C/min to the predetermined injection temperature. In a separate PTFE container, an aqueous solution of Ba(OH)₂·8H₂O (High Purity B1000, Solvay Corporation) was heated to 95°C. On achievement of the injection temperature (i.e., the temperature of the Ti gel slurry in the autoclave), the 95°C Ba(OH)₂·8H₂O solution was introduced to the injection apparatus, filtered through a 5 µm Teflon filter to remove possible BaCO₃ contaminant particles, and injected into the autoclave at varying rates. After injection, the autoclave was ramped at an approximate rate of 1.4°C/min to a 200°C reaction temperature, soaked at the reaction temperature for 10 min, and cooled to room temperature. The cooling time was not controlled and was performed with a closed circulating system and 10°C water. Therefore, initial cooling from the reaction temperature was rapid, and the approximate total cooling time was two hours. All autoclave reactions were performed under mechanical agitation at 350 rpm since this

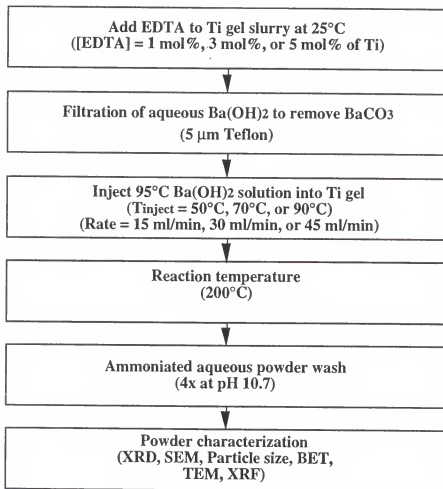


Figure 4.1. Hydrothermal synthesis, washing, and characterization flow diagram for BaTiO₃ powders with EDTA addition.

variable was shown by Kumazawa to be relatively insignificant with respect to other process variables over a range of 150-600 rpm in noninjection systems [Kum95]. Following autoclave disassembly, the target 50 g of powder per batch were washed and dried and described in 3.2.1.

4.2.2 Powder Characterization

All BaTiO₃ sample characterization was performed as described in 3.2.2. Evaluation included x-ray diffraction (XRD), particle size analysis via a light scattering method, x-ray line broadening analysis, transmission electron microscopy (TEM), nitrogen adsorption/desorption to determine the specific surface area, and x-ray fluorescence (XRF) to determine the Ba/Ti molar ratio of the product powders.

4.3 Results and Discussion

4.3.1 Phase Purity

Evaluation of the TiO_x(OH)_y gel indicated that the as-received gel was x-ray and TEM amorphous. XRD, shown in Figure 4.2, also illustrated the pseudo-cubic crystalline phase as well as equivalent peak intensity and intensity ratios for all synthesized BaTiO₃ powders. As illustrated in Figure 4.2, modest BaCO₃ contamination was noted on most powders. This is consistent with the findings of Xia and colleagues [Xia96] when employing high Ba/Ti precursor ratios (i.e., ≥ 1.5). Powder contamination may be attributed to the carbon dioxide present in the as-received Ti-gel (since the gel synthesis operation is open to the atmosphere), incomplete N₂ purging of the autoclave, or reaction of the excess barium hydroxide with atmospheric CO₂ on exposure during the washing and dewatering processes. The BaCO₃ was not expected to be formed as a result of improper solution conditions during the reaction, since a high solution pH was maintained due to the use of high Ba/Ti ratios and ≥ 0.3 M Ba(OH)₂·8H₂O as the barium precursor. Theoretical modeling [Ada90, Len93, Ute90] and empirical observations [Ben93, Cho96b, Mil90,

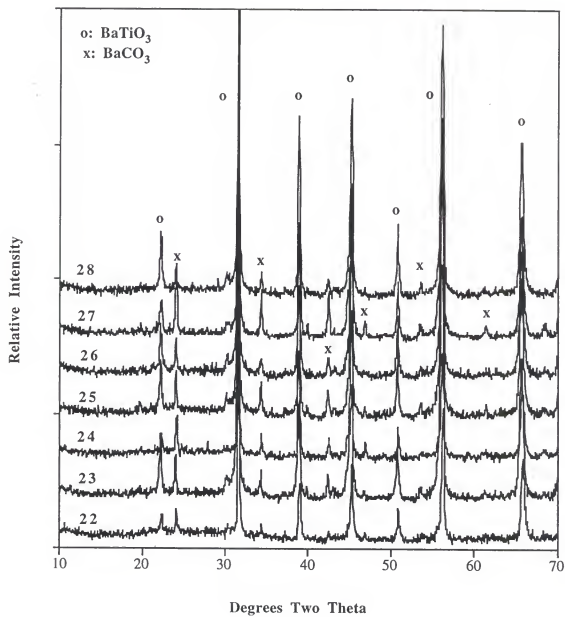


Figure 4.2. XRD analysis of the as-synthesized BaTiO₃ powder lot numbers 22-28 which illustrate XRD patterns representative of a cubic crystal structure.

Moo96] have shown that alkaline conditions are required for the synthesis of phase pure BaTiO_3 , as demonstrated in Figure 2.9. With regard to the precursor concentrations, Moon reported that $\text{Ba}(\text{OH})_2 \cdot 8\text{H}_2\text{O}$ concentrations $\geq 0.2 \text{ M}$ create the solution pH conditions (i.e., $\geq \text{pH } 13$) necessary to avoid carbonate contamination when the precursor $\text{Ba/Ti} = 1.0$ in a noninjection system [Moo96].

Other solution synthesis studies report the formation of the cubic phase at or near a Ba/Ti precursor ratio equal to 1.0 at relatively low reaction temperatures [Shi97, Viv89]. The observance of a cubic pattern is attributed to the small particle size and strain compensation for the incorporated hydroxyl point defects and/or water in hydrothermal products [Hen92b, Shi97, Sla96, Viv87, Xia96]. Charge compensation for the incorporated hydroxyls results in cation vacancies and the observed lattice strain [Shi97, Viv89]. A higher concentration of hydroxyls was noted in cubic crystallites than tetragonal crystallites [Shi97] and the incorporated hydroxyls results in an expanded lattice [Shi97, Viv89]. Nonsolution (as well as solution) derived BaTiO_3 -based ceramics with a grain size less than one micron are unable to form the 90° domains necessary to relieve the strain in the thermodynamically stable tetragonal phase [Cro98]. Subsequently, the material assumes a metastable cubic crystal structure. However, a true distinction between the tetragonal and cubic phases is not possible by standard XRD [Mil90] since the x-ray peak broadening which occurs when the particle diameter is $< 200 \text{ nm}$ does not allow the resolution of the tetragonal peaks. The utility of the peak broadening effect will be exploited later to evaluate the crystallite size and strain.

Tetragonality is observable in CPM hydrothermal particles by heating to temperatures $> 1000^\circ\text{C}$ during typical MLC processing and cooling to room temperature as observed by other investigations [Hen92b, Shi97, Viv89, Wad96]. Stress relief occurs by the removal of residual hydroxyls and formation of 90° domains following grain growth during the sintering process. On increase of the hydrothermal precursor Ba/Ti ratio to ≥ 2

and/or increase of the reaction temperature, a pure tetragonal phase has been directly formed [Kaj91, Shi97]. However, the $\geq 300^{\circ}\text{C}$ reaction temperature, the safety concern of the pressures inherent to elevated temperatures, the use of excess Ba precursor, high probability of carbonate contamination, and the ease of tetragonal restoration during firing deem the direct production of tetragonal hydrothermal powders unnecessary (if not industrially unprofitable) for capacitor applications.

4.3.2 Effect of Treatments on Coulter Particle Size of Barium Titanate

Particle size distributions measured by the Coulter LS230 indicated a number frequency mean particle size between 75-81 nm as shown in the summary of all characterization results given in Table 4.3. Though not analyzed within a design matrix, the d_{10} and d_{90} of the distributions typically were 45-50 nm and 100-140 nm, respectively. The empirically derived precision of the employed technique (including BaTiO_3 sampling fluctuations and instrumental error) taken from four separate runs was equal to ± 2.7 nm. Empirical instrument accuracy, based on silica standards, was shown to be less than $\pm 1.0\%$. Estimation of the main effect of the treatments was performed by placing the particle size raw data within the observation column of the design matrix, as described below.

4.3.2.1 Calculation of the main effects of the treatments

The naïve main effects were computed by multiplying the particle size observation of experiment number 22 (75.4 nm from Table 4.3) by the variable level value (i.e., -1 or +1) present in each column of the design matrix, Table 4.1, and inserting the product into columns A, B, C, and D of Figure 4.3. The remaining powder lots 23 through 25 were completed similarly by horizontal insertion of the observation column and multiplication to produce Figure 4.3, the completed calculation matrix. The naïve estimate for the main effect of treatment A was calculated by summing column A of Figure 4.3 and dividing the

Table 4.3. Summary of characterization results for the hydrothermal BaTiO₃ powder lot numbers 22-28 with EDTA additions.

Powder Lot Number	Crystalline Phase via XRD	Particle Morphology via TEM ^a	Mean Particle Size via Coulter (nm)	Standard Deviation of Particle Size Dist. (nm)	Specific Surface Area via 5-pnt. BET (m ² /g)	XRD Crystallite Size (nm)	XRD Crystalline Strain (%)	Ba/Ti via XRF (at CPM)
22	Cubic BaTiO ₃ ^a	E	75.4	44	17.97	30.9	0.220	1.016
23	Cubic BaTiO ₃ ^a	E,A	74.5	43	35.53	27.4	0.234	0.960
24	Cubic BaTiO ₃ ^a	E	81.0	47	25.52	25.9	0.224	0.980
25	Cubic BaTiO ₃ ^a	E	75.6	46	21.16	25.4	0.235	1.014
26	Cubic BaTiO ₃ ^a	E,A	75.0	43	24.70	17.4	0.311	1.025
27	Cubic BaTiO ₃ ^a	E	75.8	41	24.26	24.1	0.260	1.026
28	Cubic BaTiO ₃ ^a	E	77.1	40	16.79	21.9	0.311	1.006
CPM BT-16 6670-70	Cubic BaTiO ₃ ⁱ	E,B	88.7	57	15.93	28.9	0.267	1.023
CPM BT-8 R59	Cubic BaTiO ₃	E	193.0	67	8.2	24.14	0.267	1.003
Average Value of powders 22-25			76.6	45	25.05	27.4	0.228	0.993
95% Confidence Interval (if 22-25 represent only one population)			± 3.4	± 5	± 14.0	± 10.9	± 0.094	± 0.036
Physical Range			74.5- 81.0	40-47	17.8-35.5	25.4-30.9	0.220- 0.235	0.960- 1.016

i. Slight BaCO₃ contamination (ICPDS card number 5-378)ii. Moderate BaCO₃ contamination (ICPDS card number 5-578)

iii. E = equiaxed morphology, A = some asymmetrical particles, B = bimodal distribution

- (a) Calculation of naïve main effect for each treatment and average of the population, Avg. Y, assuming only one population exists for powder lot numbers 22-25.

Powder Lot	Treatment A (Inject Temp.)	Treatment B (Inject Rate)	Treatment C (Ba/Ti)	Treatment D ([EDTA])	Particle Size (in nm)
22	-75.4	-75.4	75.4	75.4	75.4
23	74.5	-74.5	-74.5	74.5	74.5
24	-81.0	81.0	-81.0	-81.0	81.0
25	75.6	75.6	75.6	-75.6	75.6
Y _i -Y (Sum Col.)	-6.3	6.7	-4.5	-6.7	306.5
Main Effect of Treatment	-3.15	3.35	-2.25	-3.35	
Avg. Y=					76.63

- (b) Estimate of variance, S^2 , from replicate runs, lots 26-28, at center point

Powder Lot	Particle Size (in nm)
26	75.0
27	75.8
28	77.1
Column Sum	227.9
Avg. Y	76.0

then

$$S^2 = \text{Sum}[(y_i - \text{Avg. Y})^2] / (n-1) \quad \text{where } n=3$$

$$S^2 = 1.12$$

- (c) Using estimated S^2 on fractional factorial design, powder lots 22-25

$$\eta = \text{Avg. Y} \pm t_{v,0.025}[S^2 * (1/n_+ + 1/n_-)]^{1/2} \quad \text{where } v = 3, n_+ = 2, \text{ and } n_- = 2$$

$$\eta = 76.63 \pm (3.182)[(1.12)(1/2 + 1/2)]^{1/2}$$

$$\eta = 76.63 \pm 3.37$$

$$P(73.3 < \eta < 80.0) = 0.95$$

Figure 4.3. Experimental calculation matrix for the particle size of BaTiO₃ powder lot numbers 22-25, including the calculation of the naïve main effects of treatments and the estimate of variance, S^2 , from the replicate powder lots 26-28.

result by half of the total number of experiments (i.e., $n/2$ or 2). The calculated main effects are located within both Figure 4.3 and Table 4.4, where a negative value for the calculated main effect indicates that the particle size varies inversely with the low and high level designations of the treatment.

4.3.2.2 Estimation of population variance

The estimate of the population variance (or width) of the four experiments of the fractional factorial design was performed by first estimating the particle size variance of the three replicate runs, experiments 26 through 28, at the center point of the design. The estimate of variance, S^2 , was calculated by the following equation where y_i is the particle size for each experiment (i.e., 75.0, 75.8, and 77.1 nm), Avg. Y is the average of the three experiments (i.e., 76.0), and n is the total number of experiments (i.e., 3).

$$S^2 = S [(y_i - \text{Avg. } Y)^2] / (n-1) = 1.12 \quad [4.1]$$

The estimate of variance, 1.12, is utilized in the calculations for the fractional factorial design to determine the statistical significance of the treatment effects.

4.3.2.3 The 95% confidence interval and statistical significance

In determination of the statistical significance of data, the null hypothesis is first assumed, that is, that the treatments (time, temperature, etc.) have no effect on the observation (in this example, the particle size). Therefore, it is assumed that all treatment effects, τ_i , equal zero in the model $y_i = \eta + \tau_i + \epsilon_i$. The physical description of the null hypothesis model that defines each particle size observation (y_i) is the result of the particle size population mean (η) plus an arbitrary inherent experimental error (ϵ_i). If the treatments have no effect as defined by the null hypothesis, then all calculated main effects should lie

Table 4.4. Summary of naïve main effects of treatments on the particle size where statistically significant treatments are distinguished by a shaded region.

	Treatment / Observed Particle Attributes	Mean Particle Size (nm)	Standard Deviation of PSD (nm)	Specific Surface Area (m ² /g)	XRD Crystallite Size (nm)	XRD Crystallite Strain (%)	Ba/Ti Product Ratio via XRF
A	Injection Temperature	-3.15	-1	6.6	-2.0	0.0125	-0.011
B	Injection Rate	3.35	3	-3.4	-3.5	0.0025	0.009
C	Ba/Ti Precursor Ratio	-2.25	0	-11.0	1.5	-0.0015	0.045
D	[EDTA]	-3.35	-3	3.4	3.5	-0.0025	-0.009
95% Confidence Interval		± 3.37	± 5	± 14.0	± 10.9	± 0.094	± 0.036

within a 95% confidence interval for the four powder population, which is given by the equation:

$$\eta = \text{Avg. } Y + t_{v,0.025}(S^2/n)^{1/2} = 76.6 \pm 3.4 \quad [4.2]$$

where the Avg. Y is the average particle size of the four runs, $t_{v,0.025}$ is the value of the Student's t-distribution for three degrees of freedom, S^2 is the estimate of variance calculated from the three replicate runs, n is the total number of experiments, four. If the naïve estimate of the main effect for any one treatment lies outside the confidence interval (CI), then the null hypothesis is refuted and the main effect cannot be assumed to belong to the single population. Therefore, the effect of the treatment is considered to be statistically significant. Conversely, if the calculated main effect of a variable lies within the CI, then it cannot be distinguished from the main population. The variable would be deemed statistically insignificant.

Table 4.4 highlights the two treatments which exhibit the greatest effect in altering the particle size of BaTiO₃ powders, the injection rate of the Ba(OH)₂ and the EDTA concentration. Since the calculated main effects of both treatments lie on the border of the confidence interval, further experimentation must be performed in order to determine the statistical significance of either treatment. Qualitatively, particle size decreases with increasing EDTA concentration and decreasing injection rate. It is important to note that a strong complexing agent such as EDTA, within the employed concentration range, affects the solubility of the Ti gel to a level which minimally modifies the particle size. The industrial implication is that minute fluctuations in the gel chemistry may produce particles of nearly similar size, since the above concentrations of a strong complexing agent exhibit only minor effects in the final particle diameter.

4.3.3 Effect of Treatments on the Barium Titanate Particle Size Distribution

Similar calculations were performed to estimate the main effect of the treatments on the BaTiO_3 particle size distribution derived from the Coulter LS230. For each treatment, the value of the calculated main effect was within the boundary of the 95% CI. Therefore, the null hypothesis was accepted. None of the four treatments modified the distribution in a statistically significant manner. The average standard deviation of the particle size distribution of the four runs was 45 nm.

4.3.4 XRD Line Profile Analysis

4.3.4.1 Effect of treatments on barium titanate crystallite size

The average crystallite size of the 4 powders was equal to 27.4 ± 10.9 nm via calculation of a 95% confidence interval from the three replicate powders. Crystallite sizes ranged between 25.4-30.9 nm. By factorial design analysis similar to that used to determine the Coulter particle size (Table 4.3), all treatments were shown to exhibit a statistically negligible effect on the crystallite size derived from planes normal to the [100]. The null hypothesis was accepted. The quantification of the crystallite size of 25-30 nm is based on a diffraction phenomena. Therefore, the crystallite size is a convoluted measurement of the crystalline substructure, including the grain size, domain size, and other defects.

The observed smaller crystallite size is comparable to the 68-95 nm and 40-52 nm hydrothermally derived BaTiO_3 crystallites reported by independent laboratories [Kum95, Viv89] which employed the amorphous Ti gel and $\text{Ba}(\text{OH})_2$ systems without $\text{Ba}(\text{OH})_2$ injection. The size also matches the 35-50 nm crystallites reported by Eckert et al. when using a static reaction of barium hydroxide and anatase precursors in a ratio of 1.0 [Eck96]. Kumazawa et al. [Kum96] showed the mean particles size to decrease from 200 nm to 55 nm with an increase of the Ba/Ti ratio when using the amorphous gel. However, the crystallite size remained constant at approximately 40-50 nm for all Ba/Ti ratios. Two

significant points are evident. First, the observed crystallite sizes match the sizes reported via several investigations [Eck96, Shv79] and are slightly smaller than the 47 nm crystallites produced by Kumazawa's experiments using the same precursor Ba/Ti. This decrease of the substructure size may be attributed to several experimental differences such as precursor preparation or the method of a precursor introduction. Second, the relatively constant crystallite size over a range of Ba/Ti precursor ratios is not unlike that reported by Kumazawa. Though the crystallite size indicates an x-ray phenomena, the observance of nearly equal particle sizes and crystallite sizes may indicate the presence of single crystals in Kumazawa's work at precursor $\text{Ba/Ti} \geq 2$.

4.3.4.2 Effect of treatments on barium titanate crystallite strain

In performing the Warren-Averbach line profile technique, calculation of the crystallite strain within a given direction is possible. The strain within the directions perpendicular to the (100) of the four powders provided an average value of 0.228%, where strains ranged between 0.220-0.235%. Similar to the evaluation of crystallite size, analysis of the treatment effects proved all treatments statistically insignificant with respect to the crystal strain, Table 4.3. As illustrated in the literature, the strain associated with as-synthesized hydrothermal particles is attributed to hydroxyl incorporation within the BaTiO_3 lattice [Hen91, Shi97, Wad96, Viv87].

BaTiO_3 powders, CPM lot R59 and CPM lot 6670-70, were synthesized from similar precursors and were acquired from CPM. The magnitude of the observed crystallite strains of lots 22-28 closely matched the measured 0.267% strain in the industrially synthesized BaTiO_3 powders. The strain within the directions perpendicular to the (h00) planes of powders produced in the initial twenty experiment design (Chapter 3) and following chapter (i.e., barium hydroxide precharging and BaTiO_3 seeding experimentation) ranges between 0.204-0.382%, where strains of 0.220-0.270% are most common. Though numerous XRD generated crystallite sizes have been reported to discern

the property versus particle size relationship of dielectric powders, fewer reports of XRD quantified crystalline strain exist. In one such study, Vivekanandan and Kutty [Viv89] reported no net strain perpendicular to the (h00) planes and a strain of 0.08-0.19% perpendicular to the (hko) planes via line broadening methods based on Cauchy and Gaussian fits.

4.3.5 Transmission Electron Microscopy

All employed sets of treatments have produced a majority of distinct, equiaxed polycrystalline particles with some asymmetrical, ellipsoidal particles. The powders exhibit diameters between 30-120 nm and an equiaxed morphology similar to particles shown in the TEM photomicrographs Figure 4.4. As illustrated by the loose agglomerate of powder lot 27 in Figure 4.4(c), the particle distributions are near monosized. The diameter of the observed particles corroborates the average 70-80 nm particle size analysis by Coulter LS230 light scattering system.

4.3.6 Effect of Treatments on Barium Titanate Specific Surface Area

The specific surface area (SSA) of the particles ranged from 18.0-35.5 m²/g and exhibited an average SSA of 25.0 m²/g. The accuracy of the stations is given by $\pm 5.0\%$ by running a standard of known SSA. The precision of the three BET stations was calculated as $\leq \pm 0.7\%$. All analyses on the hydrothermally derived BaTiO₃ powders produced a C constant ≥ 50 , thereby signifying reliable SSA data. Upon insertion of the surface area results into the statistical matrix, the calculated 95% confidence interval was determined as ± 14.0 m²/g. No treatments are statistically significant.

The inflated value of the estimate of variance, S^2 , of the SSA population (Table 4.4) is attributed to the fluctuation of the surface area of lot 28. Contrary to instinctive beliefs, the calculated main effect of the precursor Ba/Ti shows a simultaneous decrease in the particle size and surface area with increasing Ba/Ti. Previous authors have reported a

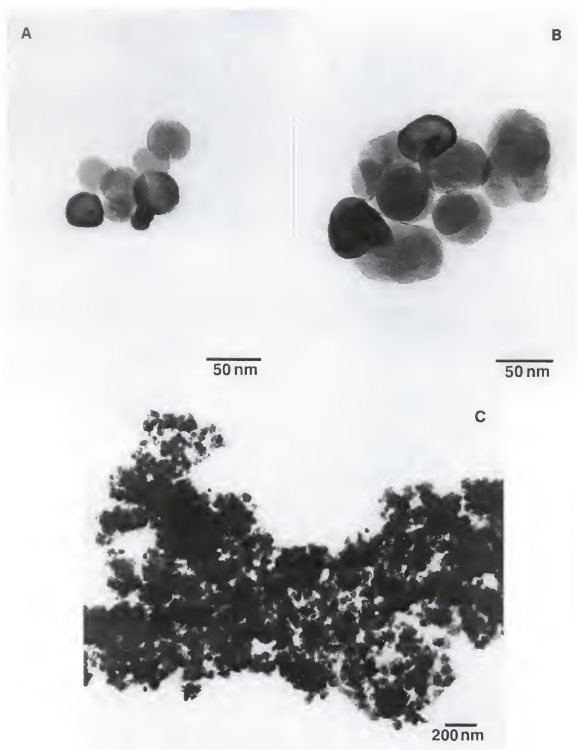


Figure 4.4. TEM photomicrographs illustrate the distinct, spherical polycrystalline particles for all lots. Most powders are representative of (a) lot 22 and (b) lot 28, and exhibit a nearly monosized distribution as shown by (c) the loose agglomerate of powder lot 27.

decrease in the particle size and assumed increase in SSA with increasing BT precursor molar ratio [Kum96, Wad95]. In addition, the calculated particle diameters from the measured SSA are smaller than the particle size reported by the Coulter LS230 and the size observed via TEM for all particles. This can be explained by the assumptions of the surface area to particle size conversion, i.e., smooth, dense, ideally spherical powders. Thus, the fluctuations may indicate a change in surface roughness, the presence of contaminant phases such as unreacted anatase or BaCO_3 , the formation of lower density BaTiO_3 particles, or slight modification of the particle symmetry. BaCO_3 contamination is expected to increase the specific surface area due to the acicular morphology of BaCO_3 when formed under hydrothermal conditions [Mil90] and lower theoretical density than BaTiO_3 (i.e., 4.3 g/cm^3 and 6.0 g/cm^3 , respectively) [Lid94]. Although not observed in the TEM photomicrographs, high SSA, loose agglomerate structures as reported by Miller may have been present in addition to the dense BaTiO_3 particles and account for the increase in SSA [Mil90]. The lowest measured product Ba/Ti, 0.96, also exhibited the highest SSA. This might be attributed to an unreacted, titanium-based contaminant phase as in the 20-experiment series. Notably, the typical SSA of the EDTA derived powders is larger than powders produced in the $\text{Ba(OH)}_2 \cdot 8\text{H}_2\text{O}$ precharging experiment series (Chapter 5).

4.3.7 Effect of Treatments on Barium Titanate Product Ba/Ti

Only the precursor Ba/Ti was shown to affect the product Ba/Ti ratio in a statistically significant manner. The direct relationship as shown in Table 4.4 is attributed to the formation of BaCO_3 contamination as described in the prior discussion of phase purity. An increase in the excess barium available in solution promotes the formation of barium carbonate from various contaminant sources of carbon dioxide.

4.4 Conclusions

Submicron, equiaxed particles which exhibited x-ray diffraction patterns representative of cubic barium titanate were synthesized between a number frequency mean

particle size of 74-81 nm, crystallite size of 25.4-30.9 nm, specific surface area of 18-36 m²/g, Ba/Ti of 0.960-1.012, and exhibited a crystallite strain of 0.22-0.23% perpendicular to the (100). Based on the variable levels employed in the current experimental design, no treatments were shown to exhibit a statistically significant effect on the particle size and distribution. EDTA additions show limited alteration of the BaTiO₃ particle size in the investigated range of EDTA concentration. However, the observed SSA of the powders synthesized in the presence of EDTA are typically larger than those produced by the Ba(OH)₂·8H₂O precharging experimental design. Further experimentation is required to elucidate the effects of EDTA and the degree of complexation of the barium and titanium species. An increase in the EDTA concentration is suspected to exhibit a more distinct effect on the BaTiO₃ particle size and reaction kinetics via modification of the hydrated titanium oxide gel solubility.

CHAPTER 5

EFFECT OF BARIUM HYDROXIDE PRECHARGING AND OTHER PROCESS VARIABLES ON HYDROTHERMALLY SYNTHESIZED BaTiO₃

5.1 Introduction

Since the discovery of barium titanate (BaTiO₃) in the 1940s, it remains the most commercially significant and widely investigated of the oxygen octahedral ferroelectrics [Her85, Kan87, Kin76, Lin77, Ras55, Ric92, Swa97]. During this time, BaTiO₃-based powders have been synthesized by conventional calcination [Alc91, Bea83, Fer91], electrochemical-hydrothermal methods [Bac92, Ben93, Ven95], hydrothermal methods [Dut94, Fla55, Hen91, Kut84, Shv79, Wad96], and solution techniques at lower temperatures [Bru93, Dog97, Kle89]. Due to the advances in multilayer capacitor (MLC) wet-laydown technology, the need to remain cost competitive in the electronic component industry, and the desire to improve the volume efficiency of capacitors (i.e., capacitance/volume), a demand exists for BaTiO₃ powders which can deliver superior performance in fired dielectric layers < 5 μm in thickness [Daw88, Kan95, Bee97, Ven98].

Solution-based techniques provide desirable characteristics such as increased chemical homogeneity, a smaller particle size, and uniform morphology [Bru93, Daw88]. The hydrothermal technique offers additional advantages, high yield and the direct production of crystalline powders at low temperatures (i.e., $\leq 200^\circ\text{C}$) in less than fifteen minutes at the reaction temperature. BaTiO₃ powders produced via other techniques, such as conventional calcination, oxalate-derived, and sol-gel-derived methods, may require additional crystallization heat treatments and/or milling prior to use in forming operations [Fax70, Phu90, Suy94]. In both scenarios, improper application of the

respective secondary processes may produce an aggregated powder unfit for use in ultrathin layers. The competitiveness of such techniques is further lessened if solution chemistry is not appreciated during wet milling and an unanticipated nonstoichiometric surface results [Ada87, And87, Cho96b, Len93]. With regard to the perceived increased cost of hydrothermally derived powders in comparison to conventional solid-state powders, the MLC manufacturing costs are offset by the ability to produce ultrathin layers and the use of decreased sintering temperatures [Abe91, Daw91], less noble electrode systems [Phu90], and decreased quantities of dielectric and metal powders [Bru93]. In addition, aqueous-based MLC fabrication techniques are relatively inexpensive and benign in comparison to the purchase and disposal costs and hazardous nature of organic solutions.

A viable dielectric layer $< 5 \mu\text{m}$ in thickness requires the use of uniform submicron powders which maintain a near-equiaxed morphology to enable a tight randomly packed, cast structure. In general, the particle size of powders precipitated from solution can be altered by control of the competition between the nucleation and growth processes [LaM50, Nyv85]. Typically, solution seeding [Bel98], alteration of the stirring rate [Soh92], and modification of the solubility and/or supersaturation of the reactant species are used to promote or inhibit either nucleation or growth [Rin96]. In contrast to some conventional solution precipitation techniques, the stirring rate has been shown to be insignificant during the hydrothermal synthesis of BaTiO_3 from 100 to 600 rpm [Kum95]. Other hydrothermal BaTiO_3 powder investigations have shown the form of the titanium precursor to be of utmost importance [Kum95, Kum96, Moo96, Shi97, Xia96]. Of the investigated precursors, the amorphous hydrated titanium oxide gels have shown an increased reactivity and the smallest BaTiO_3 particle size with respect to the crystalline oxide precursors, anatase and rutile [Kum96, Moo96, Shi97, Xia96]. In addition, researchers report the significance of the precursor Ba/Ti in the formation of

smaller particles [Kum96, Wad95] and in the promotion of hydrothermal reaction kinetics [Kan75, Xia96]. Lastly, the alkalinity of the reaction medium has been noted to improve reaction kinetics [Xia96] and even inhibit BaTiO₃ formation if the solution is not sufficiently alkaline [Ish90, Moo96]. Based on these discoveries, the following experimental design investigates the use of (1) an amount of Ba(OH)₂·8H₂O introduced to a hydrated titanium oxide (TiO_xOH_y) gel prior to the bulk Ba(OH)₂·8H₂O injection, (2) a range of Ba(OH)₂·8H₂O injection rates not investigated in the rapid injection work of the initial 20-experiment design, (3) a range of increased precursor BT molar ratios (Ba/Ti), and (4) a range of injection temperatures. A 3-experiment series also was performed to investigate the effect of particle seeding at various concentrations with a Cabot Performance Materials 16 m²/g BaTiO₃ powder (lot 6670-70, Boyertown, PA).

5.1.1 Hydrothermal Synthesis

Hydrothermal synthesis is defined, in terms of ceramic powder synthesis, as the treatment of precursors in an aqueous environment at elevated temperature and pressure to produce a crystalline substance [Daw88]. The technique was employed to synthesize BaTiO₃ for pigment applications as early 1940 [Pet40]. Most of the previous aqueous-based synthesis entailed the loading of all precursors for any given reaction within the reaction vessel, sealing the vessel, and ramping the temperature to the desired isothermal condition, where the reactants were soaked for a given time (with or without agitation) as illustrated in Chapter 2. In fact, the only investigated process which employed an injection system (other than Cabot's patented hydrothermal method [Men89a, Men89b]) was that of Her and Matijevec, in which the double injection of both titanium and barium chloride precursors was used to coprecipitate powders [Her95a]. The general noninjection reactions differ from injection systems in that high hydroxide concentrations are maintained with respect to temperature prior to the incipient precipitation. Secondly, assuming that the solution is not saturated in the noninjection system, all of the barium

precursor is available for reaction immediately following the initiation of precipitation. The rate limiting factor of the precipitation is determined by the mechanism of formation and varies with the nature of the titanium precursor. Solution conditions when using an injection system require that the initial injected $\text{Ba}(\text{OH})_2 \cdot 8\text{H}_2\text{O}$ contribute to increasing both the solution pH and the concentration of aqueous barium species, $\text{Ba}^{2+}(\text{aq})$ or $\text{BaOH}^+(\text{aq})$, to produce conditions favorable for the production of BaTiO_3 . Thus, the effect of $\text{Ba}(\text{OH})_2 \cdot 8\text{H}_2\text{O}$ addition prior to the bulk $\text{Ba}(\text{OH})_2 \cdot 8\text{H}_2\text{O}$ injection may provide insight to the differences between the noninjection and injection methods and further elucidate the effect of the $\text{Ba}(\text{OH})_2 \cdot 8\text{H}_2\text{O}$ on the final powder attributes.

5.1.2 BaTiO_3 Seeding

Generally, precipitation occurs from high supersaturation conditions which cause rapid nucleation rates. In turn, the rapid nucleation consumes a majority of the precursor stock prior to particle growth in a batch reaction. The result of solution precipitation methods is small crystals present in high concentrations of about 10^{11} to 10^{16} particles/cm³ [Soh92]. Therefore, seeding techniques require the use of high seed concentrations in order to be effective in avoiding homogeneous nucleation or heterogeneous nucleation on the vessel walls, cooling coil, or agitator components. Provided the seed concentration is sufficient and nucleation is exclusive to the seed particles, the seed concentration and overall reactant concentration may be tailored to produce a desired particle size. Bell et al. have shown hematite seeds useful in seeding the glycothermal dehydroxylation of gibbsite to produce α -alumina powders under reaction temperatures and pressures similar to the hydrothermal technique [Bel98].

The possibility of self-seeding the BaTiO_3 system with BaTiO_3 particles is suggested by several research reports, but results have not yet been reported in the hydrothermal powder literature. For example, the heterogeneous (rather than homogeneous) nucleation of BaTiO_3 occurs on anatase particles in the hydroxide-anatase

hydrothermal reaction [Chi95, Eck96, Zha96]. In electrochemical-hydrothermal and hydrothermal reactions, BaTiO_3 was grown from the reactant titanium metal substrates [Bac92, Ben93, Ish90, Kaj91, Ven95, Yos89]. Heteroepitaxial growth of BaTiO_3 from SrTiO_3 single crystals also was shown from hydrothermal solutions [Chi95]. Also supportive of the probability of seeding is the research of single crystal synthesis methods which employ various seeding techniques [Gar96, Reh98, Yoo97].

5.1.3 Experimental Design

Experimental designs have been well documented by texts throughout the 1940s and 1950s, but have yet to be employed in the solution synthesis of ferroelectric powders [And52, Coc57, Fed55, Kem52, Pla46]. The technique is especially useful in studying the hydrothermal process due to the inherent closed nature of the reaction. Presently, hydrothermal research is divided into two methods: trial and error investigations of final particle attributes, and low temperature studies to determine formation mechanisms. Due to the rapid reaction kinetics, low temperatures are necessary to enable the measurement of crystal growth [Eck96, Her88, Moo96]. Since the conclusions of low temperature studies may not be extrapolated to real process conditions with certainty, the author chose to perform a statistical post-mortem analysis based on the nucleation temperatures reported by low temperature investigations.

The use of statistical DOE allows one to efficiently screen or optimize the process to quantifiably determine the predominant variables and multivariable relationships (or interactions) which affect final product attributes. In addition, the statistical-based approach permits estimation of the reproducibility of the process and calculation of confidence intervals for all variable effects. In this research, a screening fractional factorial design was employed to gain an understanding of variable effects in the presence of a precharged concentration of $\text{Ba}(\text{OH})_2 \cdot 8\text{H}_2\text{O}$ and to determine the viable processing window.

Similar to the EDTA experimentation of Chapter 4, a 2^{4-2} fractional factorial design with center point analysis (Table 5.1) was employed in order to analyze four treatments. All treatments and levels were identical to the EDTA matrix, except that a small amount of $\text{Ba}(\text{OH})_2 \cdot 8\text{H}_2\text{O}$ was added to the titanium gel at room temperature, as shown in Table 5.2.

Table 5.1. Fractional factorial design with replicated center point to estimate the variance where columns A through D represent the investigated treatments.

Lot #	A	B	C	D	Observation
29	-1	-1	+1	+1	
30	+1	-1	-1	+1	
31	-1	+1	-1	-1	
32	+1	+1	+1	-1	
33	0	0	0	0	
34	0	0	0	0	
35	0	0	0	0	

Table 5.2. Investigated treatments and treatment level of the employed 2^{4-2} fractional factorial design. All experiments were performed with a stirring rate of 350 rpm, 200°C reaction temperature, 10 min reaction time, and BaTiO_3 product loading of 0.356 mol/L assuming complete conversion of the hydrated titanium oxide gel.

	Treatment	Low Value	Center Value	High Value
A	Temperature of $\text{TiO}_x(\text{OH})_y$ gel on injection of $\text{Ba}(\text{OH})_2 \cdot 8\text{H}_2\text{O}$ ($^\circ\text{C}$)	50	70	90
B	Injection Rate (ml/min)	15	30	45
C	Ba/Ti Precursor Ratio	1.2	1.5	1.8
D	$\text{Ba}(\text{OH})_2 \cdot 8\text{H}_2\text{O}$ Precharge Concentration (% of total charge)	2	6	10

5.2 Materials and Methods

5.2.1 Hydrothermal Synthesis

Seven BaTiO₃ powder batches were synthesized with CO₂-free deionized water, as illustrated in the process flow diagram in Figure 5.1. Variable levels and the specific variable levels for every batch are listed in Table 5.1 and Table 5.2, respectively. The titanium precursor consisted of a high surface area, 240 m²/g, amorphous hydrated titanium oxide gel (TiO_x(OH)_y) from CPM, Boyertown, PA. The gel was weighed into a Ti reaction vessel, placed in the autoclave, purged with nitrogen, sealed to the atmosphere, and ramped at approximately 1.2°C/min to the predetermined injection temperature. In a separate Teflon container, an aqueous solution of Ba(OH)₂·8H₂O was heated to 95°C. On achievement of the injection temperature (i.e., the temperature of the TiO_x(OH)_y gel slurry in the autoclave), the 95°C barium hydroxide solution was introduced to the injection apparatus, filtered through a 5 µm Teflon filter to remove possible BaCO₃ contaminant particles, and injected into the autoclave. After injection, the autoclave was ramped at an approximate rate of 1.4°C/min to a 200°C reaction temperature, soaked at the reaction temperature for 10 min under autogenous pressure (< 300 psi), and cooled to room temperature. All autoclave reactions were performed under mechanical agitation at 350 rpm since this variable was shown to be relatively insignificant with respect to other hydrothermal variables [Kum95]. The precursor Ba/Ti ratios of 1.2 and 1.8 correspond to final Ba(OH)₂·8H₂O concentrations of 0.427 M and 0.641 M, respectively.

Following autoclave disassembly, the target 50 g of powder per batch was rinsed with a deionized water wash (adjusted to pH 10.7 with ammonium hydroxide) using a centrifugation (3500 rpm) and decantation technique. The wash and solution pH adjustment are necessary to remove the excess barium precursor from solution while retaining a stoichiometric particle surface. Incongruent dissolution of barium from the

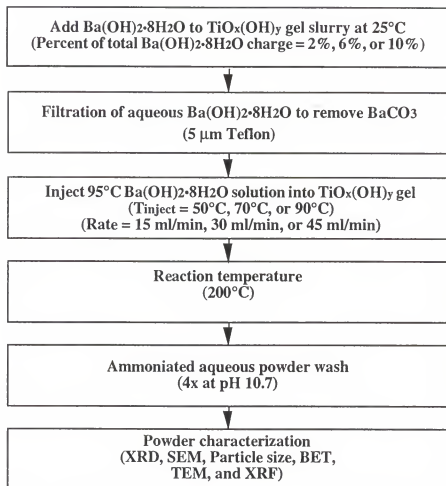


Figure 5.1. Flow diagram of hydrothermal synthesis, washing, and characterization of BaTiO_3 powder lot numbers 29-35. A percentage of the total $\text{Ba(OH)}_2 \cdot 8\text{H}_2\text{O}$ charge was introduced at room temperature prior to the bulk $\text{Ba(OH)}_2 \cdot 8\text{H}_2\text{O}$ injection.

BaTiO₃ has been well documented [Ada87, Cho96b, Len93, Ute90], yet seldom considered in recent experimental studies, as shown in Table 2.1. After the fourth and final wash, the powders were stored in the wash solution until the powders were vacuum dried at 160°C for ≥ 8 hours prior to characterization.

The three seeding experiments were conducted with the CPM BaTiO₃ powder lot 6670-70 which exhibited a specific surface area of 16 m²/g. Hydrothermal experiment numbers 36, 37, and 38 employed zero, 1×10^{10} , and 1×10^{13} seeds/ml, respectively. The highest seed concentration required 2.6 g of BaTiO₃ seeds. Thus, further increase of the seed concentration is not desirable since 1×10^{14} seeds/ml would require an amount of seeds which equal to 50% of the total weight of the target 50 g powder yield. The seeds were introduced to the titanium gel at room temperature. Barium hydroxide precharging was not employed in this experiment. A constant precursor Ba/Ti of 1.2, [Ba(OH)₂·8H₂O] of 0.257 M, injection temperature of 70°C, injection rate of 15 ml/min, reaction temperature of 200°C, and reaction time of 10 min were employed in all three experiments. Other process techniques were similar to those described in the above fractional factorial design.

5.2.2 Powder Characterization

Characterization for both the seven-experiment design and the three seeding experiments were performed similar to the methods described in 3.2.2. All properties except the particle density were investigated.

5.3 Results and Discussion

5.3.1 Phase Purity

Evaluation of the TiO_x(OH)_y gel indicated that the as-received gel was x-ray and TEM amorphous. XRD, shown in Figure 5.2, also illustrated diffraction patterns representative of the crystalline, cubic BaTiO₃ for all synthesized BaTiO₃ powders

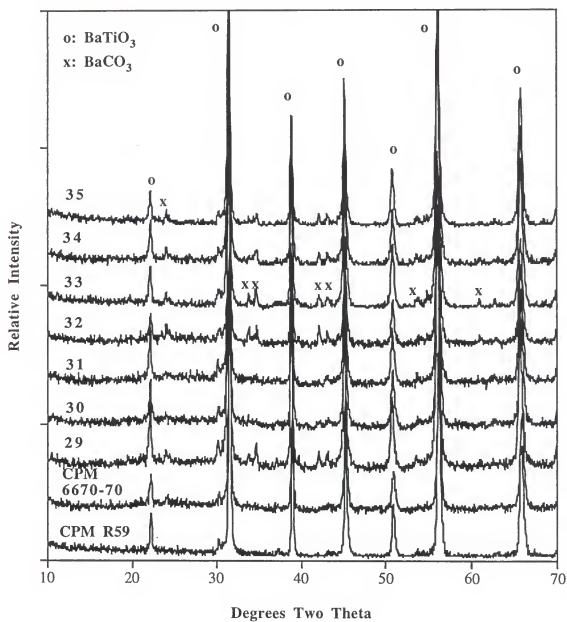


Figure 5.2. Room temperature XRD analyses of the as-synthesized BaTiO₃ powder lot numbers 29-35 and CPM powder lot numbers 6670-70 and R59, which illustrate XRD patterns representative of the cubic crystalline phase and some BaCO₃ contamination.

similar to CPM powder lots number R59 and 6670-70. As illustrated in Figure 5.2, modest BaCO_3 contamination was noted on most powders. This is consistent with the findings of Xia and colleagues [Xia96] when employing high Ba/Ti precursor ratios (i.e., ≥ 1.5). Powder contamination may be attributed to the carbon dioxide present in the as-received $\text{TiO}_x(\text{OH})_y$ gel since the gel synthesis operation is exposed to the atmosphere, incomplete N_2 purging of the autoclave, or reaction of the excess $\text{Ba}(\text{OH})_2 \cdot 8\text{H}_2\text{O}$ with atmospheric CO_2 on exposure during the washing and dewatering processes. The BaCO_3 was not formed as a result of improper final solution conditions, since a high reaction pH was maintained due to the use of high Ba/Ti ratios and $\geq 0.3 \text{ M}$ $\text{Ba}(\text{OH})_2 \cdot 8\text{H}_2\text{O}$ as the Ba precursor. The final solution pH was observed to range from pH 12.9-13.5, depending on the $\text{Ba}(\text{OH})_2 \cdot 8\text{H}_2\text{O}$ content. Theoretical modeling [Ada90, Len93, Ute90] and empirical observations [Ben93, Moo96] have shown that a solution pH > 12.0 is required for the synthesis of phase pure BaTiO_3 as demonstrated in Figure 2.9. With regard to the precursor concentration, Moon showed that $\geq 0.2 \text{ M}$ of $\text{Ba}(\text{OH})_2 \cdot 8\text{H}_2\text{O}$ is necessary to avoid the preferential formation of barium carbonate in the $\text{Ba}(\text{OH})_2 \cdot 8\text{H}_2\text{O}$ and hydrated $\text{TiO}_x(\text{OH})_y$ gel precursor system [Moo96].

Other hydrothermal synthesis studies have reported the formation of the metastable cubic phase at or near a Ba/Ti precursor ratio of 1 at relatively low reaction temperatures [Shi97, Viv89]. However, most reports note the difficulty in discerning the two phases due to the x-ray line broadening of room temperature samples and have instituted differential scanning calorimetry [Dut94, Mil90], full-width-half-maximum x-ray peak measurement versus temperature [Mil90], and the dielectric measurement of fluid composites [Mil90]. The observance of a cubic-like pattern is attributed to strain compensation for both the incorporated hydroxyl point defects and the small particle size [Sla96, Viv87, Xia96]. Shi et al. show the observation of the metastable cubic state is simultaneously noted with an increase in the concentration of hydroxyls and charge

compensating barium vacancies [Shi97]. X-ray analysis of the CPM R59 sample from room temperature to 170°C showed no visible change in the crystal structure associated with the typical 120°C tetragonal to cubic transition and thus corroborated the low temperature assessment of a cubic phase. Tetragonality was restored to CPM R59 hydrothermal particles by heating to temperatures > 1000°C. This also has been observed in other investigations [Hen92b, Shi97, Viv89, Wad96]. Restoration is attributed to the removal of residual hydroxyls and grain growth during the sintering process where initial sintering of the R59 powder at 900-950°C was measured by dilatometry at CPM. Thermogravimetric/differential thermal analysis (TG/DTA) exhibited weight loss to at least 1000°C and suggests the removal of water, as shown by Herard et al. [Her95b]. On increase of the hydrothermal precursor Ba/Ti ratio to ≥ 1.6 -2 and/or increase of the reaction temperature (240-300°C) for extended reaction times (8 h to 7 days), increased tetragonal character has been attained [Dut94, Shi97]. However, the high reaction temperature and safety concerns regarding the associated pressures, extended reaction times, use of excess barium precursor, high probability of carbonate contamination, and the ease of tetragonal restoration during normal MLC firing deem the production of tetragonal-based hydrothermal powders unnecessary (if not industrially unprofitable) for generic capacitor applications.

5.3.2 Effect of Treatments on Particle Size

Particle size distributions measured by the Coulter LS230 indicated a number frequency mean particle size between 73.2 nm and 94.6 nm, as shown in Table 5.3, the summary of characterization results. Particles of this size are representative of particles produced via the hydrothermal reaction, as shown in Table 2.1. Estimation of the main effect of the treatments was performed by placing the average particle size data within the design matrix as described below.

Table 5.3. Characterization results of the hydrothermal BaTiO₃ powder lot numbers 29-35.

Powder Lot Number	Crystalline Phase via XRD	Particle Morphology via TEM	Mean Particle Size (nm)	Standard Deviation of Particle Size Dist. (nm)	Specific Surface Area (m ² /g)	XRD Crystallite Size (nm)	XRD Crystallite Strain (%)	Ba/Ti of Product via XRF
29	Cubic BaTiO ₃ ⁱ	E ⁱⁱⁱ	73.2	40	17.8	24.7	0.204	1.012
30	Cubic BaTiO ₃ ⁱ	E,A	94.6	62	12.6	28.4	0.249	0.995
31	Cubic BaTiO ₃ ⁱ	E	88.4	57	13.4	25.8	0.278	0.982
32	Cubic BaTiO ₃ ⁱ	E	82.5	29	17.1	26.2	0.260	1.007
33	Cubic BaTiO ₃ ⁱⁱ	E,A	75.0	40	14.5	27.2	0.270	1.004
34	Cubic BaTiO ₃ ⁱⁱ	E	74.0	39	15.0	28.3	0.252	1.004
35	Cubic BaTiO ₃ ⁱⁱ	E	74.8	44	14.6	26.2	0.268	1.001
Average Value of powders 29-32			84.7	47	15.2	26.3	0.248	0.999
95% Confidence Interval ^{iv}			± 1.7	± 8	± 0.77	± 3.3	± 0.031	± 0.007
Observed Range of lots 29-32			73.2-94.6	29-62	12.6-17.8	24.7-28.4	0.204-0.278	0.982-1.012
CPM BT-16 6670-70	Cubic BaTiO ₃ ⁱ	E,B	88.7	57	15.9	28.9	0.267	1.023
CPM BT-8 R59	Cubic BaTiO ₃ ⁱ	E	193.0	67	8.2	24.14	0.267	1.003

i Slight BaCO₃ contamination (ICPDS card number 5-378)ii Moderate BaCO₃ contamination (ICPDS card number 5-378)

iii E = equiaxed morphology, A = some asymmetrical particles, B = bimodal distribution

iv Calculated confidence interval based on the S² value from lots 33-35 and assuming lots 29-32 represent only one population

5.3.2.1 Estimation of population variance

The estimate of population variance for the four batches of the fractional factorial design was performed by first estimating the particle size variance of the three replicate runs, experiments 33 through 35, at the center point of the design. The estimate of variance, S^2 , was calculated by the following equation where y_i is the particle size for each experiment (i.e., 75.0 nm, 74.0 nm, and 74.8 nm), Avg. Y is the average of the replica experiments (i.e., 74.6 nm), and n is the total number of experiments (i.e., 3).

$$S^2 = S [(y_i - \text{Avg. Y})^2] / (n-1) = 0.28 \quad [5.1]$$

The estimate of variance, 0.28, is utilized in the calculations for the fractional factorial design to determine the statistical significance of the treatment effects.

5.3.2.2 Fractional factorial matrix calculations

In determination of the statistical significance of data, the null hypothesis is first assumed, that is, that the treatments have no effect on the observation (in this example, the particle size). Therefore, it is assumed that all treatment effects, τ_i , equal zero in the model $y_i = \eta + \tau_i + \epsilon_i$. The physical description of the null hypothesis model defines each particle size observation (y_i) as the result of the particle size population mean (η) plus an arbitrary inherent experimental error (ϵ_i). If the treatments have no effect as defined by the null hypothesis, then all main effects should lie within a 95% confidence interval for the four powder population, which is given by [5.2] or [5.3]:

$$\eta = \text{Avg. Y} + t_{v,0.025}(S^2/n)^{1/2} = 84.7 \pm 1.7 \quad [5.2]$$

$$P(82.9 < \eta < 86.3) = 0.95 \quad [5.3]$$

where the Avg. Y now represents the average particle size of the four runs, $t_{v,0.025}$ is the value of the Student's t-distribution for three degrees of freedom, S^2 is the estimate of variance calculated from n, the total number of runs in the fractional factorial design. If the naïve estimate of the main effect for any one treatment lies outside the confidence

interval (CI), then the null hypothesis is refuted and the main effect cannot be assumed to belong to the single population. Therefore, the effect of the treatment is considered to be statistically significant. Conversely, if the calculated main effect of a variable lies within the CI, then it cannot be distinguished from the main population. The variable would be deemed statistically insignificant.

After calculation of the 95% confidence interval for the four powder matrix, the naïve main effects for each treatment must be computed. This is accomplished by multiplying the particle size observation of lot number 29 (73.2 nm from Table 5.3) by the variable level value (i.e., -1 or +1) present in each column of the design matrix, Table 5.1, and inserting the product into columns A, B, C, and D, Figure 5.3. Particle size insertion is performed similarly for the remaining lot numbers 30 through 32 to produce the completed calculation matrix, Figure 5.3. The naïve estimate for the main effect of treatment A is calculated by summing column A of Figure 5.3 and dividing the result by half of the total number of experiments (i.e., $n/2$ or 2). The calculated main effects are located within both Figure 5.3 and Table 5.4, where a negative value for the main effect indicates that the particle size varies inversely with the low and high level designations of the treatment.

Table 5.4 demarcates the two treatments which are statistically significant in altering the particle size of BaTiO_3 powders, the temperature of the $\text{TiO}_x(\text{OH})_y$ gel upon injection and the Ba/Ti concentration. Particle size increases with increasing injection temperature and decreasing Ba/Ti precursor molar ratio. The overall magnitude of the observed range of mean particle sizes is modest, 20 nm, yet provides direction for future research. The observed injection temperature-particle size relationship may indicate an enhancement in the growth process, however, the relationship is currently not understood. Decrease of the particle size with increase of the precursor Ba/Ti was

- (a) Calculation of naïve main effect for each treatment and average of the population, Avg. Y, assuming only one population exists for powder lot numbers 29-32.

Powder Lot	Treatment A (Inject Temp.)	Treatment B (Inject Rate)	Treatment C (Ba/Ti)	Treatment D ([EDTA])	Particle Size (in nm)
29	-73.2	-73.2	73.2	73.2	73.2
30	94.6	-94.6	-94.6	94.6	94.6
31	-88.4	88.4	-88.4	-88.4	88.4
32	82.5	82.5	82.5	-82.5	82.5
Y _i -Y (Sum Col.)	15.5	3.1	-27.3	-3.1	306.5
Main Effect of Treatment	7.75	1.55	-13.65	-1.55	
Avg. Y=					84.7

- (b) Estimate of variance, S^2 , from replicate runs, lots 33-35, at center point

Powder Lot	Particle Size (in nm)
33	75.0
34	74.0
35	74.8
Column Sum	223.8
Avg. Y	74.6

then

$$S^2 = \text{Sum}[(y_i - \text{Avg. Y})^2] / (n-1) \text{ where } n = 3$$

$$S^2 = 0.28$$

- (c) Using estimated S^2 on fractional factorial design powder lots 29-32

$$\eta = \text{Avg. Y} \pm t_{v,0.025} [S^2 * (1/n_+ + 1/n_-)]^{1/2} \text{ where } v=3, n_+=2, \text{ and } n_-=2$$

$$\eta = 84.7 \pm (3.182)[(0.28)(1/2+1/2)]^{1/2}$$

$$\eta = 84.7 \pm 1.68 \text{ nm}$$

$$P(83.0 \text{ nm} < \eta < 86.4 \text{ nm}) = 0.95$$

Figure 5.3. Experimental calculation matrix for the particle size of BaTiO₃ powder lot numbers 29-32, including the calculation of the naïve main effects of treatments and the estimate of variance, S^2 , from the replicate powder lots 33-35.

Table 5.4. Summary of naïve main effects of treatments on the particle size where statistically significant treatments are distinguished by a shaded region.

	Treatment / Observed Particle Attributes	Mean Particle Size (nm)	Standard Deviation of PSD (nm)	Specific Surface Area (m ² /g)	XRD Crystallite Size (nm)	XRD Crystallite Strain (%)	Ba/Ti Product Ratio via XRF
A	Injection Temperature	7.8	-3	-0.75	2.1	0.014	0.004
B	Injection Rate	1.6	-8	0.05	-0.5	0.042	-0.009
C	Ba/Ti Precursor Ratio	-13.7	-25	4.40	-1.7	-0.031	0.021
D	[Ba(OH) ₂ ·8H ₂ O] added to TiO _x (OH) _y gel prior to bulk Ba(OH) ₂ ·8H ₂ O injection	-1.6	8	-0.05	0.5	-0.042	0.009
95% Confidence Interval		± 1.7	± 8	± 0.77	± 3.3	± 0.031	± 0.007

reported by several researchers when using noninjection reaction vessel systems [Kum96, Wad95]. Using the injection system, the concentration of the initial charge of $\text{Ba}(\text{OH})_2 \cdot 8\text{H}_2\text{O}$ exhibited no statistically significant effect on the particle size by the creation of nuclei. This was corroborated by the trial seeding experiments, powder lot numbers 36-38, with seed concentrations of zero, 1×10^{10} , and 1×10^{13} seeds/ml, respectively. The average 91 nm, 94 nm, and 81 nm particle sizes of the respective lot numbers 36, 37, and 38 illustrated that particle nucleation and growth occurs as if no seeds were present. TEM analysis confirmed the size results and also did not indicate a bimodal distribution. Since the molar concentration of Ti remained constant at 0.356 M for all experiments, the increased Ba/Ti ratio also increases the barium concentration in solution and solution pH. Both effects are believed to promote nucleation by an enhanced dissolution and recrystallization mechanism, which is discussed in Chapter 6 with reference to the Ba/Ti effects reported by Kumazawa et al. and Wada et al. [Kum96, Wad95].

5.3.3 Effect of Treatments on Particle Size Distribution

Powder lots 29-32 exhibit an average standard deviation of the particle size distribution (PSD) of 47 ± 8 nm, as listed in Table 5.4. The naïve main effects of the injection rate and $\text{Ba}(\text{OH})_2 \cdot 8\text{H}_2\text{O}$ initial charge concentration are located on the boundary of the 95% CI. Thus, the two treatments do not clearly demonstrate statistical significance and will not be discussed. Further experimentation is required to elucidate the effects, if any. Increase of the Ba/Ti, however, markedly decreases the standard deviation of the PSD. As discussed, the increase of Ba/Ti increases the $[\text{Ba}(\text{OH})_2 \cdot 8\text{H}_2\text{O}]$. Provided a more rapid nucleation burst occurred, the ensuing PSD would narrow and more closely resemble the distribution produced by monosized particles [LaM50, Rin96].

5.3.4 XRD Line Profile Analysis

5.3.4.1 Effect of treatments on crystallite size

The average crystallite size of the powder lots 29-32 was equal to 26.3 ± 3.3 nm via calculation of a 95% confidence interval from the three replicate powders. Crystallite sizes ranged between 24.7 nm to 28.4 nm via the Warren-Averbach XRD technique. By factorial design analysis similar to that used to determine the Coulter particle size (Table 5.4), all treatments exhibit a statistically negligible effect on the crystallite size derived from planes normal to the [100]. The null hypothesis was accepted.

The observed 26.3 ± 3.3 nm crystallite size is comparable to the 68-95 nm [Viv89], 40-52 nm [Kum95], and 35-50 nm [Eck96] crystallites of hydrothermally derived BaTiO₃ reported by independent laboratories. Kumazawa et al. [Kum96] showed the mean particles size to decrease from 200 nm to 55 nm with an increase of the Ba/Ti ratio when using the amorphous gel in a noninjection system. However, at the same time the crystallite size remained constant at approximately 40-50 nm for all Ba/Ti ratios. Two significant points are evident. First, the observed near-30 nm crystallites match the sizes reported via some anatase-based reactions [Eck96, Shv79] and are somewhat smaller than the 47 nm crystallites produced by Kumazawa's experiments using the same precursor Ba/Ti and hydrated titanium gel. This decrease of the substructure size may be attributed to experimental differences such as precursor selection or the method of Ba(OH)₂·8H₂O introduction. Second, the relatively constant crystallite size over a wide range of Ba/Ti ratios in the current research and Kumazawa's work may suggest either an aggregation phenomena during particle formation or the dependence of the substructure size on the precursor particle size or surface area.

5.4.3.2 Effect of treatments on crystallite strain

In performing the Warren-Averbach line profile technique, calculation of the crystallite strain within a given direction is possible. The strain perpendicular to the

(100) of the four powders provided an average value of 0.248%, where strains ranged between 0.204-0.278%. Analysis of the treatment effects in Table 5.4 proved two treatments statistically significant with respect to the crystal strain. As the $\text{Ba(OH)}_2 \cdot 8\text{H}_2\text{O}$ injection rate is increased, the solution pH rises at a more rapid rate to a level conducive to BaTiO_3 formation [Moo96]. As the total time of the injection decreases, particles may undergo rapid growth. Thus, insufficient time may exist for the transport and release of the byproduct hydroxyls from the dehydroxylation of the $\text{TiO}_x(\text{OH})_y$ gel. It is important to note the caution with which significance is assigned. The matrix was designed primarily for the investigation of the particle size and qualitative evaluation of morphology, not crystal strain. Thus, the observed strain may be a result of factors which are an indirect result of the injection rate.

Decrease in the observed strain when increasing $\text{Ba(OH)}_2 \cdot 8\text{H}_2\text{O}$ concentrations are added to the $\text{TiO}_x(\text{OH})_y$ gel at room temperature may be attributed to the more complete dissolution and breakdown of the titanium gel in the highly alkaline environment. This effect is noted in the increased tetragonal content (and therefore lower hydroxyls concentration) produced with increasing precursor Ba/Ti [Dut94, Shi97]. Notably, the solution pH of the as-received gel slurry is equal to pH 3.5 prior to the addition of CO_2 -free deionized water and barium hydroxide.

As illustrated in the literature, the strain associated with as-synthesized hydrothermal particles is attributed to hydroxyl incorporation within the BaTiO_3 lattice as measured by Fourier transform infrared spectroscopy (FTIR) and simultaneous FTIR/TG-DTA [Hen91, Shi97, Wad96, Viv87]. For every two hydroxyls incorporated within the lattice on oxygen sites, one Ba vacancy must be created to maintain electroneutrality [Wad95]. The range of the observed crystallite strains, 0.204-0.278%, included the 0.267% strain measured in both the industrially synthesized, CPM lot R59 and CPM lot 6670-70, powders which were made from similar precursors. In addition,

the strain perpendicular to the (h00) of the $\text{Ba}(\text{OH})_2 \cdot 8\text{H}_2\text{O}$ -charged reactions were equivalent to the 0.220-0.235% and 0.247-0.259% strain produced in the EDTA experimentation lot numbers 21-28, and trial seeding runs, lots 36-38, respectively.

5.4.4 Transmission Electron Microscopy

All employed sets of treatments have produced a majority of distinct, spherical polycrystalline particles with some asymmetrical, ellipsoidal particles. The powders exhibit diameters between 40 nm to 110 nm and an equiaxed morphology similar to particles shown in the TEM photomicrographs Figure 5.4. In agreement with the large measured particle size by light scattering and the decreased surface areas, powder lot numbers 30 and 31 exhibited the largest particle size via TEM analysis.

5.4.5 Effect of Treatments on Specific Surface Area

The specific surface area of the powder lot numbers 29-35 ranged from 12.6-17.8 m^2/g , surface areas smaller in magnitude than the EDTA lots. Assumption of the null hypothesis and matrix calculations produced a 95% confidence interval of $15.2 \pm 0.8 \text{ m}^2/\text{g}$ for powder lots 29-32. As shown in Table 5.4, the precursor Ba/Ti is the only statistically significant treatment and varies directly with the surface area. As previously discussed, the increased Ba/Ti is expected to cause more rapid nucleation and subsequently smaller particles.

5.4.6 Effect of Treatments on Product Ba/Ti

Powder lot numbers 29-32 exhibited product Ba/Ti ratios near unity, an observed range from 0.982-1.012, and a calculated mean product Ba/Ti of 0.999 ± 0.007 based on the variance analysis of the replicate lots. Three treatments, the injection rate, precursor Ba/Ti, and $\text{Ba}(\text{OH})_2 \cdot 8\text{H}_2\text{O}$ initial charge, were shown to exhibit statistically significant effects. Increase of the product ratio Ba/Ti may be attributed to carbonate formation at

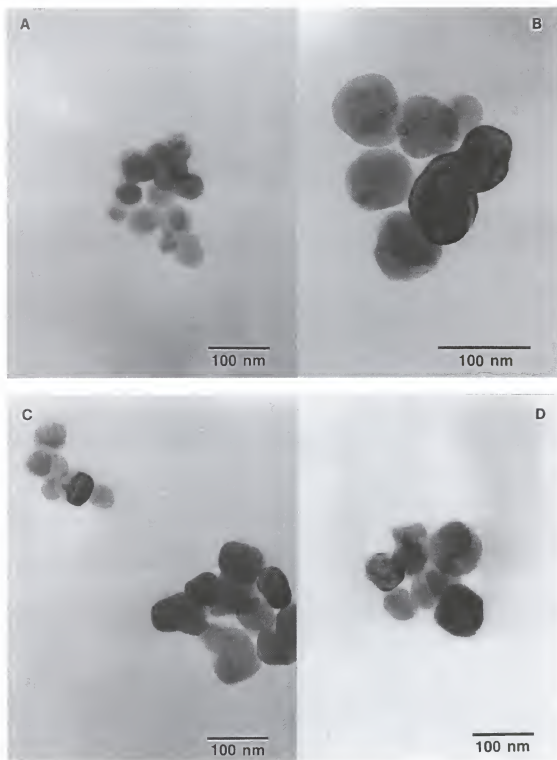


Figure 5.4. TEM photomicrographs illustrate the distinct, spherical polycrystalline particles for powder lot numbers 29-35. Most powders are equiaxed and exhibit a nearly monosized distribution, as illustrated by the powder images of (a) lot 29, (b) lot 30, (c) lot 33, and (d) lot 35.

high precursor ratios or insufficient washing, since all powders were washed under the same conditions regardless of the amount of excess barium. This is expected in the case of the increased precursor Ba/Ti and the $\text{Ba}(\text{OH})_2 \cdot 8\text{H}_2\text{O}$ concentration. The highest initial $\text{Ba}(\text{OH})_2 \cdot 8\text{H}_2\text{O}$ charge (i.e., prior to the bulk hydroxide injection) of 0.15 M is insufficient for the phase pure formation of BaTiO_3 , as shown experimentally by Moon [Moo96] assuming similar levels of carbon dioxide contamination. The inverse relationship of the product Ba/Ti and injection rate cannot be explained at this time.

5.5 Conclusions

Submicron, equiaxed barium titanate particles which represented the metastable cubic crystalline phase were synthesized between a number frequency mean particle size from 73 nm to 95 nm, crystallite size from 25 to 28 nm, specific surface area from 12.6 to 17.8 m^2/g , product Ba/Ti from 0.982 to 1.012, and exhibited a crystallite strain of 0.20% to 0.28% perpendicular to the (100). Experimental design is useful in investigating the hydrothermal technique provided that variables and variable levels are judiciously selected and controlled. Such designs provide quantifiable conclusions of particle attribute effects based on real-world process conditions. The combined effects of the precursor Ba/Ti on the particle size, size, distribution, and the specific surface area strongly suggest a rapid nucleation event. The effect of the precursor ratio in modifying the particle size is the subject of the following chapter.

CHAPTER 6 HIGH YIELD HYDROTHERMALLY SYNTHESIZED BaTiO₃ POWDERS

6.1 Introduction

Barium titanate (BaTiO₃) has been produced since the 1940s and remains the most commercially significant and widely investigated of the oxygen octahedral ferroelectrics [Her85, Kan87, Kin76, Lin77, Ras55, Ric92, Swa97]. It is widely used in a doped form as the dielectric material in multilayer capacitor (MLC) applications. The miniaturization of electronic components and desire to increase the volumetric efficiency of capacitors has led to the production of dielectric layers of ever-decreasing thickness. In 1983 a 15 μm dielectric layer was the state-of-the art thickness offered by commercial MLC producers [Kan95]. Until recently, fired dielectric layers 3 μm [Bee97, Ven98] were produced only on the laboratory scale. As wet casting processes and suspension dispersions have been refined to provide thinner commercial dielectric layers, a smaller particle size dielectric is required with an equiaxed morphology for optimum packing [Kan95]. If the particle diameters approach the magnitude of the dielectric thickness, the voids inherent to the randomly packed layers would represent a large percentage of the total thickness and may be sufficiently large to produce a short-circuit across the dielectric layer, rendering the dielectric layer useless. Subsequently, MLC manufacturers use submicron powders in order to remain competitive, and an equal importance is placed on the powder synthesis industry to produce <400 nm spherical dielectric powders.

6.2 Hydrothermal Synthesis

Hydrothermal synthesis is defined as the treatment of precursors in an aqueous environment at elevated temperature and pressure to produce a crystalline inorganic material, and was first employed to synthesize BaTiO_3 for pigment applications in 1940 [Pet40]. Research has shown the technique to be superior to other powder synthesis techniques due to the ability to directly produce crystalline, agglomerate-free, high purity powders in a relatively benign environment at low temperatures (i.e., $\leq 200^\circ\text{C}$). BaTiO_3 powders produced via other techniques, such as conventional calcination [Alc91, Bea83, Fer91], oxalate-derived [Cla56, Sch65, Sto93], and sol gel-derived [Fre95, Sha86] methods, may require additional crystallization heat treatments and/or milling prior to use in forming operations [Fax70, Her95b, Phu90, Suy94]. Improper application of the respective secondary processes may produce an aggregated powder unsuited for use in ultra-thin layers and powder surfaces which exhibit a nonstoichiometric Ba/Ti due to the incongruent dissolution of barium [Ada87, And87, Cho96b, Len93, Men89a]. Furthermore, the use of a pH controlled, aqueous-based synthesis technique is relatively inexpensive and benign in comparison to the purchase and disposal costs and hazardous nature of organic solutions.

The major commercial disadvantages of hydrothermal synthesis include the stability of the selected material within the aqueous environment, the appreciable capital equipment expenditures, and the aggregation of particles during solvent extraction [Rin96]. The first two disadvantages may be negated by adequate control of solution pH and cost analysis of the entire process lifetime based on the sales of a higher quality product. The latter limitation, aggregation on drying, can be surmounted by avoiding solvent removal from the powder until drying of the final tape as offered by a total aqueous processing (TAP) method [Ven98]. Thus, the as-synthesized wet-cake is not completely dewatered when introduced to the polymeric plasticizer, binder and other

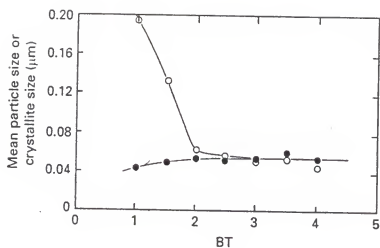
casting additives. With respect to academic interests, the disadvantages of the hydrothermal BaTiO_3 synthesis include the inaccessibility of the reaction and the rapid kinetics of the reaction precipitation process. The closed nature of the system hinders the *in situ* determination of pH and limits sampling techniques. Thus, researchers often result to post-mortem analysis of the system and deduce the complex interactions at elevated reaction conditions based on speculation.

6.2.1 Further Decrease in the Size of Hydrothermal Product

Recent hydrothermal studies employed simple noninjection systems where suspensions of barium hydroxide octahydrate ($\text{Ba}(\text{OH})_2 \cdot 8\text{H}_2\text{O}$) and hydrated titanium oxide gel ($\text{TiO}_x(\text{OH})_y$) were introduced to the autoclave at room temperature, sealed to the atmosphere, and ramped to the final reaction temperature under agitation [Kum96, Wad95]. In both laboratories, the particle size was reported to strongly rely on the precursor Ba/Ti molar ratio. Decrease in the mean particle size was observed with increase of the precursor Ba/Ti until a critical ratio, $\text{Ba/Ti}_{\text{crit}}$, was reached. Once a critical Ba/Ti was achieved, the particle size remained constant with additional increases of the precursor Ba/Ti, as shown in Figure 6.1. However, Kumazawa et al. reported a $\text{Ba/Ti}_{\text{crit}}$ of 2.0 in contrast to a $\text{Ba/Ti}_{\text{crit}}$ of 20.0 reported by Wada et al. [Kum96, Wad95]. Therefore, the suggested $\text{Ba/Ti}_{\text{crit}}$ in the two studies differed by an order of magnitude. The Ba/Ti exhibits an effect on the particle size, but side-by-side comparison of the two studies suggests that the effect of the Ba/Ti is indirect and may not be the most important variable.

During aqueous precipitation, excess barium is necessary to produce a stoichiometric powder due to the high solubility of barium [Kir78]. At high Ba/Ti ratios, Wada et al. proposed that barium species completely cover the finite gel surface area [Wad95]. Thus a critical Ba/Ti is observed, above which an increase in the

(a)



(b)

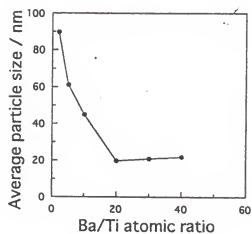


Figure 6.1. Effect of precursor Ba/Ti on the particle size of hydrothermally derived BaTiO_3 powders. The critical Ba/Ti differs by an order of magnitude in the experiments by (a) Kumazawa et al. [Kum96] and (b) Wada et al. [Wad95]. The mean particle size and crystallite size in (a) are designated by the open and filled data points, respectively.

number of excess barium ions in solution does not affect the particle size. In contrast, Kumazawa et al. offer only the findings of the ratio-size relationship and do not offer a physical or chemical interpretation. The author believes complete surface coverage occurs even in nearly equimolar precursor proportions since the gel is generally regarded as significantly more insoluble than the barium hydroxide [Bae76, Cho96b, Kir78, Moo96, Ovr79].

6.2.2 Titanium Solubility

Baes and Mesmer report the constant, limited solubility of titanium species (i.e., 1×10^{-8} M) when the solution pH is \geq pH 4 as illustrated in Figure 6.2 [Bae76]. A constant solubility is atypical of most cations in aqueous solution. Generally an increased solubility under both extremely acidic and alkaline conditions is noted. At the time of publication, Baes and Mesmer did not obtain experimental data from solutions of moderate alkalinity (i.e., $>$ pH 9) and reported the neutral species, titanium tetrahydroxide ($\text{Ti}(\text{OH})_4(\text{aq})$), to be the highest order mononuclear species observed in alkaline solution. In comparison, zirconium and hafnium, also Group IV-B elements, exhibit pentacoordinated species as shown for zirconium in Figure 6.2 [Bae76].

Pourbaix, in contrast to Baes and Mesmer, noted a theoretical increase in the solubility of titanium at high pH and postulated the existence of $\text{HTiO}_3^-(\text{aq})$, as shown in Figure 6.3. Lee utilized the same dominant species as Pourbaix to construct predominance diagrams at various temperatures and illustrated the continual decrease in the lower domain limit of $\text{HTiO}_3^-(\text{aq})$ with increasing temperature [Lee81]. Though $\text{Ti}(\text{OH})_4(\text{aq})$ is experimentally noted at room temperature, Lee reported the exclusion of the species due to the lack of thermodynamic data.

Using the general metal hydrolysis scheme proposed by Baes and Mesmer, simplistic calculation of the ionic radius ratio for Ti/OH and Zr/OH specifies that both

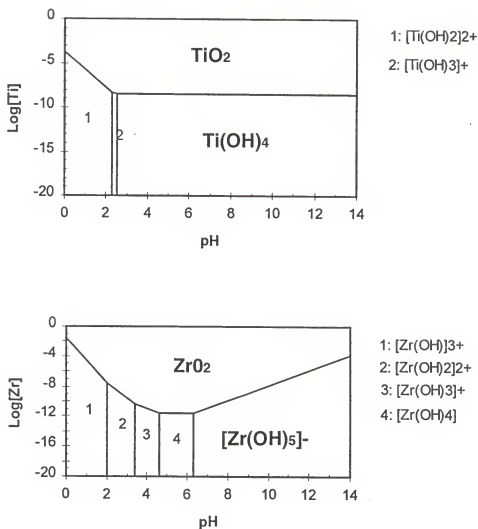


Figure 6.2. Predominance diagrams for titanium and zirconium in aqueous solution. The diagrams were constructed by the OPAL© software program based on the species reported by Baes and Mesmer [Bae76] and data acquired from the NBS thermodynamic tables [Wag82].

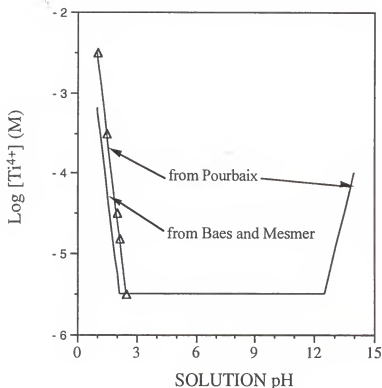


Figure 6.3. Theoretical stability diagram for aqueous TiO_2 suspensions [Bae76, Pou74].

cations should be octahedrally coordinated. Thus, the unimpeded $\text{Ti}^{4+}(\text{aq})$ ion should be capable of supporting a coordination greater than four. In fact, the first coordination sphere which surrounds most solvated cations is generally thought to be octahedrally coordinated [But88]. In the BaTiO_3 lattice, titanium is also octahedrally coordinated. Due to the behavior of similar Group IVB elements, ionic radius calculations, and the known coordination of titanium in a solid lattice, it is suggested that a pentacoordinated or hexacoordinated titanium species exists in solution and results in the increased solubility of crystalline titanium dioxides and amorphous hydrated titanium oxide gels under alkaline conditions.

6.2.3 Formation Mechanisms

Two formation mechanisms have been proposed when discussing hydrothermal precipitation: (1) *in situ* transformation and (2) dissolution and recrystallization, as shown in Figure 2.8 [Den90, Eck96]. *In situ* transformation involves the conversion of a solid reactant by initial crystallization on the precursor surface and propagation of the reaction front toward the center of the reactant particle. As the process is completed, the unreacted core is the last material to crystallize. An *in situ* transformation within the framework of the gel-hydroxide reaction would require both the inward diffusion of barium through the newly formed product BaTiO_3 layer toward the unreacted gel core and the outward diffusion of the reaction byproduct, water, for the reaction to proceed to completion. In contrast, a dissolution and recrystallization process, as its name suggests, involves the combination of soluble species to form a crystalline product.

Moon showed BaTiO_3 nucleation from the gel-hydroxide system at temperatures as low as 50°C , indicating the high reactivity of the precursor system even at a low precursor Ba/Ti of 1.0 [Moo96]. Moon's kinetics studies, performed under 75°C isothermal conditions, also illustrated a dissolution and recrystallization formation mechanism by a Hancock and Sharp analysis [Han92]. This result was corroborated by transmission electron microscopy.

In contrast, Hertl suggested the direct conversion (or *in situ* transformation) of 37 nm anatase particles to 25 nm BaTiO_3 when a high concentration of $\text{Ba}(\text{OH})_2 \cdot 8\text{H}_2\text{O}$ was employed. Using the titanium molar density, the calculation of a direct conversion reaction indicates that the total mass of a 37 nm anatase particle with a density of 3.48 g/cm^3 [Lid94] would form a minimum-sized 38 nm BaTiO_3 particle. Therefore, the 25 nm particles reported by Hertl most likely were formed by a dissolution and recrystallization process, and not direct conversion as was reported. The product particle size was coincidentally similar to the original size of the anatase particles. Furthermore,

Slamovich et al. point out the failure of Hertl's model to describe the change in BaTiO_3 particle size observed with varying reaction conditions [Sla96]. If an *in situ* transformation transpired, the size of the BaTiO_3 particles would be fixed by the size of the precursor TiO_2 .

In the gel-hydroxide system, Kumazawa et al. reported gel particles of 650 nm formed 45 nm BaTiO_3 particles [Kum96]. Complete mass conversion of the hydrated titanium gel (with an assumed density of 2.57 g/cm^3) would result in 700 nm BaTiO_3 particles, unlike the reported 45 nm particles. Once again, a dissolution and recrystallization process is supported. The above experimental observations and the theory of increasing titanium solubility with increasing solution pH suggest that a dissolution-recrystallization formation mechanism is dominant under extremely alkaline conditions. Provided that the pH is sufficiently alkaline, the formation mechanism appears dominant in the cases of both the anatase and amorphous titanium precursors.

Notably, though Hertl's assessment of the formation mechanism is believed inaccurate, Hertl recognized the importance of the $[\text{Ba}(\text{OH})_2 \cdot 8\text{H}_2\text{O}]$, rather than the precursor Ba/Ti, in controlling the BaTiO_3 particle size. In the anatase-hydroxide system Hertl evaluated various barium hydroxide concentrations from dilute conditions up to 7.0 M. Unfortunately, neither photomicrographs of the BaTiO_3 powders nor precursor Ba/Ti ratios were supplied by Hertl.

Revisiting the experimentation of Kumazawa et al. [Kum96] and Wada et al. [Wad95], the inordinate difference in the observed $\text{Ba/Ti}_{\text{crit}}$ may be explained by the significance of the $[\text{Ba}(\text{OH})_2 \cdot 8\text{H}_2\text{O}]$. In both experiments, the onset of the particle size plateau or $\text{Ba/Ti}_{\text{crit}}$ was noted at a critical $[\text{Ba}(\text{OH})_2 \cdot 8\text{H}_2\text{O}]$ of approximately 1.0-1.3 M. The exact location of the critical $[\text{Ba}(\text{OH})_2 \cdot 8\text{H}_2\text{O}]$ and particle size plateau is not known due to the noncoinciding experimental increments selected by the two separate laboratories.

It is the hypothesis of the author that the $[\text{Ba}(\text{OH})_2 \cdot 8\text{H}_2\text{O}]$ controls the particle size until a critical concentration near 1.0 M is achieved. However, even this clarification statement is less than absolute since the employed barium precursor is a hydroxide. Increase in the $[\text{Ba}(\text{OH})_2 \cdot 8\text{H}_2\text{O}]$ produces a barium concentration in solution which is thermodynamically required to coexist with stoichiometric BaTiO_3 , allows barium species to encompass the gel, promotes reaction completion via LeChâtelier's principle, increases the solution pH, and increases the concentration gradient of the barium in solution versus the unreacted titanium gel structure.

6.3 Materials and Methods

6.3.1 Titanium Gel Storage

The titanium precursor, an amorphous hydrated titanium oxide gel shipped from CPM, Boyertown, PA, exhibited a high, as-synthesized specific surface area, $\geq 200 \text{ m}^2/\text{g}$. Previous experimentation has shown BaTiO_3 powder inconsistencies when using gel synthesized more than one week prior to use in the synthesis of BaTiO_3 powders [Moo96]. Similarly, other authors specify the use of fresh gels [Shi97, Xia96]. The deleterious, room temperature aging effect is akin to the Ostwald ripening of an extremely fine colloidal system. A proper study of the hydrothermal process required the use of one gel lot to avoid drawing conclusions based on gel lot inconsistencies. The aging problem was avoided by freezing the as-received gel in 100 ml aliquots on receipt from CPM. The gels used in this study remained in the frozen state (at approximately -10°C) for seven months until 12-24 h before the gels were used in a hydrothermal reaction. On thawing, the phase separation which occurred during freezing was apparent. The once homogeneous gel (of bread dough or paste-like consistency) separated into solid and liquid portions, yet retained a high surface area, $240 \text{ m}^2/\text{g}$. The phase separation process has not yet been investigated, however, speculation promotes two theories. First, the solubility of the gel in ice is expected to be significantly lower than that of water. As ice

begins to form, the remaining liquid portion of the gel experiences an increase in the concentration of the aqueous titanium species, the solution becomes supersaturated, and precipitation may ensue. The second postulation suggests the importance of the unique volumetric expansion of water on freezing. Quite possibly, the expansion of localized entrapped water within the loosely bound colloidal gel network physically fractures the three-dimensional gel network during the freezing process.

Effectively, the freeze-thaw gel provides a liquid medium for the hydrothermal reaction without dilution. Unlike the as-synthesized gel, the post freeze-thaw gel suspension also exhibits a viscosity which allows transfer to the autoclave through industrial scale feed lines without dilution. Thus, the freeze-thaw process permits increased product loading of the autoclave, as well as a significantly extended shelf-life.

6.3.2 Hydrothermal Synthesis

Two BaTiO₃ powder batches were synthesized with CO₂-free deionized water, as illustrated in the process flow diagram in Figure 6.4. The thawed titanium gel and Ba(OH)₂·8H₂O(s) were directly weighed into a titanium reaction vessel, placed in the autoclave, purged with nitrogen, sealed to the atmosphere, and ramped at approximately 1.4°C/min to the final reaction temperature of 200°C, and soaked for 20 min. All autoclave reactions were performed under mechanical agitation at 350 rpm since this variable was shown to be relatively insignificant over a range of 150-600 rpm [Kum95]. After cooling to room temperature, the powder suspensions were washed with pH 10.7 ammoniated water and stored in Nalgene containers. The wash solution pH was adjusted to avoid incongruent dissolution of barium from the BaTiO₃ surface [Ada87, Cho96b, Len93, Ute90].

Lot number 39 consisted of a 1.03 M barium concentration similar to the previous literature [Kum96, Wad95], yet retained a precursor Ba/Ti of 1.2. The objective of the

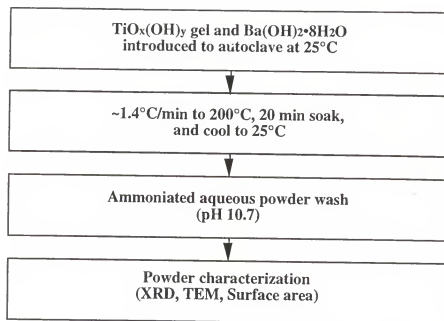


Figure 6.4. Hydrothermal synthesis, washing, and characterization flow diagram for BaTiO₃ powders produced by the noninjection system.

experiment was to test the hypothesis that a large excess of barium hydroxide (i.e., a high precursor Ba/Ti) is not necessary to form fine BaTiO₃ powders. Until the potential of the gel phase separation via the freeze-thaw process was recognized, a simultaneous high hydroxide concentration and low ratio were not possible in the gel-hydroxide system. Kumazawa et al. and Wada et al. merely added large quantities of Ba(OH)₂·8H₂O(s) to produce a large excess ratio.

Lot number 40 was performed under more extreme conditions and entailed a 2.00 M barium concentration and precursor Ba/Ti of 1.7. This was possible by extracting a small volume of the supernatant from the phase separated, thawed gel suspension. Note that both lot numbers 39 and 40 were performed without the hydroxide injection system which was employed in lot numbers 1 through 38 of the previous chapters. Therefore, lots 39 and 40 exploit the effects of the [Ba(OH)₂·8H₂O], whereas the hydroxide concentration increased gradually when using an injection system.

Furthermore, the prior fractional factorial designs employed lower, 0.4-0.6 M barium hydroxide concentrations.

6.3.3 Powder Characterization

6.3.3.1 X-ray diffraction

BaTiO₃ samples for x-ray diffraction (XRD) analysis were prepared by placing powder from the aqueous-washed suspension onto an amorphous silica slide and drying the samples in a vacuum oven at 80°C. Phase purity XRD analysis was performed from 10-90° 2 θ using CuK α radiation using a Philips Powder Diffractometer model APD 3720 system and generator (Mount Vernon, NY) at 40 kV and 20 mA in combination with a Philips automated diffraction software PW1877, version 3.6g.

6.3.3.2 Transmission electron microscopy

Transmission electron microscopy (TEM) samples were prepared by dispersion of approximately 0.01 g of vacuum dried BaTiO₃ powder in 12 ml of isopropanol by sonication. Carbon coated Cu grids were vertically dipped into the suspension and stored under vacuum prior to TEM analysis. TEM analysis was performed at 200 kV on a JEOL 200cx TEM (Boston, MA).

6.3.3.3 Specific surface area

The measurement of specific surface area was performed by conventional nitrogen adsorption/desorption by the Brunauer, Emmett, and Teller technique (BET) on a Quantachrome Autosorb-6 Sorption System (Boca Raton, FL) [Gre82]. Arid conditions were ensured by outgassing the powder in a 6 ml amorphous SiO₂ BET cell for ≥ 8 hours at 160°C under a 400 mtorr vacuum. The ascertained specific surface area is based on the linear regression of a five-point analysis.

6.4 Results and Discussion

6.4.1 Powder Lot Number 40

The as-synthesized powder lot number 40 exhibited a blue-gray hue, unlike the cream or off-white color of typical BaTiO_3 powders. This may have been caused by impurities from the Hastelloy C agitator or cooling coils under such caustic conditions. The powder was thought to be unusable as a dielectric material and was not analyzed further. The following discussion of powder characterization techniques pertains only to powder lot number 39.

6.4.2 Effect of Treatments on Phase Purity

XRD, shown in Figure 6.5, illustrates a cubic BaTiO_3 crystalline pattern. As observed in the previous experiments, a slight amount of BaCO_3 contamination was noted. Carbonate is a major contaminant in the $\text{Ba(OH)}_2 \cdot 8\text{H}_2\text{O}$ precursor and is specified by the supplier to be present in concentrations of $< 0.51\%$. However, improper handling and exposure to the atmosphere may increase carbonate concentration significantly. When the hydroxide is dissolved into solution, as in the injection process, the insoluble barium carbonate remains in the solid state and is removed prior to BaTiO_3 synthesis by an in-line filter. Thus some carbonate contamination was anticipated in lot number 39 and 40 since the as-received $\text{Ba(OH)}_2 \cdot 8\text{H}_2\text{O(s)}$ was introduced directly to the autoclave without dissolution and filtration. However, a pre-synthesis or post-synthesis filtration process is possible within the constraints of the employed system. The high concentration of barium in solution also promotes the formation of carbonate from atmospheric sources [Xia96]. Thus powder contamination also may be attributed to the carbon dioxide present in the as-received Ti-gel, incomplete N_2 purging of the autoclave, or reaction of the excess barium hydroxide with atmospheric CO_2 on exposure during the washing and dewatering processes. Due to the rapid nature of the reactive precipitation process and the inability to seed BaTiO_3 with high concentrations of BaTiO_3 particles,

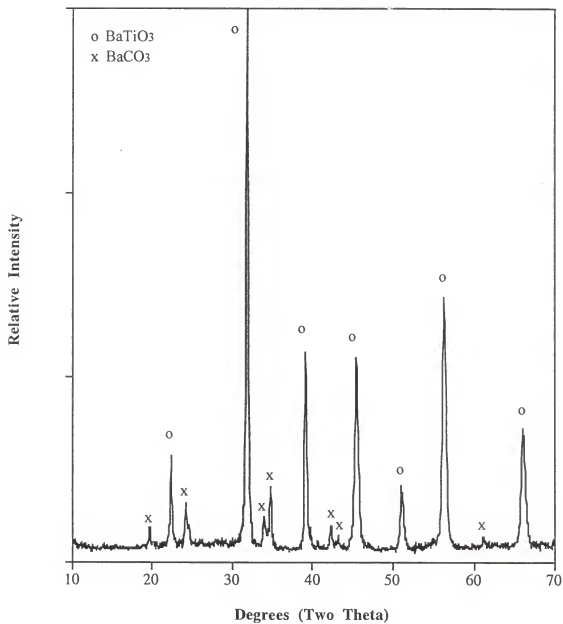


Figure 6.5. XRD of the as-synthesized BaTiO_3 powder lot number 39, which illustrates a cubic crystalline pattern with BaCO_3 contamination.

the barium titanate product attributes are expected to be consistent whether carbonate is absent or present in the system.

6.4.3 Transmission Electron Microscopy

Powder lot number 39 exhibited distinct, spherical polycrystalline particles and a near-monosized distribution. The powders exhibit diameters between 30-90 nm, an approximate average of 50 nm by visual inspection, and an equiaxed morphology as shown in the four TEM photomicrographs in Figure 6.6. These observed diameters correspond with the 45 nm and 20 nm diameters observed near the particle size plateau by Kumazawa et al. and Wada et al., respectively [Kum96, Wad95]. Therefore, particles of decreased size were produced by employing similar hydroxide concentrations and without the need for a large precursor Ba/Ti.

6.4.4 Specific Surface Area

The specific surface area of the powder lot 39 was $15.2 \text{ m}^2/\text{g}$. A C constant of 52.1 was calculated, thereby signifying reliable data from near-monolayer surface coverage by the nitrogen. The corresponding particle size, assuming ideal spheres of 6.0 g/cm^3 , is 65 nm. This corroborates the visual observation via TEM.

6.4.5 A Viable System

Unlike the previous injection systems where the $[\text{Ba}(\text{OH})_2 \cdot 8\text{H}_2\text{O}]$ in the autoclave increases with the time of injection, the noninjection process exploits the effective controlling variable of this system, the $[\text{Ba}(\text{OH})_2 \cdot 8\text{H}_2\text{O}]$. The true controlling factor (i.e., either the barium concentration or the solution pH) was not investigated, though the increase in pH was reported to increase the solubility of the titanium precursor [Sla96, Kee66]. Elevating the solution pH by introducing either inorganic or organic bases other than barium hydroxide is possible, yet may unnecessarily complicate the process. If employed, the introduction of organic mineralizers would require the controlled removal

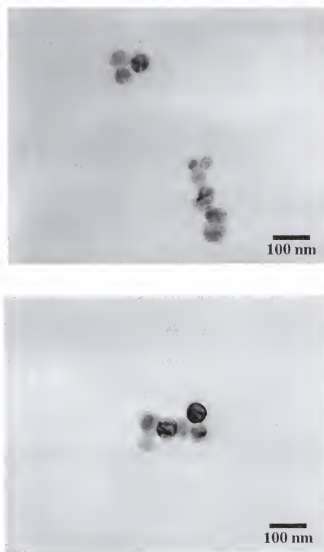


Figure 6.6. TEM photomicrographs illustrate the distinct, spherical, polycrystalline, near-monosized particles for lot number 39.

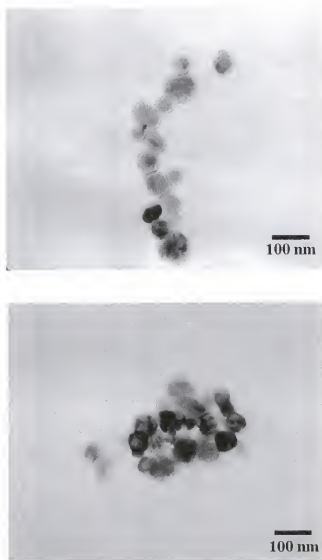


Figure 6.6.(continued) TEM photomicrographs illustrate the distinct, spherical, polycrystalline, near-monosized particles for lot number 39.

of residual species during the cofiring of MLC components. The addition of alkali metal hydroxides as mineralizers is undesirable, since the inherent residual alkali within the BaTiO_3 product increases the dielectric loss beyond tolerated dielectric classification limits and may cause exaggerated grain growth. When employing potassium and sodium hydroxides to adjust the solution pH, inductively coupled plasma spectroscopy on the digested BaTiO_3 product showed K and Na residuals of 1.76 mol % and 0.4 mol %, respectively [Her95a]. Solution pH adjustment via other alkaline earth hydroxides is limited since all Group IIA elements, with the exception of strontium, are fairly insoluble in aqueous solution [Lid94]. Regardless of the method of increase, the importance of the pH has been well noted in the formation of hydrothermal powders [Ada90, Ish90, Len93, Moo96, Sla96, Xia96] as well as coprecipitated [Fox90, Her95a] and oxalate derived powders [Sch65]. Kutty et al. postulated the solvation of the titanium phase to be rate limiting [Kut88a]. Therefore, the reaction is promoted by enhanced hydrolytic attack of the gel network by an increase in solution pH.

Similar to the alternative methods to increase solution pH, the increase in the barium concentration by other barium salts also is limited. Several undesirable factors include the limited solubility of the salts, toxic nature of the gaseous byproducts on firing, BaTiO_3 dedensification on sintering caused by high temperature decompositions, significant grain growth, adverse effects of residuals on dielectric performance, and precursor cost with respect to barium hydroxide [Dut94, Her85, Kle89, Lid94]. Though discerning the importance of the barium concentration versus the solution pH would be insightful, it is not necessary for this system.

6.4.6 Limitations

When employing the high concentrations of barium ions inherent to the high solids loading technique, additional caution must be taken to avoid barium carbonate contamination of the postsynthesized product. Also, since the noninjection system does

not involve the dissolution and filtration of the $\text{Ba}(\text{OH})_2 \cdot 8\text{H}_2\text{O}$, carbonate contamination of the precursor may remain in the final product unless removed in a prefiltration or postfiltration step. In prior research, acicular carbonate crystals of 2.0-3.0 μm in size were observed, similar to those reported by Miller [Mil90]. In addition to the concern of a final product which exhibits a decreased dielectric constant, a contaminant of this size obviously is deleterious to the production of dielectric layers $\leq 3 \mu\text{m}$. However, the relatively large contaminant size may enable filtration from the 50 nm BaTiO_3 product.

The high concentration of barium ions and high pH inherent to the high solids loading technique promote the precipitation of $\text{Ba}(\text{OH})_2 \cdot 8\text{H}_2\text{O}$ during postsynthesis cooling to room temperature as illustrated in Table 2.2. Hydroxide precipitation was not observed in this research. However, if present, the barium hydroxide could be dissolved and removed via a hot ammoniated water wash (to minimize the incongruent dissolution of the BaTiO_3 surface).

6.5 Conclusions

The high solids loading technique was not possible previously when using the as-synthesized hydrated titanium oxide gel. Prior investigation and application of the gel-hydroxide system required gel dilution with water to create a low viscosity slurry and permit a liquid medium for the hydrothermal reaction. In addition, researchers increased the solution pH by increase in the concentration of solid $\text{Ba}(\text{OH})_2 \cdot 8\text{H}_2\text{O}$ or the use of basic mineralizers. The sole increase in the hydroxide component created subsequently extremely high precursor Ba/Ti ratios and resulted in a large amount of precursor waste. The second method, the addition of basic mineralizers, is not desirable due to the contamination caused by species foreign to the current system.

The use of the freeze-thaw process provides both a low viscosity slurry and liquid reaction medium by the phase separation of the gel without significant decrease in the gel surface area. Furthermore, the solution pH can be increased by increase in both

the gel and hydroxide components because dilution is not required. The results suggest that the precursor Ba/Ti ratio is an indirect variable in affecting the particle size. A high concentration of $\text{Ba}(\text{OH})_2 \cdot 8\text{H}_2\text{O}$, while maintaining a low precursor Ba/Ti, was shown to produce fine BaTiO_3 powders without the use of excessive precursor Ba/Ti as employed by previous authors [Kum96, Wad95]. Submicron, equiaxed barium titanate particles which exhibited pseudo-cubic crystallinity and a near-monosized distribution were synthesized with an estimated average particle size of 50 nm via transmission electron microscopy and calculated 65 nm particles from a specific surface area of $15.2 \text{ m}^2/\text{g}$. The relative importance of the simultaneous increase in the barium concentration with respect to the increase in the pH has not been determined, though the solution pH is expected to exhibit a significant effect on the hydrated titanium oxide gel solubility in a dissolution and recrystallization reaction.

The increase in the solids loading enabled by the freeze-thaw process has increased the autoclave yield by a factor of 2.7 with respect to current industrial techniques. An increase in the yield of this magnitude is expected to dramatically decrease the expenditures of the powder manufacturing facility. In addition, the removal of the cost intensive injection system may be possible. Additional handling benefits are also created by the freeze-thaw technique. The shelf-life of the gel is effectively increased from one week to several months. Furthermore, the self-life allows sufficient time for gel characterization prior to use in BaTiO_3 synthesis, lessens the dependency of the autoclave synthesis on gel production, and ensures that gel will not be wasted (due to aging) in the event of unanticipated autoclave maintenance.

CHAPTER 7 CONCLUSIONS AND FUTURE WORK

7.1 Conclusions

Various hydrothermal process variables were investigated to form polycrystalline BaTiO_3 particles which were, in general, equiaxed, near monodispersed, and exhibited mean particle sizes between approximately 50 nm to 120 nm. The injection system used in the experimental design research produced mean particle sizes between 75 nm to 95 nm in contrast to the approximate 50 nm mean particle size produced by the increased loading, noninjection system. Similar to prior investigations, particles were believed to exhibit a finite concentration of hydroxyls incorporated within the lattice and the pseudo-cubic phase consistent with hydrothermal BaTiO_3 particles formed from low reaction temperatures ($\leq 200^\circ\text{C}$) and short reaction times with a precursor Ba/Ti near unity. The assignment of variable effects to the $\text{Ba}(\text{OH})_2 \cdot 8\text{H}_2\text{O} - \text{TiO}_x(\text{OH})_y$ gel precursor hydrothermal system was facilitated by the use of experimental designs to calculate confidence intervals within a process window.

The use of the rapid hydroxide injection system and the 20-experiment, 2^{7-3} fractional factorial design with center point replicate analysis, indicated the importance of the titanium precursor. Hydrothermal treatment of the $\text{TiO}_x(\text{OH})_y$ gel at 150°C caused transformation of the amorphous gel to anatase. This resulted in anatase contamination of the final BaTiO_3 powder, due in part to the rapid injection times (< 15 s), the short duration of the time (≤ 30 min) spent at the reaction temperature ($\leq 210^\circ\text{C}$), and the notably decreased kinetics and solubility of the coarsened anatase with respect to the high surface area hydroxylated gel precursor (i.e., $195 \text{ m}^2/\text{g}$ and $240 \text{ m}^2/\text{g}$, respectively).

Though the gel precursor systems did not exhibit an x-ray visible anatase contaminant, low product Ba/Ti ratios were noted by x-ray fluorescence in some batches. This has been attributed to the encapsulation of the gel network by the rapid formation of BaTiO₃. Both the observed low density and extremely high surface area of some powders is attributed to the presence of the unreacted titanium precursor. The probability of producing stoichiometric powders is believed to be greatly increased by the use of less rapid barium hydroxide injection rates, an increased concentration of barium hydroxide, and the use of the as-received amorphous gel system without hydrothermal pretreatment. Hence, these variables were further reviewed in the following experimental series.

The second experimental design, a 2⁴⁻² fractional factorial design, employed EDTA additions to the amorphous gel at room temperature prior to ramping to the hydroxide injection temperature. Stoichiometric powders were produced with mean particle sizes ranging between 75 to 81 nm. From the experimental design, the product Ba/Ti ratio was shown to increase with increase in the precursor Ba/Ti ratio. This effect is most likely attributed to increased levels of barium carbonate contamination caused by the stability of barium carbonate in alkaline solution [Ada90, Len93] and the increased availability of aqueous barium species for reaction with carbon dioxide [Xia96]. Possible sources of carbon dioxide contamination included the titanium gel precursor, incomplete nitrogen atmosphere blanketing, and exposure of the powders and the wash suspension to the atmosphere. Limited success was noted with respect to the magnitude of the particle size alteration via EDTA addition in the employed concentration range (7.1×10^{-3} - 3.5×10^{-2} M). Further experimentation is necessary to confirm or refute the statistical significance of the treatments which affect the particle size. Notably, the modest concentrations of EDTA corresponded to 1 to 5 mol% of the titanium precursor. The titanium solubility, and hence reaction kinetics, may not be markedly affected until a near 1:1 molar ratio of EDTA and titanium are employed. In addition, the highest surface area powder exhibited

the lowest product Ba/Ti and is suspected to obtain a small amount of unreacted titanium precursor.

The third experimental design employed the same fractional factorial design and reduced hydroxide injection rates as the EDTA design, with the exception that various concentrations of barium hydroxide octahydrate (rather than EDTA) were introduced to the gel at room temperature prior to the bulk injection of the aqueous barium hydroxide solution. Stoichiometric powders were produced which exhibited an equiaxed nature and mean particle diameters between 73 and 95 nm. The product ratio was shown to increase with an increase in the amount of $\text{Ba(OH)}_2 \cdot 8\text{H}_2\text{O}$ precharging concentration and, like the EDTA design, the product ratio also increased with increase in the precursor Ba/Ti ratio. Both effects were attributed to carbonate contamination.

Most notably, the $\text{Ba(OH)}_2 \cdot 8\text{H}_2\text{O}$ precharging experimental design suggested the importance of the precursor Ba/Ti (whether direct or indirect) in the modification of the particle size and the promotion of a rapid nucleation event. The light scattering measurement and rapid nucleation hypothesis were corroborated by the simultaneous and inversely proportional alteration of the surface area and the particle size distribution. The 3-experiment design which investigated differing concentration of seed particles within the gel prior to the hydroxide injection indicated that seeding does not affect the particle size and is not expected to result in epitaxial growth within the investigated variable levels.

The final two experiments, powder lots 39 and 40, expand on the results of the $\text{Ba(OH)}_2 \cdot 8\text{H}_2\text{O}$ fractional factorial design by attempting to illustrate the importance of the $[\text{Ba(OH)}_2 \cdot 8\text{H}_2\text{O}]$ rather than the precursor Ba/Ti ratio in control of the BaTiO_3 particle size. However, unlike the prior experimentation, the final two experiments employed a noninjection system. Lot 39 illustrated that a low Ba/Ti (1.2) and high solids concentration, hence increased $[\text{Ba(OH)}_2 \cdot 8\text{H}_2\text{O}]$ (1.0 M), produced an approximate mean particle size of 50 nm which maintained an equiaxed morphology and near-monosized

distribution. This is in contrast to the high precursor Ba/Ti ratios of 2 [Kum96] and 20 [Wad95], as reported by previous authors. The $\text{Ba}(\text{OH})_2 \cdot 8\text{H}_2\text{O}$ concentration exhibits a dual effect, simultaneously increasing the Ba concentration and the solution pH. At this time the sole effect of either variable is not known, however the addition of $\text{Ba}(\text{OH})_2 \cdot 8\text{H}_2\text{O}$ is preferable to other alkaline mineralizers or soluble barium salts since it does not require the introduction of precursor spectator species which are foreign to the BaTiO_3 lattice structure. An increase in the $\text{Ba}(\text{OH})_2 \cdot 8\text{H}_2\text{O}$ concentration while maintaining a low Ba/Ti is possible by the freeze-thaw process employed on the titanium gel and has resulted in an increase in the autoclave yield by a factor of 2.7 times. Lot 40, employing a high Ba/Ti = 1.7 and a $[\text{Ba}(\text{OH})_2 \cdot 8\text{H}_2\text{O}] = 2.0 \text{ M}$, produced a blue-gray powder, which may indicate the presence of impurities from the Hastelloy C impeller, cooling coil, and sampling components of the autoclave or create a reduction of the titanium. Previous authors illustrated that an upper limit to the increase of the $\text{Ba}(\text{OH})_2 \cdot 8\text{H}_2\text{O}$ concentration exists by observation of a plateau in the particle size at a critical Ba/Ti [Kum96, Wad95].

Relatively consistent particle attributes were noted for all investigated replicated runs in the three different designs. This is especially significant when considering the enhanced control and reliability expected from the possible automated control and sealed nature of an industrial scale process. The solution pH is believed to be an extremely significant variable since the solution pH dictates the nature and concentration of the aqueous species. The effect is noted in the preferential formation of $\text{Ba}^{2+}(\text{aq})$ or $\text{BaOH}^+(\text{aq})$ and the dissolution of the titanium oxide gel [Ada90, Eck96, Kee66, Ovr80]. The author suspects a polycoordinated hydroxylated species to be present in solution which exhibits a coordination greater than $\text{Ti}(\text{OH})_4(\text{aq})$, the species which was proposed to be stable at a solution $\text{pH} \geq 4$ [Bae76]. Based on calculations from the initial and final powder sizes [Her88, Wad95] and observation of a variation in particle size with the

Ba/Ti [Kum96, Wad96], the author believes that a dissolution and recrystallization growth mechanism is dominant under sufficiently high pH conditions due to the increasing solubility of the titanium precursor, regardless of the precursor phase.

The use of experimental design strategies is superior to one-variable-at-a-time tactics when screening or optimizing a process. However, it is not the intention to over-illuminate the effectiveness of DOE tactics. The results of DOE-based experiments and the confidence in the conclusions relies heavily on the design selection, choice of the variables, control of interior and exterior variables, and prudent conclusions evolved from experience with the system or knowledge of the prior literature. Experimental designs are an excellent tool to facilitate determination of the dominant process variables and complement the evaluation of a hypothesis. If attempting an experimental design technique for the first time, the author highly recommends the assistance of a statistician. Also, the use of experimental design software may further conserve research time and expenditures by automatically performing design matrix calculations.

7.2 Future Work

Previous authors investigated various large incremental precursor Ba/Ti ratios and thus incremental $[\text{Ba}(\text{OH})_2 \cdot 8\text{H}_2\text{O}]$ to suggest a critical concentration between 1.0 to 1.3 M. Thus, a more continuous investigation of the $[\text{Ba}(\text{OH})_2 \cdot 8\text{H}_2\text{O}]$ might provide the true critical $[\text{Ba}(\text{OH})_2 \cdot 8\text{H}_2\text{O}]$ in the investigated process. Also, differentiation of the effect of the $[\text{Ba}(\text{OH})_2 \cdot 8\text{H}_2\text{O}]$ would be insightful. The determination of the independent effects of the pH and barium concentration may be accomplished with highly soluble hydroxides and salts such as NaOH and BaCl_2 , respectively. Such a study may be more helpful in the optimization of other synthesis techniques which do not employ $\text{Ba}(\text{OH})_2 \cdot 8\text{H}_2\text{O}$ as the barium precursor. However, the alkali, organic, and halide contamination anticipated from the precursors [Kle89] is not anticipated to produce a dielectric material which exhibits a low dielectric loss and/or sinters to a high relative density.

A study of the solubility of titanium via ICP at high pH with respect to the coordination of the aqueous species in solution is desirable since the titanium precursor dissolution is expected to exhibit a major effect on the formation mechanism. Unless the hydroxide solution is consistently injected immediately on attainment of the injection temperature, the effect of dwell time at the injection temperature on gel aging (prior to the injection of barium hydroxide) is also important from an industrial process perspective.

Though the investigated properties are physical and chemical in nature, the electronic properties are equally important due to the sensitivity of the dielectric properties on minor compositional impurities or lattice defects. Thus a study of powder synthesis for dielectric applications is not truly complete until an investigation of the electronic properties is performed. This performance appraisal might include calculation of the dielectric constant versus temperature, temperature coefficient of capacitance, dielectric loss as a function of frequency, and a complementary measurement of the breakdown strength.

REFERENCES

- Abe87 I.K. Abe, T.M. Aoki, S.H. Rikimaru, S.T. Ito, T.K. Hidaka, and I.K. Segawa, U.S. Patent 4,643,984 (1987).
- Abe91 K. Abe and S. Matsumoto, "Processing Issues of Hydrothermal Synthesis of Fine Dielectric Powders," in Ceramics Transactions, Vol. 22, Ceramic Powder Science IV, Ed. by S. Hirano, G.L. Messing, and H. Hausner, Am. Ceram. Soc. Inc., Columbus, OH, pp. 15-25 (1991).
- Ada87 J.H. Adair, M.A. Janney, D.V. Miller, G.Y. Onoda, Jr., and R.E. Newnham, "The Surface Chemistry of Barium Titanate in Aqueous Suspension," presented at the 88th Annual Meeting of the American Ceramic Society, Pittsburgh (1987).
- Ada98 J.H. Adair, J.A. Kerchner, N.S. Bell, and M.L. Carasso, "The Application of Chemical Principles in the Synthesis of Ceramic and Metal Particles," in *Synthesis and Characterization of Advanced Materials*, ACS Symposium Series, **681**, pp. 82-94 (1998).
- Ada90 J.H. Adair, B.L. Utech, and K. Osseo-Asare, "Solubility Relationships in the Coprecipitation Synthesis of Barium Titanate in Aqueous Suspensions," presented at the Fifth U.S.-Japan Seminar on Dielectric and Piezoelectric Ceramics, Kyoto, Japan (1990).
- Ale91 J.R. Alcock, F.L. Riley, C. D'Angeli, and A.G. Thomas, "An Evaluation of Two Barium Titanate Powder Processing Routes," *Br. Ceram. Trans. J.*, **90**, pp. 152-156 (1991).
- And87 D.A. Anderson, J.H. Adair, D.V. Miller, J.V. Biggers, and T.R. Shrout, "Surface Chemistry Effects on Ceramic Processing of BaTiO₃," *Ceramic Transactions*, **1**, Nov. 1-4 (1987).
- And52 R.L. Anderson and T.A. Bancroft, Statistical Theory in Research, McGraw-Hill, New York, 1952.
- Bac92 R. Bacsa, P. Ravindranathan, and J.P. Dougherty, "Electrochemical, Hydrothermal, and Electrochemical-Hydrothermal Synthesis of Barium Titanate Thin Films on Titanium Substrates," *J. Mater. Res.*, **7** [2], pp. 423-428 (1992).
- Bae76 C.F. Baes and R.E. Mesmer, Hydrolysis of Cations, John Wiley & Sons, New York, pp. 98-157, 1976.
- Bea83 A. Beaeger, J.C. Mutin, and J.C. Niepce, "Synthesis Reaction of Metatitanate BaTiO₃," *J. Mat. Sci.*, **18**, pp. 3041-3046 (1983).
- Bec90 R.E. Becker, and W.R. Cannon, "Source of Water and Its Effect of Tape Casting Barium Titanate," *J. Am. Ceram. Soc.*, **73** [5], pp. 1312-1317 (1990).

- Bee97 J.J. Beeson, L.A. Mann, S. Venigalla, and S.A. Costantino, "Electrical and Physical Characteristics of Low-Fire X7R MLCCs with 3 μ m Active Layers and 70Ag-30Pd Electrodes," Proceedings of the 8th U.S.-Japan Seminar on Dielectric and Piezoelectric Ceramics, Plymouth, MA, pp. 180-183, October (1997).
- Bel97 N.S. Bell, "Interfacial Aspects of Glycothermally Synthesized Alpha Alumina," Ph.D. Dissertation, University of Florida (1997).
- Bel98 N.S. Bell, S-B. Cho, J.H. Adair, "Glycothermal Synthesis of Alpha Aluminum Oxide," in *Synthesis and Characterization of Advanced Materials*, ACS Symposium Series, **681**, pp. 120-133 (1998).
- Ben93 P. Bendale, S. Venigalla, J.R. Ambrose, E.D. Vernik, Jr., and J.H. Adair, "Preparation of Barium Titanate Films at 55°C by an electrochemical Method," *J. Am. Ceram. Soc.*, **76** [10], pp. 2619-2627 (1993).
- Ben92 H. Bennett and G. Oliver, XRF Analysis of Ceramics, Minerals, and Allied Materials, John Wiley & Sons, New York, pp. 1-10, 1992.
- Bog91 G.H. Bogush and C.F. Zukoski, "Uniform Silica Particle Precipitation: An Aggregative Growth Model," *J. Colloid Interface Sci.*, **132**, pp. 13-21 (1991).
- Boi88 R. Boistelle and J.P. Astier, "Crystallization Mechanisms in Solution," *J. Crystal Growth*, **90**, pp. 14-30 (1988).
- Box78 G.E.P. Box, W.G. Hunter, and J.S. Hunter, Statistics for Experiments, John Wiley & Sons, Inc., New York, 1978.
- Bru40 S. Brunauer, L.S. Deming, W.E. Deming, and E. Teller, *J. Am. Chem. Soc.*, **62**, p. 1723 (1940).
- Bru93 S.A. Bruno, D.K. Swanson, and I. Burn, "High Performance Multilayer Capacitor Dielectrics from Chemically Prepared Powders," *J. Am. Ceram. Soc.*, **76** [5], pp. 1233-1241 (1993).
- Bur51 W.K. Burton, N. Cabera, and F.C. Frank, "The Growth of Crystals and the Equilibrium Structure of Their Surfaces," *Phil. Trans. Roy. Soc. London*, **A243**, pp. 299-358 (1951).
- But88 I.S. Butler and J.F. Harrod, Inorganic Chemistry: Principles and Applications, The Benjamin/Cummings Publishing Company Inc., Redwood City, CA, 1988.
- Cau91 R. Caulcutt, Statistics in Research and Development, Second Ed., Chapman and Hall, New York, 1991.
- Cha90 F.C. Chaput and J-P. Boilot, "Alkoxide-Hydroxide Route to Synthesize BaTiO₃-Based Powders," *J. Am. Ceram. Soc.*, **73** [4] pp. 942-948 (1990).
- Che61 A.A. Chernov, *Uspekhi fiz. nauk* **73** [2], p. 277 (1961).
- Che95 H. Cheng, J.M. Zhenguo, and L. Qi, "Hydrothermal Preparation of Uniform Nanosize Rutile and Anatase Particles," *Chem. Mater.*, **7**, pp. 663-671 (1995).
- Chi88b P.-P. Chiang, M.D. Donohue, "A Kinetic Approach to Crystallization from Ionic Solution: I. Crystal Growth," *J. Colloid Interface Sci.*, **122**, pp. 230-250 (1988).

- Chi88c P.-P. Chiang, M.D. Donohue, "The Effect of Complex Ions on Crystal Nucleation and Growth," *J. Colloid Interface Sci.*, **126**, pp. 579-591 (1988).
- Chi88a P.-P. Chiang, M.D. Donohue, and J.L. Katz, "A Kinetic Approach to Crystallization from Ionic Solution: II. Crystal Nucleation," *J. Colloid Interface Sci.*, **122**, pp. 251-265 (1988).
- Chi95 A.T. Chien, J.S. Speck, F.F. Lange, A.C. Daykin, and C.G. Levi, "Low Temperature/Low Pressure Hydrothermal Synthesis of Barium Titanate: Powder and Heteroepitaxial Thin Films," *J. Mater. Res.*, **10** [7], pp. 1784-1789 (1995).
- Cho96a S.-B. Cho, "Size and Shape Control of Alpha-Alumina Particles Precipitated from 1,4-Butanediol Solution," Ph.D. Dissertation, University of Florida (1996).
- Cho96b R.E. Chodelka, "The Aqueous Processing of Barium Titanate: Passivation, Dispersion, and Binder Formulations for Multilayer Capacitors," Ph.D. Dissertation, University of Florida (1996).
- Cho97 Y.C. Choi, J. Lee, and B.S. Lee, "Improvements of the Properties of Chemical Vapor Deposited (Ba,Sr)TiO₃ Films Through Use of a Seed Layer," *Jpn. J. Appl. Phys.*, Part 1, **36** [11], pp. 6824-6828 (1997).
- Chr70 A.N. Christensen, "Hydrothermal Precipitation of Barium Titanate by Transport Reactions," *Acta Chem. Scand.*, **24** [7], pp. 2447-2452 (1970).
- Cla56 W.S. Claubach, E.M. Swiggard, and R.J. Gilchrist, "Preparation of Barium Titanyl Oxalate Tetrahydrate for Conversion to Barium Titanate of High Purity," *J. Res. Natl. Bur. Stand.*, **56**, pp. 289-291 (1956).
- Coc57 W.G. Cochran and D.R. Cox, Experimental Designs, John Wiley & Sons, Inc., New York, 1957.
- Cou73 P.R. Couchmann and W.A. Jesser, *Surface Sci.*, **34**, p. 212 (1973).
- Cro84 L.E. Cross, "Dielectric, Piezoelectric, and Ferroelectric Components," *Am. Ceram. Soc. Bul.*, **63**, pp. 586-590 (1984).
- Cro98 L.E. Cross, "The Saga of Fine Grained Barium Titanate," presented at the 100th Annual Meeting of the American Ceramic Society, Cincinnati (1998).
- Cul56 B.D. Cullity, Elements of X-Ray Diffraction, Addison-Wesley Publishing Company, Inc., Reading, MA, 1956.
- Cul78 B.D. Cullity, Elements of X-Ray Diffraction, Second Ed., Addison-Wesley Publishing Company, Inc., Reading, MA, 1978.
- Daw88 W.J. Dawson, "Hydrothermal Synthesis of Advanced Ceramic Powders," *Am. Ceram. Soc. Bulletin*, **67** [10], pp. 1673-1678 (1988).
- Daw91 W.J. Dawson, J.C. Preston, and S.L. Schwartz, "Processing Issues of Hydrothermal Synthesis of Fine Dielectric Powders," in Ceramics Transactions, Vol. 22, Ceramic Powder Science IV, Ed. by S. Hirano, G.L. Messing, and H. Hausner, Am. Ceram. Soc. Inc., Columbus, OH, pp. 27-32 (1991).

- DeH93 R.T. DeHoff, Thermodynamics in Materials Science, McGraw-Hill, Inc., New York (1993).
- Del82 R. Delhez, Th.H. de Keijser, and E.J. Mittemeijer, "Determination of Crystallite Size and Lattice Distortions Through X-Ray Diffraction Profile Analysis," *Fresenius Z Anal Chem*, **312**, pp. 1-16 (1982).
- Dem73 L.M. Dem'yanets and A.N. Lobachev, "Some Problems of Hydrothermal Crystallization," in Crystallization Processes Under Hydrothermal Conditions, Ed. by A.N. Lobachev, Consultants Bureau, New York, pp. 1-26 (1973).
- Den90 R.P. Denkwics, Jr., K.S. Tenhuisen, and J.H. Adair, "Hydrothermal Crystallization Kinetics of m-ZrO₂ and t-ZrO₂," *J. Mater. Res.*, **5**, pp. 2698-2705, (1990).
- Der41 B.V. Derjaguin and L. Landau, *Acta Physicochim. URSS*, **14**, p. 633 (1941).
- Dog97 F. Dogan, S. O'Rourke, M.X. Qian, and M. Sarikaya, "Low Temperature Synthesis of Nanophase BaTiO₃ and BaFe₁₂O₁₉ Powders," *Mat. Res. Soc. Symp. Proc. Vol. 457, Nanophase and Nanocomposite Materials II*, Materials Research Society, Pittsburgh, pp. 69-74 (1997).
- Don37 J.D.H. Donnay and D. Harker, "A New Law of Crystal Morphology Extending the Law of Bravais," *Amer. Min.*, **22**, pp. 446-467 (1937).
- Dut94 P.K. Dutta, R. Asiaie, S.A. Akbar, and W. Zhu, "Hydrothermal Synthesis and Dielectric Properties of Tetragonal BaTiO₃," *Chem. Mater.*, **6**, pp. 1542-1548 (1994).
- Eck96 J.O. Eckert, C.G. Hung-Houston, B.L. Gersten, M.M. Lencka, and R.E. Riman, "Kinetics and Mechanisms of Hydrothermal Synthesis of Barium Titanate," *J. Am. Ceram. Soc.*, **79** [11], pp. 2929-2939 (1996).
- Enü60 B.V. Enüstün and J. Turkevich, *J. Am. Chem. Soc.*, **82**, p. 4502 (1960).
- Est93 J. Estrin, "Precipitation Process," in Handbook of Industrial Crystallization, Ed. by A.S. Myerson, Butterworth-Heinemann, Boston, pp. 131-149, 1993.
- Fax70 R.C. Faxon and R.T. McGovern, U.S. Patent 3,637,531 (1970).
- Fed55 W.T. Federer, Experimental Design: Theory and Application, The Macmillian Co., New York, 1955.
- Fer91 J.F. Fernandez, P. Duran, and C. Moure, "Reaction Kinetics in the BaTiO₃ Synthesis: Influence of the TiO₂ Crystalline Structure and Morphology," Ceramics Today - Tomorrow's Ceramics, Ed. by P. Vincenzini, Elsevier, pp. 1973-1982 (1991).
- Fla55 S.S. Flaschen, "An Aqueous Synthesis of Barium Titanate," *J. Am. Chem. Soc.*, **77**, p. 6194 (1955).
- Flo53 P.J. Flory, Principles of Polymer Chemistry, Cornell University Press, Ithaca, 1953.
- Fox90 G.R. Fox, J.H. Adair, and R.E. Newnham, "Effects of pH and H₂O₂ Upon Coprecipitated PbTiO₃ Powders; Part I Properties of As-precipitated Powders," in *J. Mater. Sci.*, **25**, pp. 3634-3640 (1990).

- Fox91 G.R. Fox, J.H. Adair, and R.E. Newnham, "Effects of pH and H_2O_2 Upon Coprecipitated $PbTiO_3$ Powders; Part II Properties of Calcined Powders," in *J. Mater. Sci.*, **26**, pp. 1187-1191 (1991)
- Fre95 M.H. Frey, "Synthesis and Processing of Barium Titanate Ceramics from Alkoxide Solutions and Monolithic Gels," *Chem. Mater.*, **7**, pp. 123-129 (1995).
- Fur85 H. Furedi-Milhofer and A.G. Walton, "Principles of Precipitation of Fine Particles," in *Dispersion of Powders in Liquids*, Ed. by G.D. Parfitt, Applied Science, London, pp. 203-272 (1985).
- Gar96 M.H. Garrett and I. Mnushkina, "Techniques for Top-Seeded Solution Growth of $BaTiO_3$," *J. Crystal Growth*, **166**, pp. 550-557 (1996).
- Gib06 J.W. Gibbs, "The Equilibrium of Heterogeneous Substances," *Sci. pap.*, **1** (1906).
- Giv91 E.I. Givargizov, *Oriented Crystallization of Amorphous Substrates*, Plenum Press, New York, 1991.
- Gre82 S.J. Gregg and K.S.W. Sing, *Adsorption, Surface Area and Porosity*, Second Ed., Academic Press, p. 42, 1982.
- Hal49 W.H. Hall, *Proc. Phys. Soc.*, A62, p. 741 (1949).
- Han92 J.D. Hancock and J.H. Sharp, "Method of Comparing Solid-State Kinetic Data and Its Applications to the Decomposition of Kaolinite, Brucite, and $BaCO_3$," *J. Am. Cer. Soc.*, **55**, pp. 74-77 (1992).
- Har73 P. Hartman, "Structure and Morphology," in *Crystal Growth: An Introduction*, Ed. by P. Hartman, North-Holland, Amsterdam, pp. 367-402 (1973).
- Har80 P. Hartman and P. Bennema, "The Attachment Energy as a Habit Controlling Factor. I. Theoretical Considerations," *J. Crystal Growth*, **49**, pp. 145-156 (1980).
- Har55 P. Hartman and W.G. Perdok, "On the Relations Between Structure and Morphology of Crystals I," *Acta Cryst.*, **8**, pp. 49-52 (1955).
- Hea86 G.H. Heartling, *Ceramic Materials for Electronics: Processing, Properties, and Application*, Ed. by R.C. Buchanan, Marcel Dekker Inc., New York, pp. 139-225, 1986.
- Hea88 G.H. Heartling, "Electro-Optic Ceramics and Devices" in *Electronic Ceramics*, Ed. by L.M. Levinson, Marcel Dekker, New York, pp. 317-492 (1988).
- Hen87a D.F. Hennings, *Int. J. High Tech. Ceram.*, **3**, p. 91 (1987).
- Hen87b D.F. Hennings, R. Janssen, and P.J. Reynen, "Control of Liquid-Phase-Enhanced Discontinuous Grain Growth in Barium Titanate," *J. Am. Ceram. Soc.*, **70** [1], pp. 23-27 (1987).
- Hen78 D. Hennings and W. Mayr, "Thermal Decomposition of $(BaTi)$ Citrates into Barium Titanate," *J. Solid State Chem.*, **26**, p. 329 (1978).

- Hen91 D. Hennings, G. Rosenstein, and H. Schreinemacher, *J. Euro. Ceram. Soc.*, **8**, pp. 107-115 (1991).
- Hen92b D. Heniings and S. Schreinemacher, "Characterization of Hydrothermal Barium Titanate," *J. Euro. Ceram. Soc.*, **9**, p. 41-46 (1992).
- Hen92a M. Henry, J.P. Jolivet, and J. Livage, "Aqueous Chemistry of Metal Cations: Hydrolysis, Condensation, and Complexation," in Chemistry, Spectroscopy and Applications of Sol-Gel Glasses, Structure and Bonding, Vol. 77, Ed. by R. Reisfield and C.K. Jorgensen, Springer-Verlag, Berlin, Germany, pp. 153-206 (1992).
- Her95a Y-S. Her and E. Matijevic, "Preparation of Well-defined Colloidal Barium Titanate Crystals by the Controlled Double-jet Precipitation," *J. Mater. Res.*, **10** [12], pp. 3106-3014 (1995).
- Her95b C. Herard, A. Faivre, and J. Lemaitre, "Surface Decontamination Treatments of Undoped BaTiO₃-Part I: Powder and Green Body Properties," *J. Euro. Ceram. Soc.*, **15**, pp. 135-143 (1995).
- Her85 J.M. Herbert, Ceramic Dielectrics and Capacitors, Gordon and Breach Scientific Publishers, New York, 1985.
- Her88 W. Hertl, "Kinetics of Barium Titanate Synthesis," *J. Am. Ceram. Soc.*, **71** [10], pp. 879-883 (1988).
- Hun79 J.S. Hunter, Design of Experiments Course, distributed by the Office of Continuing Education and Extension, College of Engineering, University of Kentucky, 1979.
- Hun81 R.J. Hunter, Zeta Potential in Colloid Science: Principles and Applications, Academic Press, New York, 1981.
- Hun93 R.J. Hunter, Introduction to Modern Colloid Sceince, Oxford Science Publications, New York, 1993.
- Hur72 T.P. Hurley and A.C. McAdams, Jr., U.S. Patent 3,717,487 (1972).
- Ish90 N. Ishizawa, H. Banno, M. Hayashi, S.E. Yoo, and M. Yoshimura, *Jpn. J. Appl. Phys.*, p. 2467 (1990).
- Ish92 T. Ishihara, K. Kometani, Y. Mixuhara, and Y. Takita, *J. Am. Ceram. Soc.*, **75**, p. 613 (1992).
- Isr92 J. Israelachvili, Intermolecular and Surface Forces, Second Ed., Academic Press, New York, 1992.
- Jaf71 B. Jaffe, W.R. Cook Jr., and H. Jaffe, Piezoelectric Ceramics, Ed. by J.P. Roberts and P. Popper, Academic Press, New York, 1971.
- Kaj91 K. Kajiyoshi, N. Ishizawa, and M. Yoshimura, "Preparation of Tetragonal Barium Titanate Thin Film on Titanium Metal Substrate by Hydrothermal Method," *J. Am. Ceram. Soc.*, **74** [2] pp. 369-374 (1991).
- Kan95 H. Kanai, K. Harada, and Y. Yamashita, "Development of Large Capacitance Multilayer Ceramic Capacitors with Thin Dielectric Layers,"; presented at the Carts 95: 15th Capacitor And Resistor Technology Symposium (1995).

- Kan75 S. Kaneko and F. Imoto, "Synthesis of Fine-grained Barium Titanate by a Hydrothermal Reaction," *Nippon Kagaku Kaishi*, **6**, pp. 985-990 (1975).
- Kan87 W. Kanzig, "History of Ferroelectricity 1938-1955," *Ferroelectricity*, **74**, pp. 285-291 (1987).
- Kas87a T. Kasai and Y. Ozaki, "Preparation of Barium Titanium Precursor Sol from Metal Alkoxides," *J. Ceram. Soc. Jap.*, **95** [9], pp. 912-916 (1987).
- Kas87b T. Kasai and Y. Ozaki, "Preparation of BaTiO₃ and SrTiO₃ from Metal Alkoxides," *J. Ceram. Soc. Jap.*, **95** [10], pp. 1000-1006 (1987).
- Kee66 I. Keesmann, *Z. Anorg. Allgem. Chem.*, **346**, p. 30 (1966).
- Kem52 O. Kempthorne, The Design of Experiments, John Wiley & Sons, Inc., New York 1952.
- Kin76 W.D. Kingery, H.K. Bowen, and D.R. Uhlmann, Introduction to Ceramics, Second Ed., John Wiley & Sons, New York, 1976.
- Kir88 K.W. Kirby, "Alkoxide Synthesis Techniques for BaTiO₃," *Mater. Res. Bul.*, **23**, pp. 881-890 (1988).
- Kir78 T. Kirkpatrick, "Barium Compounds," in Kirk-Othmer Encyclopedia Chemical Technology, Vol. 3, Third Ed., John Wiley & Sons, New York, pp. 463-479 (1978).
- Kis66 K. Kiss, J. Magder, M.S. Vuksovich, and R.J. Lockhart, "Ferroelectrics of Ultrafine Particle Size, I: Synthesis of Titanate Powder of Ultrafine Particle Size," *J. Am. Ceram. Soc.*, **49** [6], pp. 291-295 (1966).
- Kle89 M.K. Klee and H.W. Brand, U.S. Patent 4,859,448 (1989).
- Klu93 D.L. Klug, "The Influence of Impurities and Solvents on Crystallization," in Handbook of Industrial Crystallization, Ed. by A.S. Myerson, Butterworth-Heinemann, Boston, pp. 65-87 (1993).
- Kos27 W. Kossel, *Nach. Ges. Wiss. Gottingen, Math.-Phys. Kl.*, p. 135 (1927).
- Kum95 H. Kumazawa, S. Annen, and E. Sada, "Hydrothermal Synthesis of Barium Titanate Fine Particles from Amorphous and Crystalline Titania," *J. Mat. Sci.*, **30**, pp. 4740-4744 (1995).
- Kum96 H. Kumazawa, T. Kagimoto, and A. Kawabata, "Preparation of Barium Titanate Ultrafine Particles from Amorphous Titania by a Hydrothermal Method and Specific Dielectric Constants of Sintered Discs of the Prepared Particles," *J. Mat. Sci.*, **31**, pp. 2599-2602 (1996).
- Kut84 T.R.N. Kutty and R. Balachandran, *Mater. Res. Bull.*, **19**, p. 1479 (1984).
- Kut88b T.R.N. Kutty and P. Murugaraj, "Hydrothermal Precipitation and Characterization of Poly titanates in the System BaO-TiO₂," *J. Mater. Sci. Let.*, **7**, pp. 601-603 (1988).
- Kut88a T.R.N. Kutty, R. Vivekanandan, and P. Murugaraj, "Precipitation of Rutile and Anatase (TiO₂) Fine Powders and Their Conversion to MTiO₃ (M=Ba, Sr, Ca) by the Hydrothermal Method," *Mater. Chem. Phys.*, **19**, pp. 533-546 (1988).

- LaM50 V.K. LaMer and R.H. Dinegar, "Theory, Production and Mechanism of Formation of Monodisperse Hydrosols," *J. Am. Chem. Soc.*, **72**, pp. 4847-4854 (1950).
- Lau62 R.A. Laudise, J.H. Crockett, and A.A. Ballman, "Hydrothermal Crystallization of Yttrium Iron Garnet on a Seed," *J. Am. Ceram. Soc.*, **45** [2], pp. 51-3 (1962).
- Lau26 M. von Laue, *Z. Krist*, **64**, p. 115 (1926).
- Lee81 J.B. Lee, "Elevated Temperature Potential - pH Diagrams for the Cr-H₂O, Ti-H₂O, Mo-H₂O, and Pt-H₂O Systems," *Corrosion*, NACE, **37**, p. 467 (1981).
- Len93 M.M. Lenka, and R.E. Riman, "Thermodynamic Modeling of Hydrothermal Synthesis of Ceramic Powders," *Chem. Mater.*, **5**, pp. 61-70 (1993).
- Li96 T. Li, "Fabrication and Characterization of Nanometer-sized Metal and Semiconductor Particles and Nanometer-sized Composites," Ph.D. Dissertation, University of Florida (1996).
- Lid94 D.R. Lide, Editor-in-Chief of CRC Handbook of Chemistry and Physics, CRC Press, Boca Raton, 1994.
- Lin77 M.E. Lines, and A.M. Glass, Principles and Applications of Ferroelectrics and Related Materials, Clarendon Press, Oxford, England, 1977.
- Liv92 J. Livage, M. Henry, and J.P. Jolivet, "Inorganic Polymerization in Aqueous Solutions," in Chemical Processing of Advance Materials, Ed. by L.L. hanch, and J.K. West, John Wiley & Sons, New York, pp. 223-237 (1992).
- Liv90 J. Livage, M. Henry, J.P. Jolivet, and C. Sanchez, "Chemical Synthesis of Fine Powders," *MRS Bulletin*, **XV** [1], pp. 18-25 (1990).
- Lor94 M.H. Loretto, Electron Beam Analysis of Materials, Second Ed., Chapman and Hall, New York, pp. 21-143, 1994.
- Mas89 R.L. Mason, R.F. Gunst, and J.L. Hess, Statistical Design and Experiments with Applications to Engineering and Science, John Wiley & Sons, Inc., New York, 1989.
- Mat88 T. Matsoukas and E. Gulari, "Dynamics of Growth of Silica Particles from Ammonia-Catalyzed Hydrolysis of Tetra-ethyl-orthosilicate," *J. Colloid Interface Sci.*, **124**, pp. 252-261 (1988).
- Maz72 K.S. Mazdiyasni, et al. U.S. Patent 3,647,364, March (1972).
- McC96 J.I. McCool, "The Analysis of Two-Factor Rolling Contact Fatigue Test Results," *Tribology Transactions*, **39** [1], pp. 59-66 (1996).
- Men89a J. Menashi, R.C. Reid, and L.P. Wagner, U.S. Patent 4,829,033 (1989).
- Men89b J. Menashi, R.C. Reid, and L.P. Wagner, U.S. Patent 4,832,939 (1989).
- Mer95 A. Mersmann, "Fundamentals of Crystallization," in Crystallization Technology Handbook, Ed. by A. Mersmann, Marcel Dekker Inc., New York, pp. 1-78 (1995).

- Mil90 D.V. Miller, "Synthesis and Properties of Nanocomposites," Ph.D. Dissertation, The Pennsylvania State University (1990).
- Moo96 J. Moon, "Hydrothermal Particle Synthesis of Barium Titanate and Particle Formation Study," Ph.D. Dissertation, University of Florida (1996).
- Mor53 G.W. Morey, "Hydrothermal Synthesis," *J. Am. Ceram. Soc.*, **36** [9], pp. 279-285 (1953).
- Mul70 B.J. Mulder, *Am. Ceram. Soc. Bull.*, **49**, p. 990 (1970).
- Mye93 A.S. Myerson and R. Ginde, "Crystals, Crystal Growth, and Nucleation," in *Handbook of Industrial Crystallization*, Ed. by A.S. Myerson, Butterworth-Heinemann, Boston, pp. 33-63 (1993).
- Nan66 G.H. Nancollas, *Interactions in Electrolyte Solutions*, Elsevier Publishing Co., New York, 1966.
- Nie83 A.E. Neilson, "Precipitates: Formation, Coprecipitation, and Aging," in *Treatise on Analytical Chemistry, Part I. Theory and Practice*, Second Ed., Vol. 3, Ed. by I.M. Kolthoff and P.J. Elving, John Wiley & Sons, Inc., pp. 304-306 (1983).
- Nyv85 J. Nyvlt, O. Sohnel, M. Matuchova, and M. Broul, *The Kinetics of Industrial Crystallization*, of Chemical Engineering Monographs Vol.19, Elsevier, New York, 1985.
- Oha73 M. Ohara, and R.C. Reid, *Modelling Crystal Growth Rates from Solution*, Prentice Hall, London, 1973.
- Oss88 K. Osseo-Asare, F.J. Arriagada, and J.H. Adair, "Solubility Relationships in the Coprecipitation Synthesis of Barium Titanate: Heterogeneous Equilibria in the Ba-Ti-C₂O₄-H₂O System"; *Ceramic Transactions*, Vol. 1, *Ceramic Powder Science II A*, Ed. by G. Messing, E.R. Fuller Jr., and H. Hausner, American Ceramic Society, Westerville, OH, pp. 47-53 (1988).
- Ost97 W. Ostwald, *Z. physik. Chem. (Leipzig)*, **22**, p. 289 (1897).
- Ott73 E.P.K. Ottens, "Nucleation in Continuous Agitated Crystallizers," Ph.D. Dissertation, Delft University of Technology, Delft (1973).
- Ott72 E.P.K. Ottens, A.H. Janse, and E.J. DeJong, *J. Crystal Growth*, **13** [14], p. 500 (1972).
- Ove52 J.Th.G. Overbeek, *Colloid Science, Vol. 1*, Ed. by H.R. Kruyt, Elsevier, New York, p. 115 (1952).
- Ovr80 N.A. Ovramenko, L.I. Shvets, F.D. Ovcharenko, and B. Yu Kornilovich, "Kinetics of Hydrothermal Synthesis of Barium Metatitanate," *Inorganic Materials*, Plenum Publishing, **15** [11], p. 1560-1562 (1979).
- Ovr79 N.A. Ovramenko, L.I. Shvets, F.D. Ovcharenko, and B. Yu Kornilovich, "Kinetics of Hydrothermal Synthesis of Barium Metatitanate," *Izv. Akad. Nauk SSSR, Neorganicheskiye Materialy*, **15** [11], p. 1982-1985 (1979).
- Oza83 Y. Ozaki, "Ultrafine Electroceramic Powder Preparation from Metal Alkoxides," *Ferroelectrics*, **49**, pp. 285-296 (1983).

- Pet40 J.H. Peterson, "Process of Producing Insoluble Titanates," U.S. Patent 2,216,655, (1940).
- Pfa91 G. Pfaff, "BaTiO₃ Preparation by Reaction of TiO₂ with Ba(OH)₂," *J. Euro. Ceram. Soc.*, **8**, pp. 35-39 (1991).
- Pla46 R.L. Plackett and J.P. Burman, "The Design of Optimum Multifactorial Experiments," *Biometrika*, **34**, pp. 255-272 (1946).
- Phu90 P.P. Phule and S.H. Risbud, "Review; Low Temperature Synthesis and Processing of Electronic Materials in the BaO-TiO₂ system," *J. Mat. Sci.*, **25**, [2B], pp. 1169-1183 (1990).
- Pou74 M. Pourbaix, Atlas of Electrochemical Equilibria in Aqueous Solutions, Second Ed., National Association of Corrosion Engineers, Houston, TX, 1974.
- Pou91 G. Pouskuleli, T.A. Wheat, A. Ahmad, S. Varma, and S.E. Prasad, "Application of Statistical Design in Materials Development and Production," SPIE Vol. 1590, Submolecular Glass Chemistry and Physics (1991).
- Pow98 K. Powers, "The Development and Characterization of Sol Gel Substrates for Chemical and Optical Applications," Ph.D. Dissertation, University of Florida (1998).
- Ran88a A.D. Randolph and M.A. Larson, "Crystallization Kinetics," in Theory of Particulate Processes: Analysis and Techniques of Continuous Crystallization, Academic Press, Inc., San Diego, CA, pp. 109-134 (1988).
- Ran88b A.D. Randolph and M.A. Larson, Theory of Particulate Processes: Analysis and Techniques of Continuous Crystallization, Academic Press Inc., San diego, CA (1988).
- Ras55 D.E. Rase and R. Roy, "Phase Equilibrium in the System BaO-TiO₂," *J. Am. Ceram. Soc.*, **38** [3], pp. 102-113 (1955).
- Ree88 J.S. Reed, Introduction to the Principles of Ceramic Processing, John Wiley & Sons, New York, 1988.
- Reh98 P.W. Rehrig, G.L. Messing, and S. Trolier-McKinstry, "Kinetics of Surface Templated Grain Growth of BaTiO₃ Single Crystals," presented at the 100th Annual Meeting of the American Ceramic Society, Cincinnati (1998).
- Ric92 D.W. Richerson, Modern Ceramic Engineering, Marcel Dekker, Inc., New York, 1992.
- Rin96 T. Ring,, Fundamentals of Ceramic Powder Processing and Synthesis, Academic Press, New York, 1996.
- Sch20 P. Scherrer, *Nachr. Ges. Wiss. Gottingen*, p. 98 (1920).
- Sch65 F. Schrey, "Effect of pH on the Chemical Preparation of Barium-Strontium Titanate," *J. Am. Ceram. Soc.*, **48** [8], pp. 401-405 (1965).
- Seg89 D. Segal, Chemical Synthesis of Advanced Ceramic Materials, Cambridge University Press, New York, pp. 114-121, 1989.

- Sha86 A. Shaikh and G.M. Vest, "Kinetics of BaTiO₃ and PbTiO₃ Formation from Metallo-Organic Precursors," *J. Am. Ceram. Soc.*, **69** [9], pp. 682-688 (1986).
- Shi97 E-W. Shi, C-T Xia, W-Z. Zhong, B-G. Wang, and C-D Feng, "Crystallographic Properties of Hydrothermal Barium Titanate Crystallites," *J. Am. Ceram. Soc.*, **80** [6], pp. 1567-1572 (1997).
- Shv79 L.I. Shvets, N.A. Ovramenko, and F.D. Ovcharenko, "Hydrothermal Synthesis of Highly-Dispersed Barium Titanate," *Dokl. Akad. Nauk SSSR*, **248** [4], pp. 889-891 (1979).
- Sla96 E.B. Slamovich and I.A. Aksay, "Structural Evolution I. Hydrothermally Processed (<100°C) BaTiO₃ Films," *J. Am. Ceram. Soc.*, **79** [1], pp. 239-247 (1996).
- Smi89 R.M. Smith and A.E. Martell, Critical Stability Constants Volume 6: Second Supplement, Plenum Press, New York, pp. 96-99, 1989.
- Smol17 M. von Smoluchowski, *Z. Phys. Chem.*, **92**, p. 129 (1917).
- Soh92 O. Sohnel and J. Garside, Precipitation; Basic Principles and Industrial Applications, Butterworth-Heinemann Ltd., 1992.
- Spa98 D.I. Spang, A.S. Safari, and I. Burn, "Properties of Donor Doped BaTi(Mn,Mg)O₃-SiO₂ Sintered in Reducing Atmospheres," presented at the 100th Annual Meeting of the American Ceramic Society, Cincinnati (1998).
- Stö68 W. Stöber, A. Fink, and E. Bohn, *J. Colloid Interface Sci.*, **26**, pp. 62-69 (1968).
- Sto93 M. Stockenhuber, H. Mayer, and J.A. Lercher, "Preparation of Barium Titanates from Oxalates," *J. Am. Ceram. Soc.*, **76** [5], pp. 1185-1190 (1993).
- Stu92 W. Stumm, Chemistry of the Solid-Water Interface, John Wiley & Sons, Inc., New York, 1992.
- Suw78 Y. Suwa, Y. Sugimoto, and S. Naka, "Preparation of Compounds in BaO-TiO₂ System by Coprecipitation from Alkoxides," *J. Jpn. Soc. Powder Powder Metall.*, **25** [5], pp. 164-167 (1978).
- Suy94 Y. Suyama and M. Nagasawa, "Synthesis of Single-Crystal Barium Titanium Isopropoxide Complex to Form Barium Titanate," *J. Am. Ceram. Soc.*, **77** [2], pp. 603-605 (1994).
- Swa97 S.L. Swartz, T.R. Shrout, and T. Takenaka, "Electronic Ceramics R&D in the U.S., Japan, Patent History," *Am. Ceram. Soc. Bull.*, **76** [7], pp. 59-65 (1997).
- Tay61 A. Taylor, "The Determination of Size and Perfection of Grains in Stress-Free Polycrystalline Metals," X-Ray Metallography, John Wiley & Sons, Inc., pp. 656-723 (1961).
- Ute90 B.L. Utech, "The Effect of Solution Chemistry on Barium Titanate Ceramics," M.S. Thesis, The Pennsylvania State University (1990).
- Val20 J. Valasek, *Phys. Rev.*, **15**, p. 537 (1920).

- Van90 G.M. VanRosmalen and P. Bennema, "Characterization of Additive Performance on Crystallization: Habit Modification," *J. Cryst. Growth*, **99**, pp. 1053-1060 (1990).
- Ven95 S. Venigalla, "Analysis and Performance of Electrochemically Synthesized Barium Titanate Films and Electrolytic Capacitors," Ph.D. Dissertation, University of Florida (1995).
- Ven98 S. Venigalla, D.V. Miller, and S.A. Costantino, "High Performance, Aqueous-Based Ceramic Dielectric Materials for <3 μm Active Layer MLCC Applications," presented at the 100th Annual Meeting of the American Ceramic Society, Cincinnati (1998).
- Ver48 E.J.W. Verwey and J.Th.G. Overbeek, Theory of Stability of Lyophobic Colloids, Elsevier, New York, 1948.
- Viv89 R. Vivekanandan and T.R.N. Kutty, "Characterization of Barium Titanate Fine Powders Formed From Hydrothermal Crystallization," *Powder Technology*, **57**, pp. 181-192 (1989).
- Viv87 R. Vivekanandan, S. Philip, and T.R.N. Kutty, "Hydrothermal Preparation of Ba(Ti,Zr)O₃ Fine Powders," *Mat. Res. Bull.*, **22**, pp. 99-108 (1987).
- Wad95 S. Wada, T. Suzuki, and T. Noma, "Preparation of Barium Titanate Fine Particles by Hydrothermal Method and Their Characterization," *J. Ceram. Soc. Jpn.*, **103** [12], pp. 1220-1227 (1995).
- Wad96 S. Wada, T. Suzuki, and T. Noma, "Role of Lattice Defects in the Size Effect of Barium Titanate Fine Particles," *J. Jap. Ceram. Soc.*, **104** [5], pp. 383-392 (1996).
- Wag82 D.D. Wagman, W.H. Evans, V.B. Parker, R.H. Schumm, I. Halow, S.M. Bailey, K.L. Churney, and R.L. Nuttall, The NBS Tables of Chemical Thermodynamic Properties, American Chemical Society and American Institute of Physics, **11**, Supplement No. 2, 1982.
- Wan94 S.F. Wang, J.P. Dougherty, W. Huebner, and J.G. Pepin, "Silver-Palladium Thick-Film Conductors," *J. Am. Ceram. Soc.*, **77** [12], pp. 3051-3072 (1994).
- Wil53 G.K. Williamson and W.H. Hall, *Acta Metallurgica*, **1**, pp. 22-31 (1953).
- Wil87 K.L. Williamson, Introduction to X-Ray Spectrometry, Allen and Unwin, Boston, 1987.
- Wul01 G. Wulff, *Z. Krist.*, **34**, p. 449 (1901).
- Xia96 C-T. Xia, E-W. Shi, W-Z. Zhong, and J-K. Guo, "Hydrothermal Synthesis of BaTiO₃ Nano-Microcrystals," *J. Crystal Growth*, **166**, pp. 961-6 (1996).
- Xu92 Z. Xu, H.K. Chae, M.H. Frey, and D.A. Payne, "Chemical Processing and Properties of Nanocrystalline BaTiO₃," *Mater. Res. Soc. Symp. Proc.*, **271**, pp. 339-344 (1992).
- Yoo97 Y.S. Yoo, M.K. Kang, J.H. Han, H. Kim, and D.Y. Kim, "Fabrication of BaTiO₃ Single Crystals Using the Exaggerated Grain Growth Method," *J. Euro. Ceram. Soc.*, **17** [14], pp. 1725-1727 (1997).

- Yos89 M. Yoshimura, S.E. Yoo, M. Hayashi, and N. Ishizawa, *Jpn. J. Appl. Physics*, 28, L2007 (1989).
- Zha96 L. Zhao, A.T. Chien, F.F. Lange, and J.S. Speck, "Microstructural Development of BaTiO₃ Powders Synthesized by Aqueous Methods," *Comm. J. Mater. Res.*, **11** [6], pp. 1325-1328 (1996).
- Zhi90 Z. Zhingang and Z. Gang, *Ferroelectrics*, **101**, p. 43 (1990).
- Zog96 D. Zogbi, Ceramic Capacitors World Markets, Technologies, and Opportunities, a 1996-2000 Technical Economic Analysis, Paulmanok Publications, Inc., Apex, N.C. (1996).

BIOGRAPHICAL SKETCH

Jeff was born to Cliff and Suzanne Kerchner on April 26, 1972, in Binghamton, NY. The family moved to the Boyertown, PA area in 1974 shortly after the arrival of his baby sister, Karen. As you might imagine, the two-year-old youth was not consulted when deciding to relocate the familial homestead. However, had it not been for this move he would never have met his good friends, Jon Rothermel and Mike Cha, or Jeannie, his high school sweetheart.

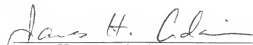
He attributes much of his leadership skills, gumption, and overall success to his parents, who raised him under strict Quaker law (just kidding). In truth, he owes much of his mechanical aptitude and problem solving to his grandfathers and father, who included him in even the largest of home-related projects. If Jeff had followed his childhood dreams, he would now be employed as either the Lone Ranger or a fireman. Thankfully, his mother fostered these notions only in his presence.

Jeff's first thoughts of an engineering profession were sparked by Mrs. Loeben, his junior high science teacher, and a field trip to a Drexel University sponsored robotics convention. His entrance into the world of ceramics was initiated by an intriguing high school trip to Penn State to visit Sue Cha, a studying ceramic engineer and the sister of his friend, Mike. As a PSU undergraduate, a friend referred him to Dr. Stephen Costantino at Cabot Performance Materials, where he obtained his first taste of an industrial environment during the summer prior to his junior year. Due to his diligence, he was the only undergraduate working at Cabot who was extended invitations, which he readily accepted, to work during the winter and spring breaks. His alternating terms spent in


industry and undergraduate semesters were an invaluable experience as he focused his collegiate textbook knowledge to real-world processing. Since matriculation to the University of Florida Ph.D. program under the advisement of Dr. James Adair, he has taken on many projects and group related activities which have strengthened both his role as a leader and his communication skills.

On March 4, 1995, Jeff married Jeannie in mystical Castle Ottis on the shores of Vilano Beach, FL. During their precious time outside of the laboratory, they have enjoyed many walks through the Floridian jungle and quality time with their two ferocious felines, Emerson and Lily. After graduation, they will anxiously await the arrival of their first child (tentatively scheduled on December 5, 1998).


I certify that I have read this study and that in my opinion it conforms to acceptable standards of scholarly presentation and is fully adequate, in scope and quality, as a dissertation for the degree of Doctor of Philosophy.


James H. Adair, Chair
Associate Professor of Materials Science
and Engineering


I certify that I have read this study and that in my opinion it conforms to acceptable standards of scholarly presentation and is fully adequate, in scope and quality, as a dissertation for the degree of Doctor of Philosophy.


David E. Clark
Professor of Materials Science and
Engineering


I certify that I have read this study and that in my opinion it conforms to acceptable standards of scholarly presentation and is fully adequate, in scope and quality, as a dissertation for the degree of Doctor of Philosophy.


Robert T. DeHoff
Professor of Materials Science and
Engineering

I certify that I have read this study and that in my opinion it conforms to acceptable standards of scholarly presentation and is fully adequate, in scope and quality, as a dissertation for the degree of Doctor of Philosophy.


Michael D. Sacks
Professor of Materials Science and
Engineering

I certify that I have read this study and that in my opinion it conforms to acceptable standards of scholarly presentation and is fully adequate, in scope and quality, as a dissertation for the degree of Doctor of Philosophy.


James D. Winefordner
Graduate Research Professor of
Chemistry

I certify that I have read this study and that in my opinion it conforms to acceptable standards of scholarly presentation and is fully adequate, in scope and quality, as a dissertation for the degree of Doctor of Philosophy.



Stephen A. Costantino
Business Manager Barium Titanate
Cabot Performance Materials

This dissertation was submitted to the Graduate Faculty of the College of Engineering and to the Graduate School and was accepted as partial fulfillment of the requirements for the degree of Doctor of Philosophy.

August, 1998



Winfred M. Phillips
Dean, College of Engineering

Karen A. Holbrook
Dean, Graduate School